

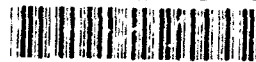
FEBRUARY 1993

PAGE 01

ISSN — 0142-2464

01 FEB 93

AD-A264 051



(2)

# INTERNATIONAL JOURNAL OF Numerical

## Electronic Networks, Devices and Fields

Special Issue on the Workshop on  
Discrete Time Domain Modelling of Electromagnetic  
Fields and Networks, Part 2

DISTRIBUTION STATEMENT A  
Approved for public release  
Distribution Unlimited

DTIC  
ELECTE  
APR 22 1993  
S C D

Managing Editor WOLFGANG HOEFER  
Editor, Europe BRIAN TUCK

 **WILEY**  
Publishers since 1807

Chichester · New York · Brisbane · Toronto · Singapore

# INTERNATIONAL JOURNAL OF Numerical Modelling

Electronic Networks,  
Devices and Fields

## MANAGING EDITOR

**Wolfgang J. R. Hoefer**

NSERC-MPR Teltech Research Chair in RF-  
Engineering, Department of Electrical & Computer  
Engineering, P.O. Box 3055, University of Victoria,  
Victoria, B.C., Canada V8W 3P6

## EDITOR, EUROPE

**Brian Tuck**

Department of Electrical and Electronic Engineering,  
University of Nottingham, University Park, Nottingham  
NG7 2RD, UK

## EDITORIAL ADVISORY BOARD

**John M. Arnold**

Department of Electronic Engineering,  
University of Glasgow, Glasgow, UK

**Martin J. Balchin**

School of Electrical Engineering,  
University of Bath, Claverton Down, Bath  
BA2 7AY, UK

**John Bandler**

Department of Electrical Engineering,  
McMaster University, Hamilton, Ontario,  
Canada L8S 4L8

**Adalbert Beyer**

Fachbereich Elektrotechnik,  
Universität-GH-Duisburg,  
Bismarckstrasse 69,  
4100 Duisburg 1, Germany

**Dennis H. Choi**

Department of Electrical Engineering,  
University of Regina, Regina,  
Saskatchewan, Canada S4S 0A2

**Christos Christopoulos**

Department of Electrical and Electronic  
Engineering,  
University of Nottingham, University  
Park, Nottingham NG7 2RD, UK

**George Costache**

Department of Electrical Engineering,  
University of Ottawa, Ottawa, Ontario,  
K1N 6N5, Canada

**Donard de Cogan**

School of Information Systems,  
University of East Anglia,  
Norwich NR4 7TJ, UK

**Leopold B. Felsen**

Department of Electrical Engineering and  
Computer Science, Polytechnic  
Institute of New York, Route 110,  
Farmungdale, New York 11735, USA

**Ron L. Ferrari**

Trinity College,  
Cambridge CB2 1TQ, UK

**Ernest M. Freeman**

Department of Electrical Engineering,  
Imperial College,  
Exhibition Road,  
London SW7 2BT, UK

**Ichiro Fukai**

Department of Electrical Engineering,  
Hokkaido University,  
Sapporo 060, Japan

**Peter Gough**

Solid State Electronics Division,  
Philips Research Laboratories,  
Cross Oak Lane, Redhill,  
Surrey RH1 5HA, UK

**Martyn R. Harris**

Department of Electrical Engineering,  
University of Southampton,  
Highfield, Southampton SO9 5NH

**Tatsuo Itoh**

66-147A ENG IV,  
Department of Electrical Engineering,  
405 Hilgard Avenue, Los Angeles,  
CA 90024-1594, USA

**Rolf H. Jansen**

Industrial Microwave and HF Techniques,  
Burohaus am See  
Am Brühl 17  
4040 Ratingen 1, Germany

**Yukio Kagawa**

Department of Electrical Engineering,  
Okayama University,  
Okayama 700, Japan

**Arthur J. Lowery**

Photonics Research Laboratory,  
Department of Electrical and  
Electronic Engineering,  
University of Melbourne,  
Parkville, Victoria 3052, Australia

**Alexander Marincic**

Faculty of Electrical Engineering,  
University of Belgrade,  
Bulevar Revolucije 73,  
PO Box 816, 11001 Belgrade,  
Yugoslavia

**Edmund K. Miller**

Leader Group MEE-3, MS J580,  
Los Alamos National Laboratory,  
Los Alamos,  
New Mexico 87545, USA

**Kenzo Miya**

Nuclear Engineering Research Laboratory,  
Faculty of Engineering,  
University of Tokyo,  
Bunkyo-ku, Tokyo 113, Japan

**Takayoshi Nakata**

Department of Electrical Engineering,  
Okayama University, Tsushima,  
Okayama 700, Japan

**Michel Ney**

Department of Electrical Engineering,  
University of Ottawa, Ottawa, Ontario,  
Canada K1N 6N5

**Giakos Y. Philippou**

ERA Technology Ltd,  
Cleeve Road, Leatherhead,  
Surrey KT22 7SA, UK

**Simon Joseph Polak**

Philips Medical Systems Nederland,  
Veenpluis 4-6, P.O. Box 10.000,  
5680 DA Best, The Netherlands

**Susan H. Pulko**

Department of Electronic Engineering,  
University of Hull,  
Hull HU6 7RX, UK

**Alain E. Ros**

Electronic Laboratory,  
Faculté des Sciences et des Techniques  
22 BP 582-ABIDJAN 22,  
Rep. de CÔTE D'IVOIRE

**Peter Russer**

Technische Universität München,  
Lehrstuhl für Hochfrequenztechnik,  
Arcisstrasse 21,  
8000 München 2, Germany

**Pierre Saguet**

Laboratoire d'Electromagnetisme,  
ENSERG, Avenue des Martyrs 38,  
Grenoble 38031, France

**Peter Silvester**

Electrical Engineering Department,  
McGill University,  
3480 University Street,  
Montreal, PQ, Canada H3A 2A7

**Christopher M. Snowden**

Department of Electrical &  
Electronic Engineering,  
The University of Leeds,  
Leeds LS2 9JT, UK

**Roberto Sorrentino**

Istituto di Elettronica,  
Università di Perugia,  
Via Carli, 24,  
I-06100 Perugia, Italia

**Frederick M. Tesche**

6921 Spanky Branch Drive,  
Dallas, Texas 75248, USA

**Bill Trowbridge**

Vector Fields Ltd,  
24 Bankside, Kidlington,  
Oxford OX5 1JE, UK

**Thomas Weiland**

Electrical Engineering Department,  
T.H. Darmstadt,  
Merckstrasse 25,  
D-6100 Darmstadt, Germany

**Alvin Wexler**

President, Quantic Laboratories Inc.,  
200-281 McDermot Avenue,  
Winnipeg, Canada R3B 0S9

**Ingo Wolff**

Fachbereich Elektrotechnik,  
Universität-GH-Duisburg,  
Bismarckstrasse 69,  
4100 Duisburg 1, Germany

**Norinobu Yoshida**

Department of Electrical Engineering,  
Faculty of Engineering, Hokkaido  
University, Sapporo 060, Japan

**Olek C. Zienkiewicz**

Department of Civil Engineering,  
University College of Swansea,  
Singleton Park, Swansea SA2 8PP, UK

**Advertising:** For details contact—

Michael J. Levermore, Advertisement Sales, John Wiley & Sons Ltd., Baffins Lane, Chichester, Sussex PO19 1UD, England (Telephone  
0243 770351; fax 0243 775878; telex 86290).

**To subscribe:** Orders should be addressed to: Subscriptions Department, John Wiley & Sons Ltd., Baffins Lane, Chichester, Sussex  
PO19 1UD, England. 1993 subscription price US\$250.00. *International Journal of Numerical Modelling: Electronic Networks, Devices and  
Fields* (ISSN 0894-3370) is published quarterly by John Wiley & Sons Ltd., Baffins Lane, Chichester, Sussex, England. Second class  
postage paid at Jamaica, NY 11431. Air freight and mailing in the U.S.A. by Publications Expediting Services Inc., 200 Meacham  
Avenue, Elmont, NY 11003. Copyright © 1993 by John Wiley & Sons Ltd. Typeset in the U.K. by Photo-graphics, Honiton, Devon.  
Printed and bound in Great Britain by Page Bros, Norwich. Printed on acid-free paper.

**U.S.A. POSTMASTERS:** Send address changes to *International Journal of Numerical Modelling: Electronic Networks, Devices and Fields*,  
c/o Publications Expediting Services Inc., 200 Meacham Avenue, Elmont, NY 11003.

INTERNATIONAL JOURNAL OF NUMERICAL MODELLING:  
ELECTRONIC NETWORKS, DEVICES AND FIELDS

CONTENTS

Special Issue on the Workshop on Discrete Time Domain Modelling of  
Electromagnetic Fields and Networks

*Munich, 24-25 October, 1991*

Part 2

*Guest Editor: Professor Dr Peter Russer*

VOLUME 6, ISSUE No 1

*February 1993*

Editorial.....	1
Efficient Analytical-Numerical Modelling of Ultra-wideband Pulsed Plane Wave Scattering from a Large Strip Grating: L. Carin and L. B. Felsen .....	3
Calculating Frequency-domain Data by Time-domain Methods: M. Dehler, M. Dohlus and T. Weiland .....	19
The Hilbert Space Formulation of the TLM Method: P. Russer and M. Krumpholz ..	29
Spatially Weighted Numerical Models for the Two-dimensional Wave Equation: FD Algorithm and Synthesis of the Equivalent TLM Model: N. R. S. Simons and A. A. Sebak .....	47
Multiport Approach for the Analysis of Microwave Non-linear Networks: M. I. Sobhy, E. A. Hosny and M. A. Nassef .....	67

Abstracted/indexed in 'CAD/CAM Abstracts', 'Cambridge Scientific Abstracts', 'Engineering Index', 'INSPEC', 'Mathematical Reviews', 'Telecommunications Abstracts'

93 4 20 137

IJNFEX 6 (1) 1-82 (1993)  
ISSN 0894-3370

93-08512



3698

## EDITORIAL

The direct time-domain modelling of electromagnetic fields and high-frequency circuits meets with growing interest. Modern powerful computers make feasible the applications of time-domain methods in the modelling of electromagnetic fields and networks. The advantages of time-domain methods are their high flexibility, their potential to include non-linear effects and time-dependent parameters, and their transparency with respect to concepts and algorithms. Time-domain analysis elucidates the physical principles underlying the phenomena and supports a creative design of circuits and systems. For these reasons, time-domain methods are of high interest for the development of CAD tools for the modelling of microwave and millimetre-wave integrated circuits, and broad-band microwave devices, antennas, circuits and systems. The combination of field concepts and network concepts allows the segmentation of complex structures and to apply full wave analysis to the segments.

This special issue is the second of three parts comprising contributions to the workshop on the German IEEE MTT/AP Joint Chapter and the German IEEE CAS Chapter on **Discrete Time Domain Modelling of Electromagnetic Fields and Networks** on 24 and 25 October 1991 at the Technische Universität München. The first part was published in vol. 5, no. 3 of the Journal. The purpose of this workshop, organized by Peter Russer and Josef Nossek under the sponsorship of the European Research Office (ERO) of the US Army, was to bring together researchers dealing with time-domain simulation and transient phenomena in fields and networks.

PETER RUSSER

DTIC QUALITY INSPECTED +

Accession For	
NTIS CRA&I	<input checked="" type="checkbox"/>
DTIC TAB	<input checked="" type="checkbox"/>
Unannounced	<input checked="" type="checkbox"/>
Justification	
By	
Distribution /	
Availability Codes	
Dist	Avail and/or Special
A-1	

## EFFICIENT ANALYTICAL-NUMERICAL MODELLING OF ULTRA-WIDEBAND PULSED PLANE WAVE SCATTERING FROM A LARGE STRIP GRATING

LAWRENCE CARIN AND LEOPOLD B. FELSEN

*Weber Research Institute/Electrical Engineering Department, Polytechnic University, Farmingdale, NY 11735, U.S.A.*

### SUMMARY

Ultra-wideband (UWB) pulsed plane wave scattering from a large but finite strip grating in free space is analysed in the frequency domain via decomposition into plane wave spectra, implemented numerically by the method of moments, and then inverted into the time domain (TD). To make this procedure practical under UWB conditions, closed form expressions are derived for interaction integrals involving widely separated expansion and testing functions. These closed forms are based on a judicious choice of the basis functions, and on asymptotic methods for reducing the integrals. Although large separation distances are assumed, the expressions have been found to be accurate for separations as small as 0.1 wavelengths. The TD self terms can also be evaluated efficiently. To test the frequency domain algorithm, comparisons are made with available data in the literature for surface currents and far-field scattering from multiple strips. New short pulse TD results are shown as well.

### 1. INTRODUCTION

Plane wave scattering from a collection of periodically arranged elements continues to be a topic of interest. Periodic arrays of patches or slots have been used for microwave and millimetre-wave frequency selective surfaces.<sup>1</sup> Strip gratings have found use in optical spectrometers<sup>2</sup> and as dispersive elements in pulse compression systems.<sup>3</sup> Although truncated in space, the arrays are usually electrically large and are therefore often treated by analysing an ideal infinitely periodic array. In such studies, the problem reduces to the much simpler investigation of scattering from a single unit cell. Recently, however, attention has been given to the effects of array truncation.<sup>1,4-7</sup>

Nearly all investigations of scattering from arrays of elements have been performed in the frequency domain.<sup>1,4-7</sup> With current interest in impulse or UWB radar,<sup>8</sup> the time-dependent scattering of short pulses from such configurations is gaining in importance. Moreover, the availability of picosecond and femtosecond lasers makes these studies relevant also to the interaction of infrared or optical pulses with gratings. It is the purpose of this paper to develop an efficient technique for the analysis and numerical calculation of UWB pulse scattering from a large but finite collection of elements. The basic phenomena associated with such scattering can be modelled by the strip array prototype adopted here.

For UWB radars, the commonly accepted definition of a UWB pulse is one having a bandwidth of 25 per cent or more with respect to the centre frequency.<sup>8</sup> For the present study, an alternative definition is more appropriate: the UWB pulse must contain sufficient energy at wavelengths  $\lambda_0$  ranging from  $\lambda_0 \ll D$  to  $\lambda_0 \gg D$ , where  $D$  is the characteristic size of the scatterer; this range of wavelength accommodates at the extremes high resolution of local features as well as collective wave phenomena associated with global features. To develop techniques for the general analysis of UWB scattering from a large but finite collection of elements, an array of planar strips in free space has been selected as a prototype problem. For this case, which is of interest in its own right, the characteristic size  $D$  for the UWB pulse is the strip width.

To analyse UWB scattering efficiently, special considerations must be addressed. If the problem is first analysed in the frequency domain and then converted to the time domain via the Fourier transform, thousands of frequency points are often required to get accurate time-domain results. If one were to apply previously developed frequency-domain techniques<sup>1,4-7</sup> directly to such a

problem, the CPU time required would be so excessive as to make the analysis impracticable. To avoid this difficulty, the present study utilizes a hybrid numerical/analytical technique. This involves application of a spectral-domain formulation, with a moment method solution. Closed form asymptotic expressions are developed for reaction integrals that contain expansion and testing functions separated by  $0.1\lambda_0$  or more. This method leads to a highly efficient and accurate procedure.

The paper is organized as follows. Section 2 deals briefly with the spectral domain formulation of time-harmonic plane wave scattering from a collection of strips in free space. Sections 3 and 4 are concerned with the techniques proposed to make such a formulation practicable for UWB pulsed scattering applications. In particular, the basis functions and integration techniques are discussed in detail. Numerical results are presented in Section 5. Comparisons are made with available frequency-domain data in the literature, followed by new time-domain results. Conclusions that can be drawn from this work are summarized in section VI.

## 2. FORMULATION AND FREQUENCY-DOMAIN SOLUTION STRATEGY

This section deals with time-harmonic plane wave scattering from a finite array of perfectly conducting infinitesimally thin strips in free space. Referring to Figure 1, the surfaces of the various strips are assumed to be perpendicular to  $y$ , and the fields in this two-dimensional problem are assumed to be independent of  $z$ . Unlike previous studies that have performed the analysis by using the two-dimensional free space (space domain) Green's function,<sup>4-6</sup> the problem is formulated here in the spectral domain (with respect to  $x$ ). This is done for two reasons: (i) as shown in section 3, one obtains thereby a convenient and efficient asymptotic representation, and (ii) this method is readily extended to more complicated configurations involving layered dielectrics. Because spectral domain formulations have been used for several related problems,<sup>9-11</sup> this section contains only a brief summary of those issues which are of importance for the present investigation.

Assuming a plane wave incident obliquely on the strips in Figure 1, and applying the boundary condition for the electric field on the perfect conductors, one arrives at the expression:

$$y \times (\mathbf{E}^i + \mathbf{E}^s) = 0 \quad (1)$$

A bold-face symbol denotes a vector quantity and a tilde, later on, identifies quantities in the spectral domain. The boundary condition in (1) is applied on the surface of each strip. Here,  $\mathbf{E}^i(x,y)$  is the incident vector electric field in the absence of the strips, while  $\mathbf{E}^s(x,y)$  is the scattered vector electric field produced by the electric surface currents  $\mathbf{J}(x',y')$  induced on the strips. The scattered field can be expressed as (an  $e^{j\omega t}$  time-dependence is assumed and suppressed henceforth)

$$\mathbf{E}^s(x,y) = \int_C \tilde{\mathbf{G}}(\mathbf{k}_x, y; y') \cdot \mathbf{J}(\mathbf{k}_x, y') e^{-j\mathbf{k}_x \cdot (x-x')} d\mathbf{k}_x \quad (2)$$

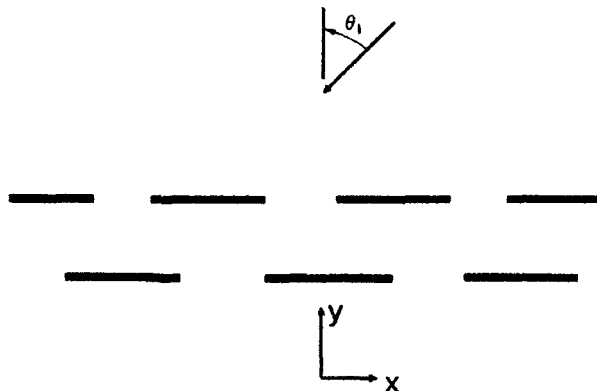


Figure 1. Example of a multilayer strip grating in free space

where  $\hat{G}(k_x, y; y')$  and  $\hat{J}(k_x, y')$  are the dyadic Green's function and surface current, respectively, in the  $k_x$  spectral wavenumber domain. The contour of integration  $C$  is assumed to run initially along the real  $k_x$  axis. Because the problem is two-dimensional, only a single component of surface current (longitudinal or transverse) is induced for a given polarization (TE or TM,<sup>12</sup> respectively). Therefore, only a single component of the dyadic Green's function is required for a given incident polarization. The required component of the spectral domain Green's function is

$$\hat{G}^h(k_x, y; y') = \frac{Z^h}{2} e^{-1\sqrt{k_0^2 - k_x^2}|y - y'|} \quad (3)$$

with  $k_0 = \omega\sqrt{\mu_0\epsilon_0}$ . For TM and TE waves, respectively, it is well known that the wave impedances are given by

$$\begin{aligned} Z^h &= \frac{\sqrt{k_x^2 - k_0^2}}{j\omega\epsilon_0} \\ Z^e &= \frac{j\omega\mu_0}{\sqrt{k_x^2 - k_0^2}} \end{aligned} \quad (4)$$

The boundary condition in (1) is enforced numerically by first expanding the unknown surface currents  $\mathbf{J}(x', y')$  in a known set of basis functions  $\mathbf{f}_k(x', y')$  with unknown coefficients  $a_k$ :

$$\mathbf{J}(x', y') = \sum_{k=1}^{N_b} a_k \mathbf{f}_k(x', y') \quad (5)$$

By applying a Galerkin testing procedure<sup>13</sup> to (1), one obtains

$$-\int_S \mathbf{E}^i(x, y) \cdot \mathbf{f}_m^*(x, y) dx = \sum_{k=1}^{N_b} a_k \int_C \tilde{\mathbf{f}}_m^*(k_x, y) \cdot \hat{G}(k_x, y; y') \cdot \tilde{\mathbf{f}}_k(k_x, y') e^{-1\sqrt{k_0^2 - k_x^2}(x_m - x_k)} dk_x \quad (6)$$

for  $m = 1, 2, \dots, N_b$ . Here,  $x_i$  represents the location (in  $x$ ) of the centre of the basis function  $\mathbf{f}_i$ , and superscript \* denotes the complex conjugate. The integral on the left side of (6) extends over the surface  $S$  of a particular strip. By expanding the currents and applying the testing procedure on each strip, an  $N_b \times N_b$  matrix equation is produced, where  $N_b$  is the total number of basis functions. From this equation one can determine the basis function coefficients, and from (5) and (2), respectively, the currents and scattered fields.

For a plane wave incident at angle  $\Theta_i$  (see Figure 1),  $\mathbf{E}^i(x, y)$  can be expressed as

$$\mathbf{E}^i(x, y) = \mathbf{c} e^{jk_0 \sin \Theta_i x} e^{jk_0 \cos \Theta_i y} \quad (7)$$

where  $\mathbf{c}$  is a vector constant. For TE incidence,  $\mathbf{c}$  is in the  $z$ -direction while for TM incidence,  $\mathbf{c}$  lies in the  $x$ - $y$  plane but depends on the angle of incidence. Using Parseval's theorem, the left side of (6) can be evaluated trivially as

$$\int_S \mathbf{E}^i(x, y) \cdot \mathbf{f}_m^*(x, y) dz = e^{jk_0 \cos \Theta_i y} e^{jk_0 \sin \Theta_i x_m} \tilde{\mathbf{f}}_m^*(k_x = -k_0 \sin \Theta_i, y) \cdot \mathbf{c} \quad (8)$$

One usually selects basis functions that have closed form spectral domain representations; therefore the computational effort in this formulation involves the numerical evaluation of the integrals on the right-hand side of (6).

### 3. FREQUENCY-DOMAIN IMPLEMENTATION FOR UWB SIGNALS

The integrals on the right side of (6) can be expressed in the generic form

$$I_{mk} = \int_C h(k_x, y_m, y_k) e^{-1\sqrt{k_0^2 - k_x^2}\Delta_y} e^{-1k_x \Delta_x} dk_x \quad (9)$$

where  $\Delta_y = |y_m - y'_k|$  and  $\Delta_x = x_m - x'_k$ . Here,  $y_m$  and  $y'_k$  locate the position in  $y$  of testing function  $m$  and expansion function  $k$ , respectively. For UWB applications, the separation  $L = \sqrt{\Delta_x^2 + \Delta_y^2}$  between expansion and testing functions will range from zero to several wavelengths. Therefore, to make the analysis of UWB pulse scattering practicable, special considerations are required for the evaluation of integrals of the form in (9).

### 3.1. Basis functions

Because integrals as in (9) must be calculated over an ultra-wide bandwidth and the efficiency of such integrations determines the ultimate speed of the algorithm, it is desirable to derive a closed form asymptotic expression for (9) when  $L$  is large relative to wavelength. As will be demonstrated below, it is possible to derive such an expression that is accurate even when  $L$  is a small fraction of a wavelength.

Success in this endeavour is dictated in large part by the choice of basis functions. It is desirable to use basis functions with simple spectral-domain representations. For this reason, the complete domain basis functions chosen here, which do not explicitly enforce the edge condition, are

$$f_x(x') = \sin\left[\frac{k\pi(x' + W/2)}{W}\right], \quad \left|\frac{W}{2}\right| \leq x' \quad (10)$$

where  $W$  is the strip width. Note that in (10), the explicit  $y'$  dependence of  $f_k(x', y')$  has been suppressed. This  $y'$  dependence is manifested in the fact that, in general, the strip width  $W$  will be different for each strip and therefore will depend on the layer in which the strip is located. The spectral domain representation of  $f_k(x')$  is

$$\tilde{f}_k(k_x) = j \sin(k_x W/2) s_k(k_x) \quad (11)$$

for  $k$  even, and

$$\tilde{f}_k(k_x) = \cos(k_x W/2) s_k(k_x) \quad (12)$$

for  $k$  odd, with  $s_k(k_x)$  defined as

$$s_k(k_x) = \frac{1}{k_x - \frac{k\pi(-1)^k}{W}} - \frac{1}{k_x + \frac{k\pi(-1)^k}{W}} \quad (13)$$

The spectral representation of the basis function therefore consists of a trigonometric function which, in general, varies rapidly with respect to the remaining algebraic expression  $s_k$ . It should be noted that the commonly used triangular subsectional basis functions also can be written as the product of a rapidly varying trigonometric function and a function that varies slowly in comparison. Since many subsectional basis functions are usually required per wavelength,<sup>4</sup> they were not chosen for the present investigation into UWB scattering.

### 3.2. Asymptotic representation

The integrals that need be evaluated can be grouped into two types: (i) for TM waves

$$I_{mk}^{TM} = \frac{1}{\omega \epsilon_0} \int_C \tilde{f}_m^*(k_x) \sqrt{k_0^2 - k_x^2} \tilde{f}_k(k_x) e^{-i\sqrt{k_0^2 - k_x^2} \Delta_y} e^{-ik_x \Delta_x} dk_x \quad (14)$$

and (ii) for TE waves



$$I_{mk}^{TE} = \omega\mu_0 \int_C \tilde{f}_m^*(k_x) \frac{1}{\sqrt{k_0^2 - k_x^2}} \tilde{f}_k(k_x) e^{-j\sqrt{k_0^2 - k_x^2}\Delta_y} e^{-jk_x\Delta_x} dk_x \quad (15)$$

By grouping the trigonometric parts of the basis functions, after decomposition, with the exponentials in (14) and (15),  $I_{mk}^{TE}$  and  $I_{mk}^{TM}$  each can be expressed as a sum of integrals of the form

$$K_{mk}^{TM} = \frac{1}{j\omega\epsilon_0} \int_C \sqrt{k_x^2 - k_0^2} s_m(k_x) s_k(k_x) e^{-j\sqrt{k_0^2 - k_x^2}\Delta_y} e^{-jk_x\Delta_x} e^{jk_x nW} dk_x \quad (16)$$

and

$$K_{mk}^{TE} = j\omega\mu_0 \int_C \frac{s_m(k_x) s_k(k_x)}{\sqrt{k_x^2 - k_0^2}} e^{-j\sqrt{k_0^2 - k_x^2}\Delta_y} e^{-jk_x\Delta_x} e^{jk_x nW} dk_x \quad (17)$$

respectively, with  $n$  either 0, 1, or  $-1$ .

These integrals can be approximated to a high degree of accuracy using standard asymptotic techniques.<sup>14</sup> It is convenient to introduce the following change of variables:

$$L_1 \sin \Theta \equiv \Delta_x + nW, \quad L_1 \cos \Theta \equiv \Delta_y, \quad L_1 \equiv \sqrt{(\Delta_x + nW)^2 + \Delta_y^2}, \quad k_x = k_0 \sin \zeta \quad (18)$$

which transforms (16) and (17) into the following simpler equations (see Reference 14 for the integration path in the  $\zeta$ -plane):

$$K_{mk}^{TM} = \omega\mu_0 \int_C s_m(\zeta) s_k(\zeta) \cos^2 \zeta e^{-j\Omega \cos(\Theta - \zeta)} d\zeta \quad (19)$$

$$K_{mk}^{TE} = \omega\mu_0 \int_C s_m(\zeta) s_k(\zeta) e^{-j\Omega \cos(\Theta - \zeta)} d\zeta \quad (20)$$

with  $\Omega = k_0 L_1$ . These integrals are evaluated most efficiently along the steepest descent path (SDP) with saddle point at  $\zeta = \Theta$ .<sup>14</sup> By performing a first-order asymptotic evaluation of (19) and (20) around the saddle point, one finds

$$K_{mk}^{TM} \sim \omega\mu_0 \sqrt{\frac{2\pi}{\Omega}} s_m(k_x = k_0 \sin \Theta) s_k(k_x = k_0 \sin \Theta) \cos^2 \Theta e^{-j\Omega} e^{j\pi/4} \quad (21)$$

$$K_{mk}^{TE} \sim \omega\mu_0 \sqrt{\frac{2\pi}{\Omega}} s_m(k_x = k_0 \sin \Theta) s_k(k_x = k_0 \sin \Theta) e^{j\Omega} e^{j\pi/4} \quad (22)$$

Inspection of (21) reveals a problem: for the important case of  $\Theta = \pm\pi/2$  (expansion and testing function on the same plane), (21) predicts  $I_{mk}^{TM} = 0$  for all  $m$  and  $k$ . This is because an  $x$ -directed current will have no far-field  $x$ -component of electric field along its axis. Therefore the first order approximation in (21) is only valid in the far field. A second-order asymptotic evaluation is in general quite difficult. However, for the special case of  $\Theta \approx \pm\pi/2$ , a second order approximation of (19) readily yields

$$K_{mk}^{TM} \sim j\omega\mu_0 \sqrt{\frac{2\pi}{\Omega^3}} s_m(k_x = k_0 \sin \Theta) s_k(k_x = k_0 \sin \Theta) e^{-j\Omega} e^{j\pi/4} \quad (23)$$

To perform higher-order asymptotic evaluations, one approximates the slowly varying part of the kernel with a few terms of its Taylor series, and therefore one must differentiate the slowly varying term of the kernel.<sup>14</sup> This is trivial for the kernel in (19) when  $\zeta = \pi/2$  because the derivatives of  $s_m(\zeta)$  and  $s_k(\zeta)$  drop out in view of the vanishing of the  $\cos^2(\zeta)$  term. This fact was used to derive the approximation in (23) for  $\zeta \approx \pi/2$ . A thorough test of (21)–(23) has been performed

for a wide range of strip widths and separations. It has been found that these expressions give good agreement with the numerical evaluation of (14) and (15) for strip separations greater than  $0.1\lambda_0$ . As an example, a comparison between the asymptotic expressions and numerical integration is presented in Figure 2 for  $I_{73}^{\text{TM}}$ . Good agreement is seen over the entire bandwidth. Likewise, results for the induced currents and scattered fields computed from (21)–(23) in both the time and frequency domains were found to be in nearly complete agreement with results calculated by the numerical integration of (14) and (15) (less than 1 per cent difference). As a practical matter, it should be pointed out that one must use L'Hopital's rule for  $k_0 \sin \Theta = \pm k\pi/W$  to get good agreement over the entire bandwidth.

In summary, use of the asymptotic expressions to replace strictly numerical procedures results in a tremendous reduction in CPU time when considering UWB plane wave scattering from a

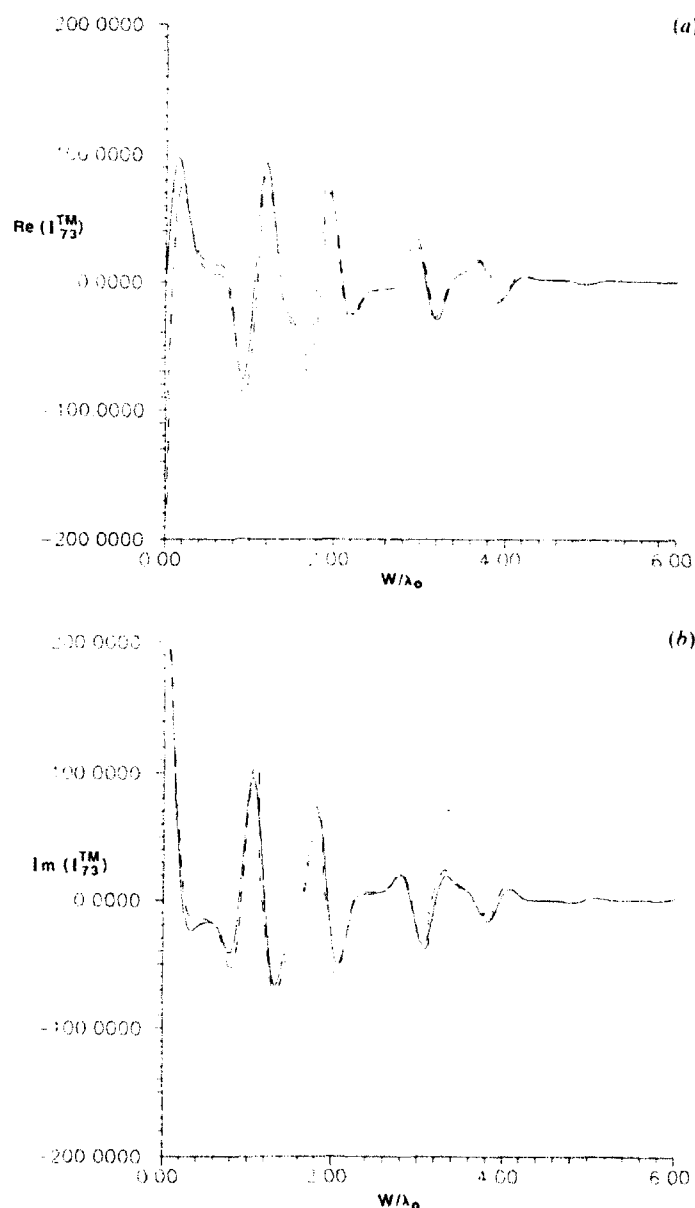


Figure 2. Real and imaginary parts of  $I_{73}^{\text{TM}}$  v.  $W/\lambda_0$ , where  $\lambda_0 = 2\pi/k_0$  is the free space wavelength, and the strip separation equals the strip width  $W$ . The solid line represents the numerical evaluation of (15) while the dashed line represents the asymptotic approximation. (a) Real part. (b) Imaginary part

collection of strips. This is true especially when the expansion and testing functions are separated by a wavelength or more. The accuracy of the asymptotics, as confirmed by comparison between the numerical and asymptotic evaluations of the integrals, is achieved only when the trigonometric parts of the spectral basis functions are grouped with the exponential functions. This is because the trigonometric parts of the spectral basis functions may have variations equal to, or greater than, those of the exponential functions; therefore, they must be combined with the rapidly varying parts of the integrands when applying asymptotics.

### 3.3. Integration along SDP

For expansion and testing functions separated by less than  $0.1\lambda_0$ , the asymptotic forms in (21)–(23) are less accurate and another efficient means of evaluating (14) and (15) is required. For such cases, (14) and (15) are evaluated numerically along the SDP.<sup>14</sup> Although this is obviously more time-consuming than evaluation of the closed form expressions (21)–(23), it is more efficient than performing the integral along the real  $k_x$  axis.

### 3.4. Self term

The above-mentioned techniques are useful for expansion and testing functions separated in space, and hence associated with different strips. For the self terms, however, the expansions and testing functions occupy the same strip and are therefore not spatially separated ( $\Delta_x = \Delta_y = 0$ ). Again (14) and (15) can be reduced to a sum of integrals of the form in (16) and (17), respectively. However, since  $\Delta_x = \Delta_y = 0$ , (21)–(23) are not valid for  $n = 0$  or for  $W < 0.1\lambda_0$ . In a related problem, it has been demonstrated that integrals of the form (14) and (15) vary slowly with frequency when  $\Delta_x = \Delta_y = 0$ .<sup>9</sup> This can be understood by realizing that the self terms sample essentially the near fields of the expansion function, and the near fields generally vary less strongly with frequency than their far-field counterparts.

UWB scattering requires very fine sampling of the frequency spectrum in order to furnish accurate time-domain results. Realizing that (14) and (15) vary slowly with frequency for  $\Delta_x = \Delta_y = 0$ , the self terms' integrals need be computed only at points along a relatively coarse frequency grid. The values of the integral between points along the coarse grid can be computed accurately by use of a simple extrapolation procedure.<sup>9</sup> This technique of computation for the self terms over an ultra-wide bandwidth has been applied in the results to be presented subsequently, and it leads to significant reduction in CPU time.

### 3.5. Summary of integration techniques

In summary, for expansion and testing functions separated in space by  $0.1\lambda_0$  or more, the asymptotic expressions (21)–(23) are used for the computation of the reaction integrals. For expansion and testing functions separated in space by less than  $0.1\lambda_0$ , numerical integration is performed along the SDP. The expressions (21)–(23) require virtually no CPU time; the integration along the SDP is very efficient and less time-consuming than real axis integration. The time-consuming part of the algorithm for UWB applications involves the computation of the self terms. Realizing, however, that these integrals vary slowly with frequency, the self terms are computed only at points along a relatively coarse frequency grid. All self term integrals at frequency points between the grid points are efficiently computed using linear extrapolation. It should also be noted that due to reciprocity, there are many redundant integrals in the moment method matrix. Taking advantage of this redundancy and using the integration techniques summarized above, UWB pulsed plane wave scattering from a collection of conducting strips becomes tractable. It is believed that these and related techniques can be extended to other classes of UWB scattering problems.

## 4. INVERSION INTO THE TIME DOMAIN

In order to obtain accurate results for UWB pulsed plane wave scattering, it is necessary that a sufficiently large number of frequency-domain points be used before Fourier transforming into the time domain. The integrals which vary most rapidly with frequency will be those associated with the most widely separated expansion and testing functions. An estimate of the required number of frequency points required can therefore be found by examining (21)–(23). The term in these expressions having the most rapid variation with frequency is  $e^{-j\Omega}$ . Assume that  $L_1 = L_{\max}$  is the largest separation encountered in the problem under study, and that  $\omega_{\max}$  is the highest frequency component needed to resolve the incident pulse. The term  $e^{-jk_0 L_{\max}}$  will therefore range from 1 to  $e^{-jk_0 \max L_{\max}}$ , where  $k_0 \max$  is the free space wavenumber at  $\omega_{\max}$ . If  $N$  frequency points are taken per period of oscillation, then  $Nk_0 \max L_{\max}/2\pi$  frequency samples are required. Here is an example of what this implies: for  $L_{\max} = 0.3$  m,  $\omega_{\max} = 28.3$  rad/s (100 GHz), and  $N = 10$ , the frequency spectrum must be discretized from 0 to 100 GHz in 100 MHz increments. This explains why it is essential that the frequency-domain results be computed as efficiently as possible.

The above considerations apply only to time-domain quantities computed directly by the moment method procedure described earlier: the time-dependent currents. To compute the scattered field, other considerations are necessary. In the far-field approximation, the time-dependent scattered fields are computed from integrals of the form

$$E(x, y, t) = \int h(x, y, \omega) e^{-jk_0 r} e^{j\omega t} d\omega \quad (24)$$

where  $r$  is the distance from the centre of a given strip to the observation point  $(x, y)$ . The expression  $h(x, y, \omega)$  is a function of the surface currents which are properly described in the frequency domain by the discretization procedure discussed above. If the observation distance  $r$  from a given strip is larger than  $L_{\max}$  (as it usually will be), then  $e^{-jk_0 r}$  will vary more quickly than  $e^{-jk_0 L_{\max}}$ , and the frequency discretization may not be sufficient to describe the time-dependent scattered fields accurately. A very simple procedure can be used to overcome this difficulty. Equation (24) can be rewritten as

$$E_1(x, y, \gamma) = \int h(x, y, \omega) e^{j\omega \gamma} d\omega \quad (25)$$

where  $\gamma = t - r/c$ . The expression  $h(x, y, \omega)$  involves only the basis functions and the Green's function for observation of the fields on the surface of the strips. The discretization required to resolve  $E_1(x, y, \gamma)$  is the same as that required of the currents, and  $E(x, y, t)$  can be found easily by shifting  $E_1(x, y, \gamma)$  by a time  $r/c$ .

It should be noted that the far-field approximation will in general not be valid for significantly low-frequency components associated with a given incident pulse. However, pulses radiated by practical antennas often have a weakly excited low-frequency spectrum so that (25) remains applicable for scattered field evaluation in most observation regions of interest, including those relatively close to the array (but 'far' from each strip). All time-dependent fields in the present study have been computed using (25) in conjunction with the FFT.

## 5. RESULTS

## 5.1. Frequency domain

To the authors' best knowledge, there are no results in the literature for UWB pulsed scattering from a collection of strips. Therefore, to check the accuracy of the computer code, comparisons have been made with available frequency-domain results. For all frequency domain calculations, a total of 12 basis functions was used per strip. For TM and TE incidence, respectively, Figures

3(a) and 3(b) show the normalized currents induced on three coplanar strips by a normally incident plane wave ( $\theta_i = 0$ ). The strip widths and separations are  $\lambda_0/4$ . The calculations reveal good agreement with data computed by Cwik and Mittra.<sup>4</sup> It is of interest to examine how the trigonometric basis functions resolve the edge condition for the case of TE incidence. From Figure 3(b) it is seen that the calculated currents oscillate around the solution found when the edge condition is used in the basis functions<sup>15</sup> (dashed curve). As the number of trigonometric basis functions is increased on each strip, the oscillations become more closely confined around the dashed curve. Although, for the TE case, a large number of basis functions is required to obtain adequate convergence for the *currents*, it has been determined that 12 basis functions are sufficient to obtain convergence for the scattered *far fields* (to better than 1 per cent). Therefore, the far fields are not sensitive to the above discrepancies in the surface currents.

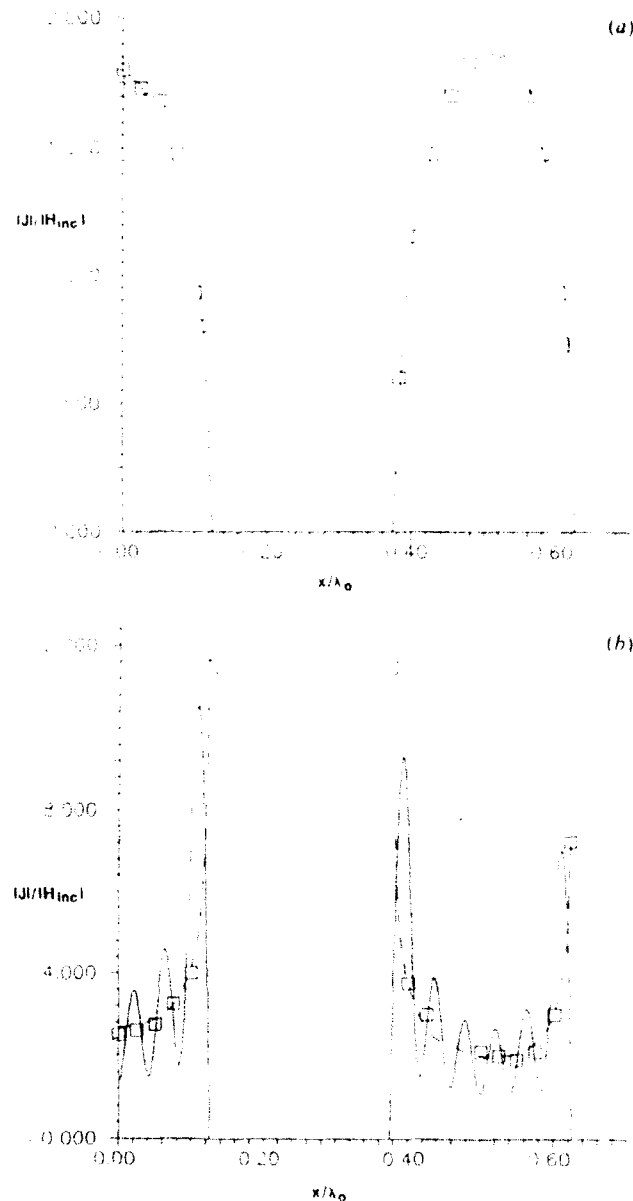


Figure 3. Normalized surface currents introduced by TM and TE plane waves incident vertically on three strips of strip width and separation equal to  $\lambda_0/4$ . The solid line represents the results of this work and the squares represent results from Reference 4. (a) TM polarization. (b) TE polarization. The dashed line was computed by including the edge condition in the basis functions<sup>15</sup>

Figures 4(a) and 4(b) show the scattered far field due to a TM and TE plane wave, respectively, incident at  $\theta_i = 60^\circ$  upon five coplanar strips. The strip widths are  $0.1\lambda_0$ , and the separation between consecutive strips is  $0.4\lambda_0$ . These results can be compared with data computed recently by Matsushima and Itakura (Figures 6(a) and 6(c)).<sup>5</sup> It is difficult to transfer the data accurately from the figures in Reference 5 (because of their small size), but excellent agreement is noted upon comparison. It is worth mentioning that the basis functions in Reference 5 for TE incidence satisfy the edge condition while those here do not. Nevertheless, the agreement between Figure 4(b) and the results in Reference 5 is excellent for all observation angles except very near  $\pm\pi/2$  (abrupt drop in the pattern of Figure 4(b)). The discrepancy over this very small range of observation angles, which may in fact be due to the edge condition deficiency of the basis functions in (10), does not detract from the utility of the algorithm employed here.

### 5.2. Time domain

To demonstrate the capabilities of the numerical code for UWB pulsed scattering from a large collection of strips, TE and TM scattering from 15 coplanar strips in free space has been considered. The strips each have width  $W$  and separation  $2W/3$ . The incident pulse, normalized to the width  $W$ , and its frequency spectrum are shown in Figure 5. All time-domain results are plotted as a function of  $\tau$ , where  $\tau$  is the time required by a plane wave to travel a distance  $W$  in free space. Note that the incident pulse has a temporal length shorter than  $\tau$  so that it is capable of resolving individual scattering from the strip edges.

The 15 coplanar strips are identified as follows: the centre strip is defined as strip 0, the seven strips to the right of the centre strip are labelled 1 to 7 from left to right, and the seven strips to the left of the centre strip are labelled  $-1$  to  $-7$  from right to left. The  $t = 0$  time reference is defined as the time when the incident pulse reaches the centre of strip 0. Figures 6(a) and 6(b) show the scattered fields produced by TM and TE plane waves, respectively, incident at an angle  $\theta_i = 20^\circ$ . The scattered fields are observed at a distance  $50W/3$  directly above the centre of strip 0, and the scattered field amplitude is normalized to the peak amplitude of the incident pulse. In addition, the left edge of each strip is labelled 'a', while the right edge is labelled 'b'. On each strip, the incident pulse will first hit edge 'b' and subsequently edge 'a'. In Figures 6(a) and 6(b), the travel time of a wavefront along a straight line from a given edge to the observation point is

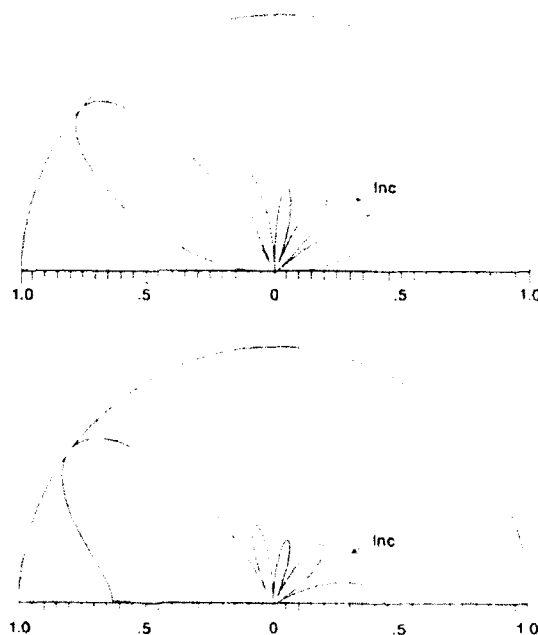


Figure 4. Normalized scattered far field due to TM and TE plane waves incident on five coplanar strips of width  $0.1\lambda_0$  and separation  $0.4\lambda_0$ . The waves are incident at  $\theta_i = 60^\circ$ . (a) TM polarization. (b) TE polarization

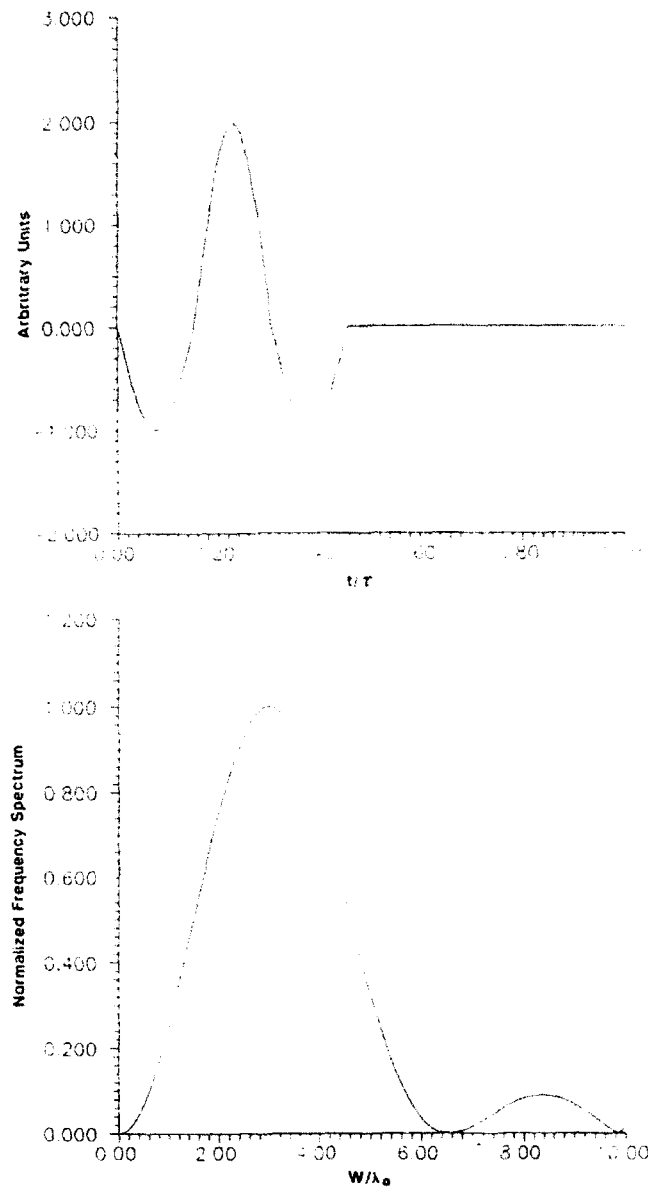


Figure 5. Incident plane wave pulse and its corresponding normalized frequency spectrum. (a) Pulse shape  $v. t/\tau$ , where  $\tau$  is the time required for a plane wave to travel a distance  $W$  (strip width) in free space. The pulse consists of three sections of a sine wave, with two lobes of equal amplitude 1 below the zero axis and one lobe of amplitude 2 above the zero axis. (b) Normalized frequency spectrum  $v. W/\lambda_0$ .

labelled for all strips to the left of centre. Note that as one moves further to the left along the strip array, the scattered pulses from individual edges become more distinct. It can be shown that for the chosen strip distribution and incidence angle, the scattered wavefronts from the edges of strips 0–7 arrive at the observer at nearly the same time; therefore, these signals are not individually resolvable. It is also interesting to note that the waveform scattered from a given edge is different for the TE and TM cases. For the TM case, the scattered field from edge 'b' is weaker than that from edge 'a', whereas the opposite is true for the TE case.

The coplanar strip array has two scales: the strip width and the strip separation. By considering the late-time response, and focusing on the time delays between the series of repetitive waveforms, one can develop a scheme by which these two scales of the scattering cells can be estimated from the data. The time delay between consecutive strong and weak signals gives information about

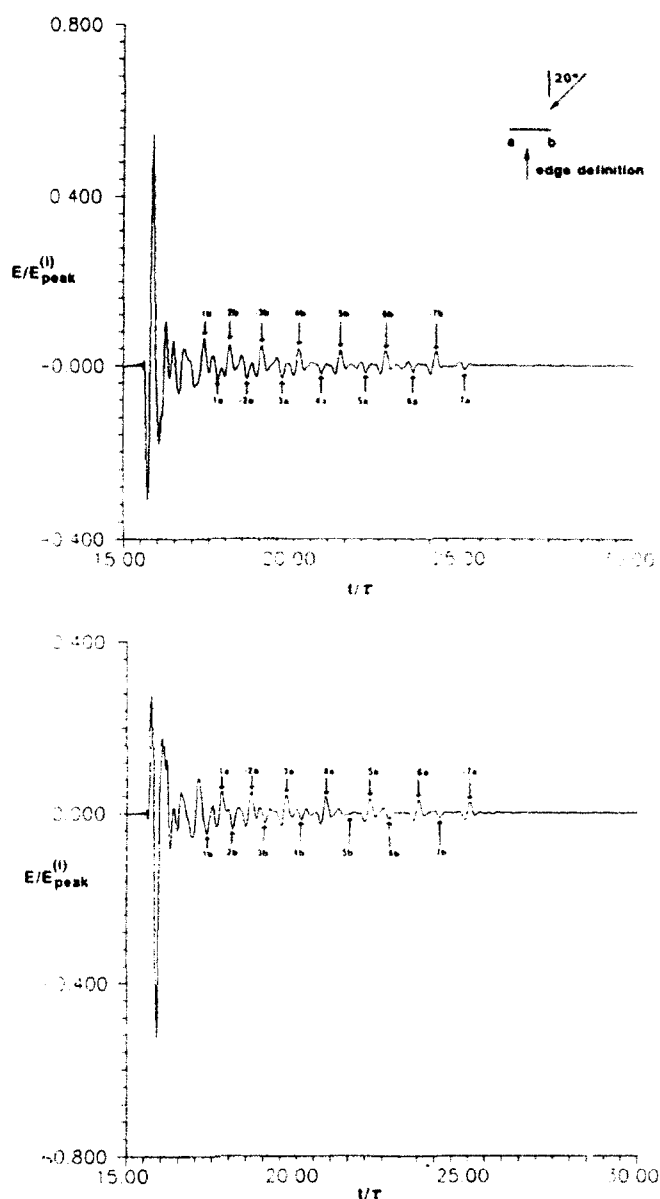


Figure 6. Time-dependent scattered fields due to TM and TE plane wave pulse in Figure 5, incident at  $\theta_i = 20^\circ$  upon 15 coplanar strips of equal width  $W$  and separation  $2W/3$ . The strips are labelled as follows: the centre strip is strip 0, the seven strips to the right of the centre strip are labelled 1 to 7 from left to right, and the seven remaining strips are labelled -1 to -7 from right to left. The left edge of each strip is labelled 'a', the right edge is labelled 'b'. The travel times, to the observer, of wavefronts from the edges of the seven strips to the left of the centre strip are identified by arrows. The time reference  $t = 0$  is the time at which the plane wave first hits the centre of strip 0, and the observation point is  $50W/3$  directly above the centre of strip 0. (a) TM polarization. (b) TE polarization

the strip width, while the time delay between consecutive large (or small) pulses gives information about the strip separation. It is believed that the insight gained from such simple investigations will be useful for understanding the scattering of UWB pulses from a more general class of scattering configurations. A detailed analysis and explanation of these and other results obtained with the present algorithm will be submitted separately for publication.<sup>16,17</sup>

Finally, some observations are made about the time-dependent surface currents induced on the strips. In Figures 7(a) and 7(b), respectively, are shown the induced currents on strip 0 for the TM and TE cases investigated in Figure 6. The currents are plotted as a function of time at three



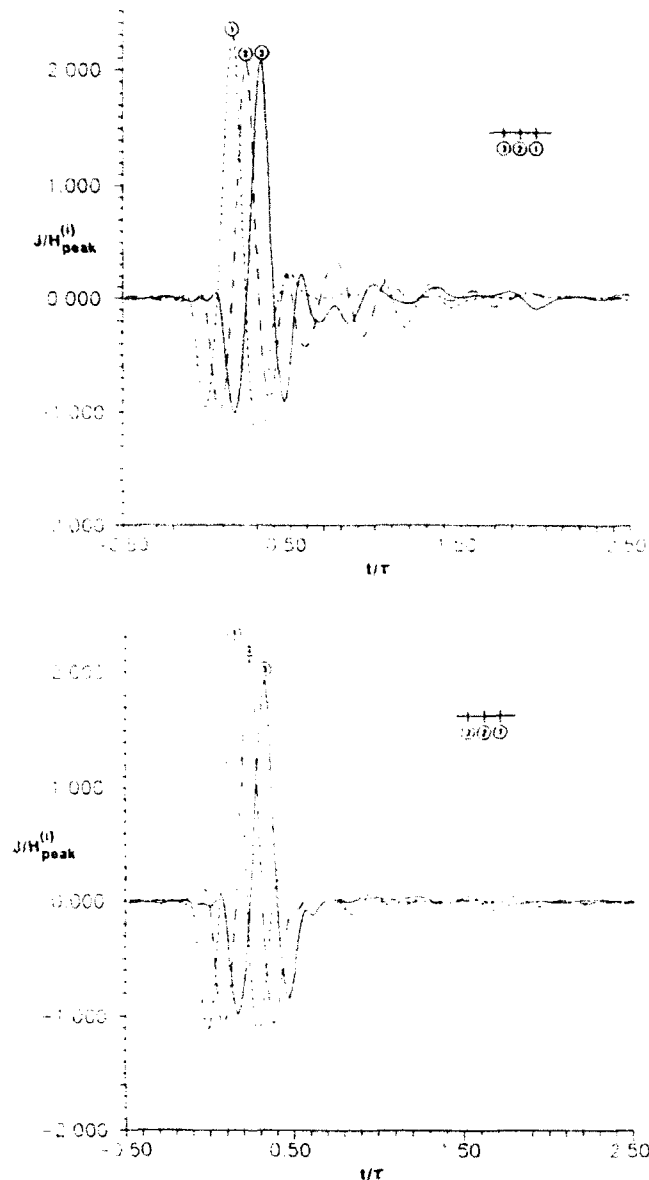


Figure 7. Time-dependent currents induced on the centre strip of the 15-strip array by the TM and TE pulsed plane waves in Figure 6. Curves 1, 2, and 3 are for positions  $x = W/4$ ,  $x = 0$ , and  $x = -W/4$ , respectively, on a strip of width  $W$  with centre at  $x = 0$ . (a) TM polarization. (b) TE polarization

locations along strip 0: at  $x = -W/4$ ,  $x = 0$ ,  $x = W/4$  (with the strip centre at  $x = 0$ ). The TM incident wave induces surface currents which propagate in the  $x$ -direction, and can therefore be expected to give rise to resonances between the strip edges. For the TE case, however, the induced currents are longitudinal ( $z$ -direction) and are therefore expected to interact less strongly between the strip edges. These expectations are confirmed upon examining Figures 7(a) and 7(b), where the late-time oscillations in the TM case are much more pronounced than in the TE case.

The 15-strip results above were computed on an IBM 6000 RISC workstation with 12 basis functions used per strip. The time-dependent data required calculations at 2500 frequency points (before inversion to the time domain), with results obtained after about 6.5 hours of CPU time (for an average of less than 10 CPU seconds per frequency point).

## 6. CONCLUSIONS

An efficient formulation has been developed for the analysis of UWB pulsed scattering from a large collection of planar strips in free space. By the spectral domain solution strategy, which has been summarized in section 3.5, closed-form asymptotic approximations have been derived for reaction integrals involving expansion and testing functions separated by greater than  $0.1\lambda_0$ . This, coupled with the extrapolation procedure used for the self terms, dramatically reduces CPU time and makes the analysis of UWB scattering tractable. The procedures developed in this paper have been applied to a broad parametric study of UWB scattering by different arrangements of strips, to various processing techniques of the time-domain data, and to direct and quantitative interpretation of the data by time-domain wave processes. These investigations will be published separately.<sup>16,17</sup> It is also intended to extend the algorithm discussed here to more complicated environments involving dielectric layers. The information gathered from these explorations may find use in the interpretation of UWB radar data from large periodic and quasi-periodic multi-scale environments, such as ocean waves.

## REFERENCES

1. T. R. Schimert, A. J. Brouns, C. H. Chan and R. Mittra, 'Investigation of millimeter-wave scattering from frequency selective surfaces', *IEEE Trans. Microwave Theory Tech.*, **39**, 315-322 (1991), and the references therein.
2. M. Born and E. Wolf, *Principles of Optics*, Macmillan, New York, 1964.
3. E. B. Treacy, 'Optical pulse compression with diffraction gratings', *IEEE J. Quantum Electron.*, **5**, 454-459 (1969).
4. T. Cwik and R. Mittra, 'The effects of the truncation and curvature of periodic surfaces: a strip grating', *IEEE Trans. Antennas Propagat.*, **36**, 612-622 (1988).
5. A. Matsushima and T. Itakura, 'Singular integral equation approach to electromagnetic scattering from a finite periodic array of conducting strips', *J. of Electromag. Waves Appl.*, **5**, 545-562 (1991).
6. W. A. Walker and C. M. Butler, 'A method for computing scattering by large arrays of narrow strips', *IEEE Trans. Antennas Propagat.*, **32**, 1327-1334 (1984).
7. L. Gurel and W. C. Chew, 'Recursive algorithms for calculating the scattering from N strips or patches', *IEEE Trans. Antennas Propagat.*, **38**, 507-515 (1990).
8. R. S. Vickers, 'Ultra-wideband radar—potential and limitations', *IEEE MTT-Symp. Dig.*, 371-374 (1991).
9. E. H. Newman and D. Forrai, 'Scattering from a microstrip patch', *IEEE Trans. Antennas Propagat.*, **35**, 245-251 (1987).
10. D. M. Pozar, 'Radiation and scattering from a microstrip patch on a uniaxial substrate', **35**, 613-621 (1987).
11. D. R. Jackson, 'The RCS of a rectangular microstrip patch in a substrate-superstrate geometry', *IEEE Trans. Antennas Propagat.*, **38**, 2-8 (1990).
12. S. S. H. Naqvi, 'A comment on the use of TE/TM polarization notation', *IEEE Trans. Antennas Propagat.*, **38**, 584 (1990).
13. R. F. Harrington, *Field Computation by Moment Methods*, Kreiger, Malabar, FL, 1982.
14. L. B. Felsen and N. Marcuvitz, *Radiation and Scattering of Waves*, Prentice Hall, Englewood Cliffs, NJ, 1972, Chs. 4 and 5.
15. E. G. Farr, C. H. Chan and R. Mittra, 'A frequency-dependent coupled-mode analysis of multiconductor microstrip lines with applications to VLSI interconnection problems', *IEEE Trans. Microwave Theory Tech.*, **34**, 307-310 (1986).
16. L. Carin and L. B. Felsen, 'Design oriented parametrization of finite periodic strip gratings', *IEEE Microwave and Guided Wave Letts.*, Sept. (1992).
17. L. Carin and L. B. Felsen, 'Time harmonic and transient scattering by finite periodic flat strip arrays: hybrid (ray) - (Foguet mode) - (MOM) algorithm and its GTD interpretation', submitted to *IEEE Trans. Antennas and Prop.*

## Authors' biographies:

**Lawrence Carin** was born in Washington, DC on 25 March 1963. He received the B.S., M.S., and Ph.D. degrees, all in electrical engineering, from the University of Maryland, College Park, in 1985, 1986, and 1989, respectively.

He is now an Assistant Professor with the Electrical Engineering Department at Polytechnic University. His present research interests include the analysis of electromagnetic waves in planar and quasi-planar structures, optoelectronics, and ultra-wideband electromagnetics.

Dr. Carin is a member of Tau Beta Pi and Eta Kappa Nu.

**Leopold B. Felsen** was born in Munich, Germany, on 7 May 1924. He received the B.E.E., M.E.E., and D.E.E. degrees from the Polytechnic Institute of Brooklyn, Brooklyn, N.Y., in 1948, 1950 and 1952, respectively.

During World War II he was concerned with work on electronic ballistics—calibration devices in the U.S. Army. Since 1948 he has been with Polytechnic Institute of Brooklyn, now Polytechnic University, and since 1978 he holds the position of Institute Professor, now renamed University Professor. From 1974 to 1978, he was Dean of Engineering. On a leave of absence during 1960-1961 he served as a Liaison Scientist with the London Branch of the Office of Naval Research. His research work has dealt with a variety of areas in electromagnetic radiation and diffraction theory, and his recent interest is centred primarily on general techniques for wave propagation in various disciplines, including optics, acoustics, mechanics of submerged

structures, and seismology, in addition to electromagnetics. He is author or co-author of more than 250 papers, and author or editor of several books. He has held visiting professorships at universities in the U.S. and abroad. In 1967, 1971, and 1988, he was in the Soviet Union as an invited guest of the Soviet Academy of Sciences, and in 1981, he was invited for a six-week stay to the People's Republic of China.

Dr. Felsen is a member of Eta Kappa Nu, Tau Beta Pi, Sigma Xi, and a Fellow of the Institute of Electrical and Electronic Engineers (IEEE), the Optical Society of America as well as the Acoustical Society of America. He is listed in numerous biographical volumes. He was an Associate Editor of *Radio Science*; he is now an Associate Editor of *Wave Motion* and an Editor of the *Wave Phenomena Series* of Springer-Verlag. In 1974, he was a Distinguished Lecturer for the IEEE Antennas and Propagation Society. He was awarded a Guggenheim Fellowship for 1973, the Balthasar van der Pol Gold Medal from URSI in 1975, an honorary doctorate from the Technical University of Denmark in 1979, a Humboldt Foundation Senior Scientist Award in 1981, an IEEE Centennial Medal in 1984, a Sackler Fellowship from Tel Aviv University in 1985, an IBM Visiting Fellowship from Northeastern University in 1990, and the IEEE Heinrich Hertz Medal for 1991. Also, awards have been bestowed on several papers authored or co-authored by him. In 1977, he was elected to the National Academy of Engineering. He has served as Vice-Chairman and Chairman of both the U.S. and the International URSI Commission B.

## CALCULATING FREQUENCY-DOMAIN DATA BY TIME-DOMAIN METHODS

M. DEHLER, M. DOHLUS AND T. WEILAND

*Technische Hochschule Darmstadt, Fachbereich 18, FG TEMF, Schloßgartenstraße 8, 6100 Darmstadt, Germany*

### SUMMARY

We show the derivation of parameters in the frequency domain from time-domain data. Far-field characteristics are obtained by a convolution formula with the harmonic field amplitudes, which are obtained via a Fourier transform or by sampling. The electric field of filter ports is expanded into the discrete eigenmodes. By this method, a monochromatic exact open boundary can be formulated and the fields divided into the incident and the reflected part. For wide band operation an *a posteriori* error correction scheme is presented.

### INTRODUCTION

The analysis of electromagnetic components can typically be subdivided into two tasks. First the mathematical problem is defined and solved yielding the electromagnetic fields as a function of one temporal and three spatial co-ordinates. The second task, we focus on in this paper, consists of reducing and filtering the result.

One common method of eliminating the time-dependency is to assume harmonic time-dependence. In the case of constant, time-invariant materials Maxwell's equations are decoupled for different frequencies and transform to quasistatic differential equations. Furthermore derived parameters such as wave amplitudes are used to describe the solution in order to obtain a formulation, which is analogous to a discrete network.

The direct solution of the frequency-domain problem using finite differences or similar methods has the following disadvantages. The equation system is complex and therefore twice as large as in the time domain. When calculating near-resonances the algebraic condition may become very bad. One has to eliminate the spurious, non-physical solutions. Also we have to repeat the solution process for each frequency.

The alternative is to calculate the time-domain response of the electromagnetic component and to derive the frequency-domain parameters. In the following we show the calculation of far-field transforms and scattering parameters with some applications. For the numerical solution, the finite integration algorithm for the spatial discretization in combination with a leapfrog scheme for the time integration was used.<sup>1,2</sup>

### FAR-FIELD CHARACTERISTICS

One disadvantage of finite difference and finite element methods is that all computations are restricted to a finite grid. Part of this problem can be overcome by introducing radiation boundary operators simulating an infinite mesh size. The direct calculation of far-field characteristics of, for example, antennas is still infeasible, since the grid has to be extended to distances, where the near fields have ebbed off.

Therefore we have to strip off the electromagnetic fields inside the grid of their near-field parts. The far field then can be written as

$$\mathbf{E}_{\text{far}}(r, \Theta, \Phi) = \frac{e^{-jkr}}{r} \mathbf{F}(\Theta, \Phi) \quad (1)$$

a plane wave in radial direction with the far-field transform  $\mathbf{F}(\Theta, \Phi)$  as the directional pattern.

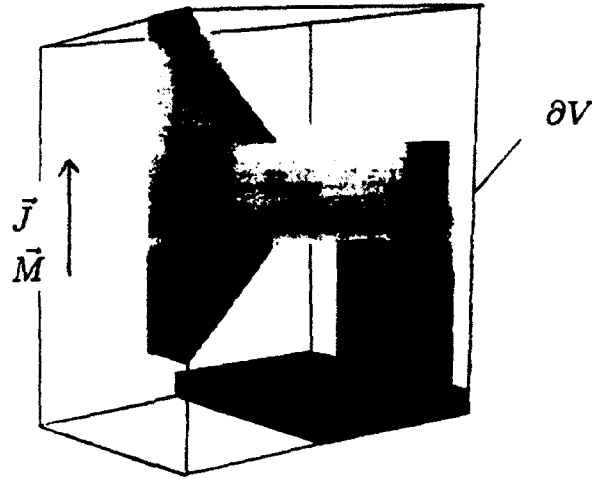


Figure 1. Integration surface around radiator

We include the radiating structure in a volume as shown in Figure 1 and substitute the radiating sources by equivalent electric and magnetic surface currents, given by the tangential electric and magnetic components along the surface. The far field can be calculated by convoluting the surface currents with the far fields of elementary electric and magnetic dipoles:<sup>1</sup>

$$\mathbf{F}(\Theta, \phi) = \frac{j\omega}{4\pi} \oint_{\partial V} e^{i\mathbf{r} \cdot \mathbf{r}'} \left\{ \mathbf{e}_r \times (\mathbf{r} \times (\mathbf{n} \times \mathbf{B})) - \frac{1}{c} \mathbf{e}_r \times (\mathbf{n} \times \mathbf{E}) \right\} dA \quad (2)$$

where  $\mathbf{n}$  is the normal to the integration surface,  $\mathbf{e}_r$  the normalized radiation vector and  $\mathbf{r}'$  the point of integration.  $\mathbf{E}$  and  $\mathbf{B}$  denote complex time harmonic electric and magnetic field amplitudes respectively.

The time harmonic field amplitudes can be obtained either by using a time harmonic excitation and sampling

$$\underline{\mathbf{E}} = \mathbf{E}(t_0) - j\mathbf{E}(t_0 + T/4) \quad (3)$$

$$\underline{\mathbf{B}} = \mathbf{B}(t_0) - j\mathbf{B}(t_0 + T/4) \quad (4)$$

( $T$  denotes the length of the harmonic period and  $t_0$  has to be a time, where the fields have reached their harmonic state), or by an on-line Fourier transform.

### FAR FIELD OF A CORRUGATED HORN

As an example we show the calculation of the far field of a corrugated horn. The structure shown in Figure 2 is rotationally symmetric and was calculated in  $rz$ -geometry using 65,000 mesh points.

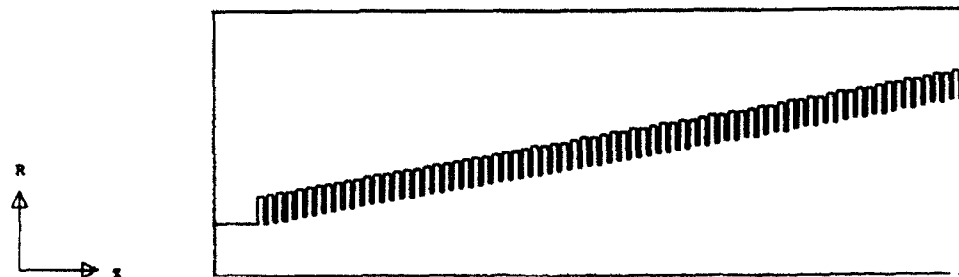


Figure 2. Geometry of the corrugated horn

As excitation a pulsed sine wave was used. The geometrical parameters, normed with the design frequency  $k_0 = \omega_0/c$ , are

inner diameter of waveguide	$bk_0$	3.25
steepness	$\theta$	$10^\circ$
number of grooves	$N$	72
depth of the grooves	$t/\lambda_0$	0.27
distance between two grooves	$l_p/\lambda_0$	0.1
width of the grooves	$l_r/\lambda_0$	0.067

Figure 3 shows the time response of the radial field on the horn axis. The time harmonic fields were calculated by a Fourier transform.

Figure 4 shows the far-field transform in a polar plot and Figure 5 in a logarithmic scale. For comparison the results calculated by R. Erb<sup>6</sup> by a mode-matching technique are drawn as a dashed line. Both results show good agreement except near 90 degrees. This is due to a different modelling. R. Erb assumed radiation into a halfspace with an infinitely conducting screen, whereas here a finite structure was calculated.

### SCATTERING PARAMETERS

When describing multiports, we have discrete ports and a discrete spectrum of eigenmodes which set up the field inside the waveguides connecting the multiport to other components. So we use a scattering matrix

$$[\underline{b}_1(j\omega) \underline{b}_2(j\omega) \dots \underline{b}_n(j\omega)]^t = S [\underline{a}_1(j\omega) \underline{a}_2(j\omega) \dots \underline{a}_n(j\omega)]^t \quad (5)$$

to describe the relationship between incoming and reflected wave amplitudes.

The transverse electromagnetic fields are described in the frequency domain by a superposition of incoming and reflected waves

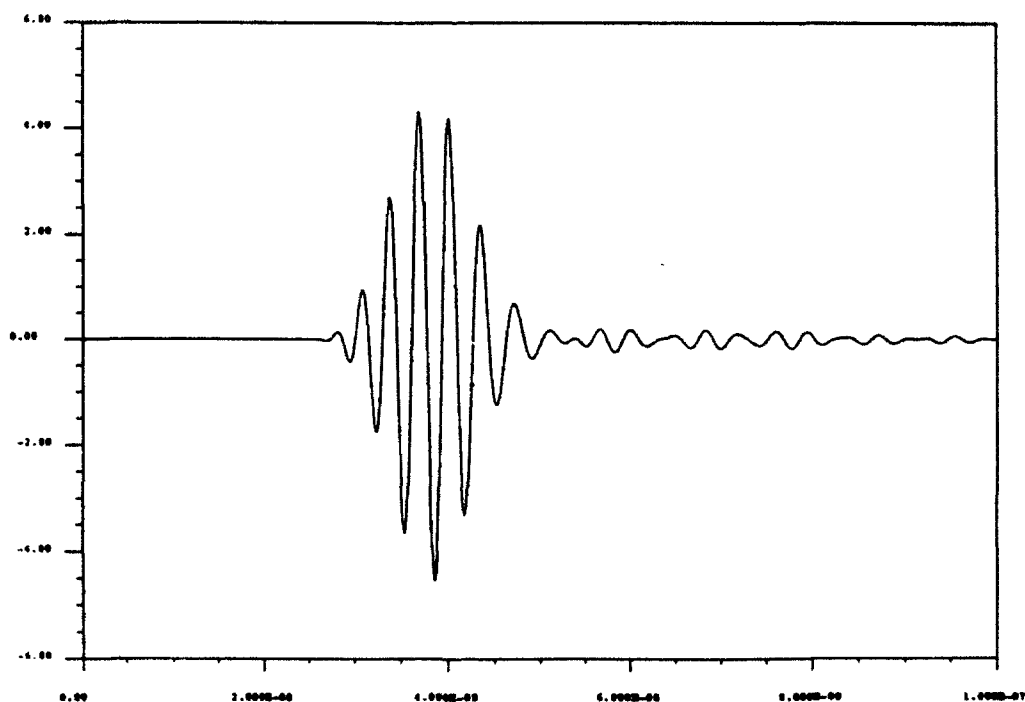


Figure 3. Field in the horn aperture v. time

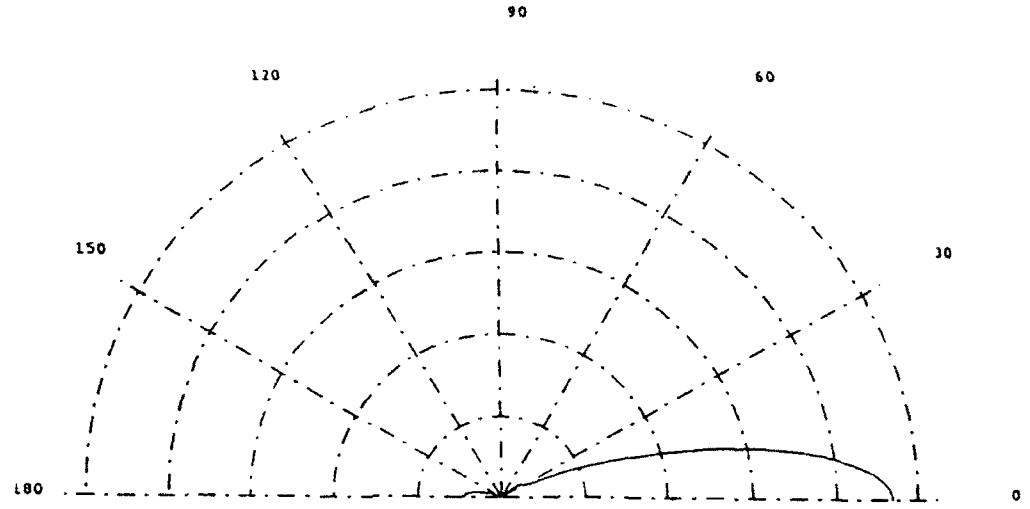


Figure 4. Polar plot of the far field (E-plane)

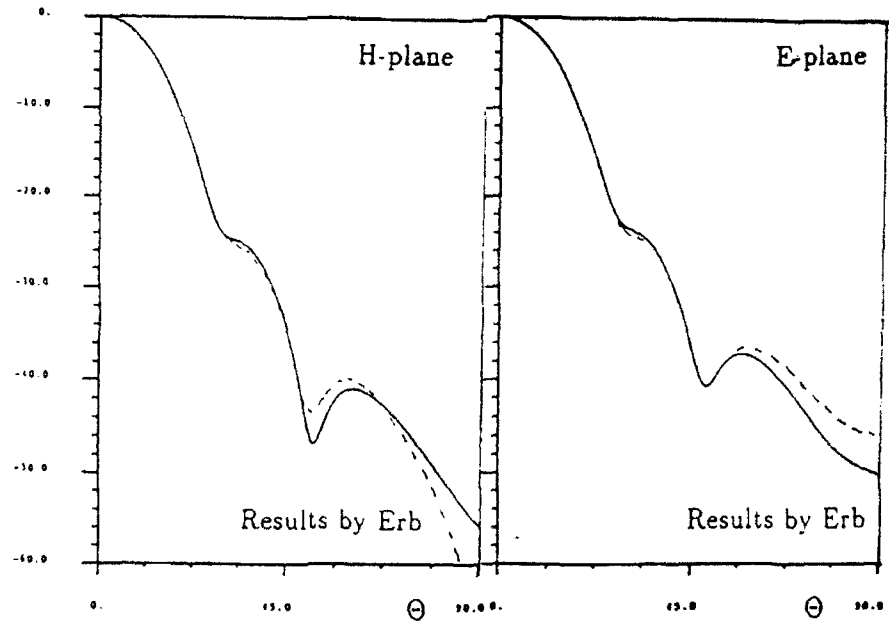


Figure 5. Logarithmic plot of far field (dashed line results by R. Erb)

$$\mathbf{E}(\mathbf{r}, \omega) = \sum_v \frac{\mathbf{E}_v(x, y, j\omega)}{f_v(j\omega)} [a_v(j\omega)e^{-\gamma_v(j\omega)z} + b_v(j\omega)e^{\gamma_v(j\omega)z}] \quad (6)$$

with the real power normalization factor

$$f_v(j\omega) = \sqrt{\iint |\mathbf{E}_v(x, y, j\omega) \times \mathbf{H}_v^*(x, y, j\omega)| dA} \quad (7)$$

For the further derivation we use the weighted wave parameters  $\tilde{a}_v(j\omega) = a_v(j\omega)/f_v(j\omega)$ ,  $\tilde{b}_v(j\omega) = b_v(j\omega)/f_v(j\omega)$  and formulate the time-domain equation

$$\mathbf{E}(\mathbf{r}, t) = \sum_v \mathbf{E}_v(x, y, t) * [\tilde{a}_v(t) * P_v(t, z) + \tilde{b}_v(t) * P_v(t, -z)] \quad (8)$$

with a double convolution. The frequency dependencies have been replaced by time dependencies and

$$P_v(t, z) = \frac{1}{2\pi} \int_{-\infty}^{\infty} e^{-\gamma_v(j\omega)z} e^{j\omega t} d\omega \quad (9)$$

describes the waveguide propagation. In homogeneously filled waveguides we can find frequency-independent transverse fields  $\underline{\mathbf{E}}_v(x, y)$  that are orthogonal.

With this in mind we look at the following model of a transmission line (Figure 6).  $z = 0$  denotes the outermost grid line at the waveguide port,  $z = \delta z$  is the grid line one step inside and  $A(t)$  and  $B(t)$  are the transverse electromagnetic fields. Both can be expanded in terms of the discrete two-dimensional eigenmodes ( $A_v(t)$ ,  $B_v(t)$ ). The coefficients are composed of an incident and a reflected wave amplitude:

$$z = 0 : \underline{A}_v(j\omega) = \underline{a}_v(j\omega) + \underline{b}_v(j\omega) \quad (10)$$

$$z = \delta z : \underline{B}_v(j\omega) = \underline{a}_v(j\omega) \underline{P}_v(j\omega)^{-1} + \underline{b}_v(j\omega) \underline{P}_v(j\omega) \quad (11)$$

with

$$\underline{P}_v(j\omega) = e^{-\gamma_v(j\omega)\delta z} \quad (12)$$

We can realize boundary conditions, that are exact for at least one frequency  $\omega_M$  when we approximate the propagation filter  $\underline{P}_v(j\omega)$  by a recursive digital filter  $\underline{P}'_v(j\omega)$  similar to classic open boundaries<sup>4,5</sup> with  $\underline{P}_v(j\omega_M) = \underline{P}'_v(j\omega_M)$ . With this filter we write analogue equations for the approximated wave amplitudes

$$z = 0 : \underline{A}_v(j\omega) = \underline{a}'_v(j\omega) + \underline{b}'_v(j\omega) \quad (13)$$

$$z = \delta z : \underline{B}_v(j\omega) = \underline{a}'_v(j\omega) \underline{P}'_v(j\omega)^{-1} + \underline{b}'_v(j\omega) \underline{P}'_v(j\omega) \quad (14)$$

and formulate a recursion for the unknown reflected amplitude

$$\tilde{b}'_v(t) = P'_v(t) * [B_v(t) - P'_v(t) * \tilde{a}'_v(t)] \quad (15)$$

The quality of the boundary condition is determined by the filter approximation, but we can calculate the true (weighted) wave amplitudes  $\underline{a}_v(j\omega)$ ,  $\underline{b}_v(j\omega)$  in a correction step after the time-domain field calculation. The amplitudes  $\underline{A}_v(j\omega)$ ,  $\underline{B}_v(j\omega)$  have a real physical meaning, so it is possible to substitute them in the above equations to yield the following relationship

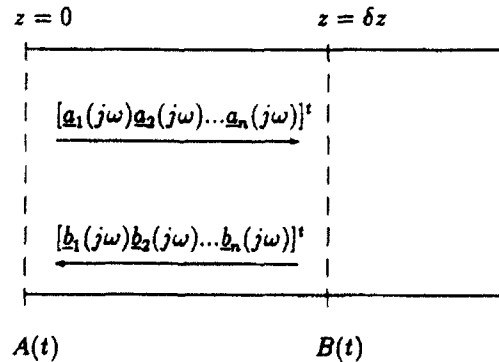


Figure 6. Model of a transmission line



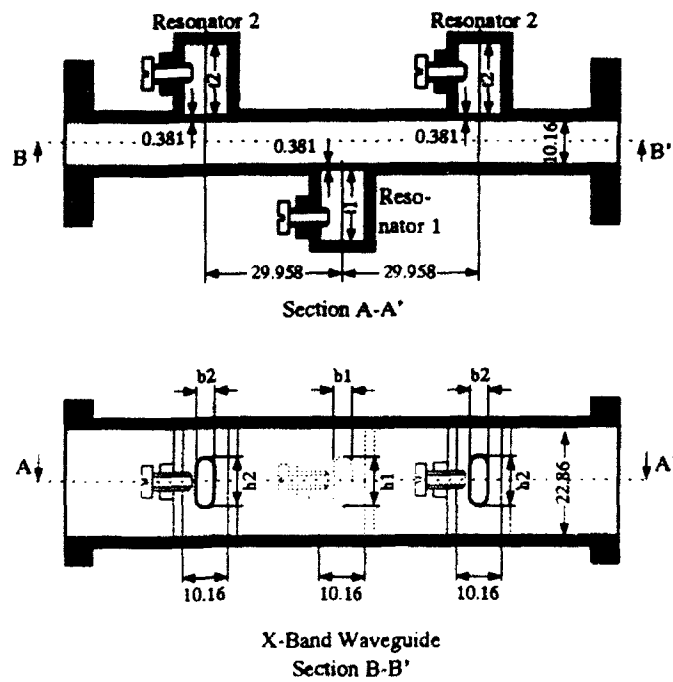


Figure 7. Geometry of the waveguide band-stop filter

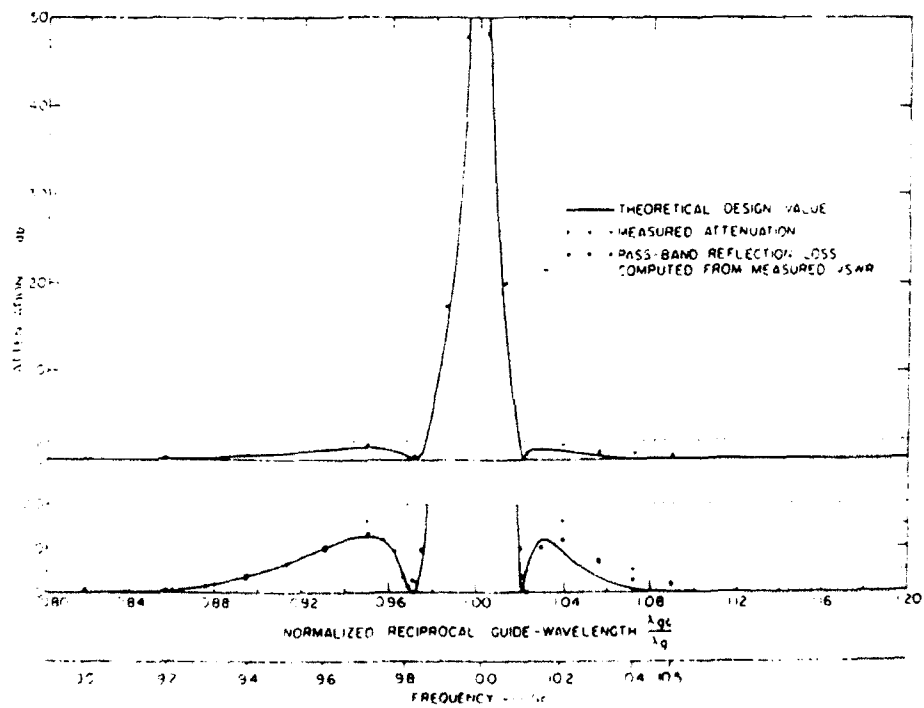


Figure 8. Measured transmission

$$\begin{bmatrix} \underline{a}_v(j\omega) \\ \underline{b}_v(j\omega) \end{bmatrix} = f_v(j\omega) \begin{bmatrix} 1 & 1 \\ \underline{P}_v(j\omega)^{-1} & \underline{P}_v(j\omega) \end{bmatrix}^{-1} \begin{bmatrix} 1 & 1 \\ \underline{P}'_v(j\omega)^{-1} & \underline{P}'_v(j\omega) \end{bmatrix} \begin{bmatrix} \underline{a}'_v(j\omega) \\ \underline{b}'_v(j\omega) \end{bmatrix} \quad (16)$$

By this technique one can calculate a set of vectors  $[\underline{a}_1(j\omega) \ \underline{a}_2(j\omega) \dots \underline{a}_n(j\omega)]^t$  and  $[\underline{b}_1(j\omega) \ \underline{b}_2(j\omega) \dots \underline{b}_n(j\omega)]^t$  for different stimulations  $[\underline{a}'_1(j\omega) \ \underline{a}'_2(j\omega) \dots \underline{a}'_n(j\omega)]^t$  to solve the scattering matrix  $S$ .

### BAND-STOP FILTER

As an example the results calculated for a waveguide band-stop filter operating in the X-band are shown in Figure 7. In Figure 8 we have the measured and in Figure 9 the calculated transmission.<sup>7</sup> For comparison, results calculated by a mode-matching technique are drawn in with a dashed line.<sup>8</sup>

For a better estimation of the error the curves are shown in Figure 10 using a range of transmission from 0 to -5 dB. It can be clearly seen, that the results agree within 0.15 dB.

### CONCLUSIONS

In this paper we have presented two methods of deriving frequency-domain results from time-domain data. Far-field characteristics are calculated by applying a convolution to the tangential time harmonic electromagnetic components on the surface of the radiator. These fields can be either sampled, using a monochromatic excitation, or obtained via a Fourier transform.

For the calculation of scattering parameters, we perform a mode expansion of the electromagnetic fields inside the ports. The modal coefficients can be used to obtain an exact open boundary when using narrow-band signals and contain all information of incident and reflected wave amplitudes. The systematic error introduced due to the inexact open boundaries in a wide band range can be compensated by an *a posteriori* error-correction scheme.

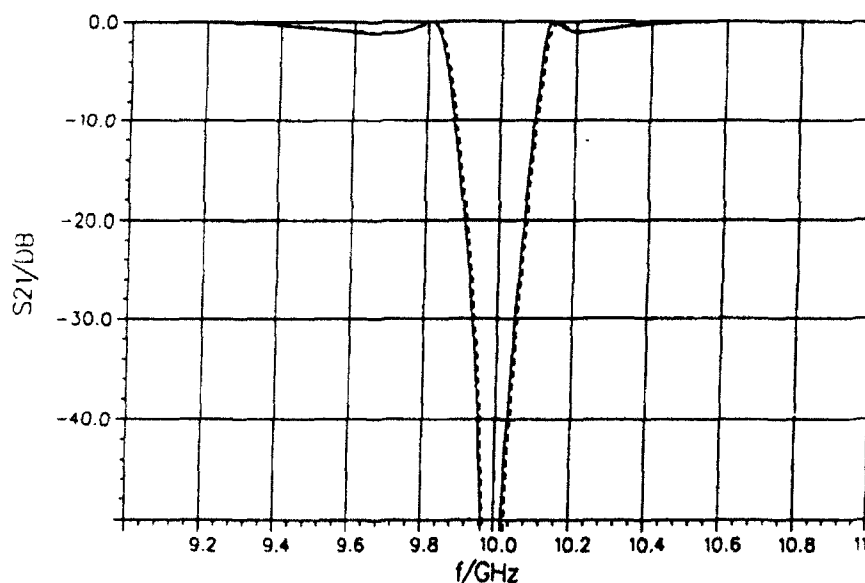


Figure 9. Calculated transmission (dashed line results obtained by mode matching)

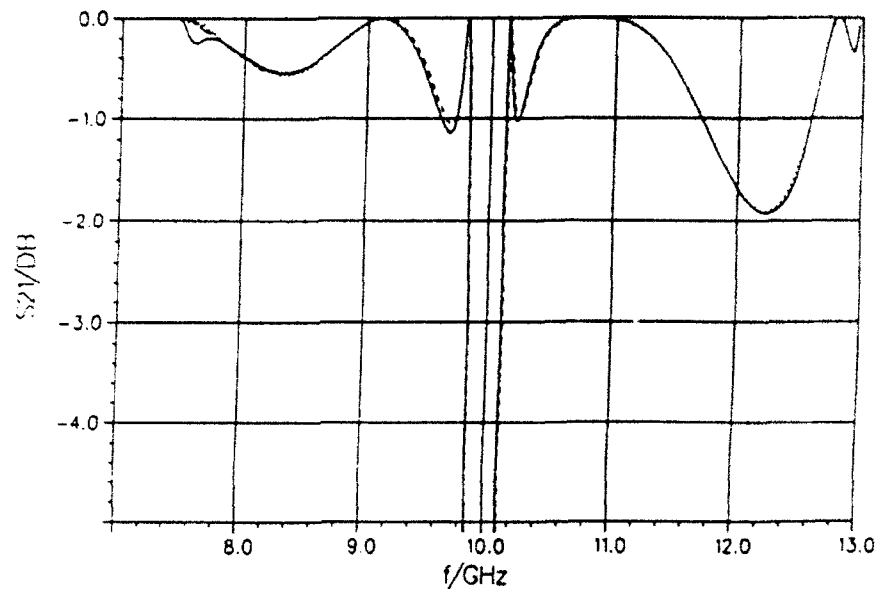


Figure 10. Calculated transmission (dashed line results obtained by mode matching)

#### REFERENCES

1. K. S. Yee, 'Numerical solution of initial boundary value problems involving Maxwell's equations in isotropic media', *IEEE, AP-14*, 302-307 (1966).
2. Th. Barts, J. Browman, R. K. Cooper, M. Dehler, M. Dohlus, F. Ebeling, A. Fischerauer, G. Fischerauer, P. Hahne, R. Klatt, F. Krawczyk, M. Marx, T. Pröpper, G. Rodenz, D. Rusthoi, P. Schütt, B. Steffen, T. Weiland and S. G. Wipf, 'Maxwell's grid equations', *Frequenz*, **44**, 9-16 (1990).
3. K. Umashankar and A. Taflov, 'A novel method to analyze electromagnetic scattering of complex objects', *IEEE, EMC-24*, 397-405 (1982).
4. G. Mur, 'Absorbing boundary conditions for the finite-difference approximation of the time-domain electromagnetic-field equations', *IEEE, EMC-23*, 377-382 (1981).
5. T. Moore, J. Blaschek, A. Taflov and G. Kriegsmann, 'Theory and application of radiation boundary operators', *IEEE, AP-36*, 1797-1805 (1988), and references therein.
6. R. Erb, 'Systematische Untersuchung mathematischer Modelle zur Berechnung rotationssymmetrischer Rillenhornstrahler', *Fortschr.-Ber. VDI-Reihe 21*, No. 33, VDI-Verlag (1988).
7. L. Young, G. L. Matthaei, E. M. T. Jones, 'Microwave band-stop filters with narrow band stops', *IRE, MTT-10*, 416-427 (1962).
8. B. Geib., Personal communication.

#### Authors' biographies:

**J. Martin Dohlus** was born in Erlangen, Germany in 1957. He received the Dipl.-Ing. degree in electrical engineering from the Universitaet Erlangen, in 1985. Since 1989, he has been working at the Technische Hochschule Darmstadt. His present research interests are in the areas of applications of numerical field calculations, especially in hyperthermia.



**Thomas Weiland**, born in 1951, studied electrical engineering and mathematics at the Technische Hochschule Darmstadt. In 1977 he received his Ph.D. In his thesis he worked out a finite difference method in the frequency domain and applied it to loss-free and lossy waveguide mode computation, which resulted in unique solutions, *a priori* free of spurious modes.

As fellow at the European Institute for Nuclear Research (CERN, Switzerland) he continued his work on electromagnetic computing extending Yee's algorithm to include fields of moving charges.

At the Deutsches Elektronen Synchrotron DESY in Hamburg he founded in 1983 an international collaboration for three-dimensional electromagnetic simulation. The software package, called MAFIA, which resulted from this collaboration, has been in use since 1984, in 22 countries, and was the first widely distributed 3D code for radio-frequency field simulation.

In 1984 he published a basic paper on the matrix formulation of Maxwell's equations and the uniqueness of numerical solutions. His formulation of Maxwell's equations as a set of matrix equations forms the basis

for a program package which can solve virtually any electromagnetic field problem starting from statics, high-frequency fields and transient fields up to time-domain problems, including free-moving charges.

For his contributions to the field of scientific computing he received in 1986 the 'Physics Prize' of the German Physical Society, the 'Prize for Achievements in Accelerator Physics and Technology' of the US Particle Accelerator School and the 'Leibniz Prize' from the German Research Association in 1987.

His work on electromagnetic simulation was always connected with practical work on accelerators. He was involved in designing and running the forefront high-energy physics accelerators such as LEP in CERN and HERA at DESY.

Since 1989 he has been a full professor at the Technische Hochschule Darmstadt, Germany, and head of the department of 'Theory of Electromagnetic Fields'.



**Micha Dehler** was born in Neuendettelsau, Germany in 1963. From 1984 to 1989 he studied electrical engineering at the Technische Hochschule Darmstadt, where he finished with the Dipl.-Ing. degree. Since 1989 he has been working there in the department of 'Theory of Electromagnetic Fields' towards his doctoral degree.

His main research interest is electromagnetic field theory, with emphasis on numerical modelling and simulation.

## THE HILBERT SPACE FORMULATION OF THE TLM METHOD

PETER RUSSER AND MICHAEL KRUMPHOLZ

*Lehrstuhl für Hochfrequenztechnik, Technische Universität München, Arcisstrasse 21, D-8000 Munich 2, Germany*

### SUMMARY

The Hilbert space representation of the TLM method for time-domain computation of electromagnetic fields and the algebraic computation of the discrete Green's function are investigated. The complete field state is represented by a Hilbert space vector. The space and time evolution of the field state vector is governed by operator equations in Hilbert space. The discrete Green's functions may be represented by a Neumann series in space- and time-shift operators. The Hilbert space representation allows the description of the geometric structures by projection operators, too. The system of difference equations governing the time evolution of the electromagnetic field in configuration space is derived from the operator equation for the field state vector in the Hilbert space.

### 1. INTRODUCTION

The TLM (transmission line matrix) method developed and first published in 1971 by Johns and Beurle is a discrete time-domain method for electromagnetic field computation.<sup>1-3</sup> In this paper, the Hilbert space representation of the TLM method is presented and applied to the algebraic computation of discrete Green's functions. The Hilbert space representation is a very general and powerful concept in field theory.<sup>4</sup> Whereas in the electromagnetic theory Hilbert space methods are mainly used for solving the field equations, as, for example, in the moment method,<sup>5</sup> in quantum theory, the fundamental theoretical concepts have been formulated in Hilbert space.<sup>6,7</sup>

The state of a discretized field can be represented by a vector in the Hilbert space. The specification of the mesh node connections and the boundary conditions is done by operators in the Hilbert space. The Hilbert space representation also allows the description of geometric structures by projection operators. The space and time evolution of the field state vector is governed by operator equations.

In field theory, field propagation in spatial domains may be treated using Green's functions.<sup>8</sup> The concept of Green's functions may also be applied to discrete time-domain field computation.<sup>9</sup> Discrete time-domain Green's functions allow the modelling of the relation between the field values on the boundaries if knowledge of the field in the spatial domains beyond the boundaries is not required.

In this paper, the algebraic computation of the discrete Green's function is investigated. Our approach is based on a Hilbert space representation of the space- and time-discretized electromagnetic field. The discrete Green's functions may be represented by a Neumann series in space- and time-shift operators. The system of difference equations governing the time evolution of the electromagnetic field in configuration space is derived from the operator equation for the field state vector in the Hilbert space. First results are presented for the two-dimensional case.

### 2. THE TWO-DIMENSIONAL TLM METHOD

The electromagnetic field is discretized within space and time. The space is modelled by a mesh of transmission lines connecting the sample points in space. The field computation algorithm consists of two steps:

- The propagation of wave pulses from the mesh nodes to the neighbouring nodes.
- The scattering of the wave pulses in the mesh nodes.

In the following, we restrict our considerations to the two-dimensional case with the transverse electric field. In the shunt TLM model, voltage wave amplitudes are used instead of total voltage and current. The voltage wave amplitudes of the incident and the reflected waves are given by  ${}_k a_{m,n}$  and  ${}_k b_{m,n}$ . The left index,  $k$ , denotes the discrete time co-ordinate and the right indices,  $m$  and  $n$ , denote the two discrete space co-ordinates. We consider the TLM mesh to be composed by elementary TLM shunt node four-ports as shown in Figure 1, where each of the four arms is of length  $\Delta l/2$ . The scattering in this elementary four-port is connected with the time delay  $\Delta t$ .

The scattering of the wave pulses is described by

$$\begin{bmatrix} b_1 \\ b_2 \\ b_3 \\ b_4 \end{bmatrix}_{k+1, m, n} = S \begin{bmatrix} a_1 \\ a_2 \\ a_3 \\ a_4 \end{bmatrix}_{k, m, n} \quad (1)$$

with the scattering matrix  $S$  given by

$$S = \begin{bmatrix} -\frac{1}{2} & \frac{1}{2} & \frac{1}{2} & \frac{1}{2} \\ \frac{1}{2} & -\frac{1}{2} & \frac{1}{2} & \frac{1}{2} \\ \frac{1}{2} & \frac{1}{2} & -\frac{1}{2} & \frac{1}{2} \\ \frac{1}{2} & \frac{1}{2} & \frac{1}{2} & -\frac{1}{2} \end{bmatrix} \quad (2)$$

With the scattering, a time delay of  $\Delta t$  is associated and therefore, the time index,  $k$ , is incremented by one. The scattered pulses are the incident pulses of the neighbouring elementary cell. This is described by

$$\begin{aligned} {}_{k+1} a_{1, m, n} &= {}_k b_{2, m-1, n} \\ {}_{k+1} a_{2, m, n} &= {}_k b_{1, m+1, n} \\ {}_{k+1} a_{3, m, n} &= {}_k b_{4, m, n-1} \\ {}_{k+1} a_{4, m, n} &= {}_k b_{3, m, n+1} \end{aligned} \quad (3)$$

### 3. THE DISCRETE FIELD STATE SPACE

In the TLM model, the field state at a given discrete time is described completely by specifying the amplitudes of the four wave pulses incident to each mesh node. The space of the voltage wave amplitudes of the incident and the reflected waves  ${}_k a_{l, m, n}$  and  ${}_k b_{l, m, n}$  is the four-dimensional real

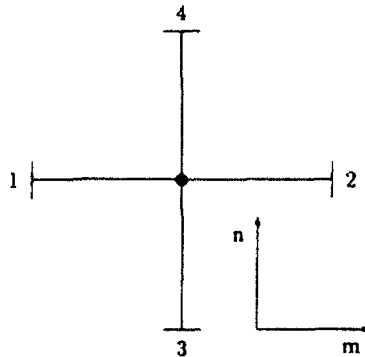


Figure 1. A two-dimensional TLM shunt node four-port

vector space  $\mathcal{R}^4$ . In order to develop our formalism in a more general way we introduce the four-dimensional complex vector space  $\mathcal{C}^4$  for representing the wave amplitudes  ${}_k a_{m,n}$  and  ${}_k b_{m,n}$ .

In order to describe the whole mesh state, we introduce the Hilbert space  $\mathcal{H}_m$  which allows the mapping of each mesh node onto an orthonormal set of base vectors of  $\mathcal{H}_m$ . The time states are represented by the Hilbert space  $\mathcal{H}_t$ . With each pair of discrete spatial co-ordinates  $(m,n)$  a basis vector of  $\mathcal{H}_m$  is associated and with each  $k$ , a basis vector of  $\mathcal{H}_t$  is associated. We now introduce the state space  $\mathcal{H}$  given by the Cartesian product of  $\mathcal{C}^4$ ,  $\mathcal{H}_m$  and  $\mathcal{H}_t$ .

$$\mathcal{H} = \mathcal{C}^4 \otimes \mathcal{H}_m \otimes \mathcal{H}_t \quad (4)$$

The space  $\mathcal{H}$  is a Hilbert space, too. The complete time evolution of the field state within the whole three-dimensional space-time may now be represented by a single vector in  $\mathcal{H}$ . Using the bra-ket notation introduced by Dirac,<sup>6</sup> the orthonormal basis vectors of  $\mathcal{H}$  are given by the bra-vectors  $\langle k;m,n|$ . The ket-vector  $|k;m,n\rangle$  is the Hermitian conjugate of  $\langle k;m,n|$ . The orthogonality relations are given by

$$\langle k_1;m_1,n_1|k_2;m_2,n_2\rangle = \delta_{k_1,k_2} \delta_{m_1,m_2} \delta_{n_1,n_2} \quad (5)$$

The incident and reflected voltage waves are represented by

$$|a\rangle = \sum_{k=-\infty}^{+\infty} \sum_{m=-\infty}^{+\infty} \sum_{n=-\infty}^{+\infty} \begin{bmatrix} a_1 \\ a_2 \\ a_3 \\ a_4 \end{bmatrix}_{m,n} |k;m,n\rangle \quad (6)$$

and

$$|b\rangle = \sum_{k=-\infty}^{+\infty} \sum_{m=-\infty}^{+\infty} \sum_{n=-\infty}^{+\infty} \begin{bmatrix} b_1 \\ b_2 \\ b_3 \\ b_4 \end{bmatrix}_{m,n} |k;m,n\rangle \quad (7)$$

in the Hilbert space  $\mathcal{H}$ . We define the shift operators  $X$ ,  $Y$  and their Hermitian conjugates  $X^*$  and  $Y^*$  by

$$\begin{aligned} X|k;m,n\rangle &= |k;m+1,n\rangle \\ X^*|k;m,n\rangle &= |k;m-1,n\rangle \\ Y|k;m,n\rangle &= |k;m,n+1\rangle \\ Y^*|k;m,n\rangle &= |k;m,n-1\rangle \end{aligned} \quad (8)$$

The operators  $X$  and  $Y$  shift the field state by one interval  $\Delta l$  in the positive  $m$ - and  $n$ -direction, respectively. Their Hermitian conjugates  $X^*$  and  $Y^*$  shift the field state in the opposite direction.

We define the time shift operator  $T$ . The time shift operator increments  $k$  by 1, i.e. it shifts the field state by  $\Delta t$  in the positive time direction. If the time shift operator is applied to a vector  $|k;m,n\rangle$ , we obtain

$$T|k;m,n\rangle = |k+1;m,n\rangle \quad (9)$$

We introduce the connection operator  $\Gamma$  given by

$$\Gamma = \begin{bmatrix} 0 & X & 0 & 0 \\ X^* & 0 & 0 & 0 \\ 0 & 0 & 0 & Y \\ 0 & 0 & Y^* & 0 \end{bmatrix} \quad (10)$$

With the connection operator  $\Gamma$ , equation (3) yields the operator equation

$$|b\rangle = \Gamma |a\rangle \quad (11)$$

describing the mesh connections. The operator  $\Gamma$  is Hermitian and unitary:

$$\Gamma = \Gamma^\dagger = \Gamma^{-1} \quad (12)$$

Therefore we obtain from equations (11) and (12)

$$|a\rangle = \Gamma |b\rangle \quad (13)$$

We now express equation (1) in the Hilbert space notation by

$$|b\rangle = \mathbf{T} \mathbf{S} |a\rangle \quad (14)$$

This equation describes the simultaneous scattering within all the mesh node four-ports according to Figure 1. The scattering by a mesh node causes the unit time delay  $\Delta t$ .

Figure 2 shows an example of a spatial domain within a TLM mesh. This spatial domain is specified by a given set of mesh four-ports. A spatial domain  $D$  in our TLM mesh may be specified by projection operators. We define the domain projection operator  $\mathbf{P}_D$  which projects a state vector  $|a\rangle$  on the domain  $D$ :

$$\mathbf{P}_D |a\rangle = |a\rangle_D \quad (15)$$

This projection operator may be written in dyadic notation as the sum of the projection operators on the nodes belonging to the domain  $D$ :

$$\mathbf{P}_D = \sum_{m \in D} \sum_{n \in D} |k;m,n\rangle \langle k;m,n| \quad (16)$$

In the same way, we define the inner domain projection operator  $\mathbf{P}_I$  and the boundary projection operator by

$$\mathbf{P}_I |a\rangle = |a\rangle_I \quad (17)$$

$$\mathbf{P}_B |a\rangle = |a\rangle_B \quad (18)$$

with

$$\mathbf{P}_I = \mathbf{P}_I \mathbf{P}_D \quad (19)$$

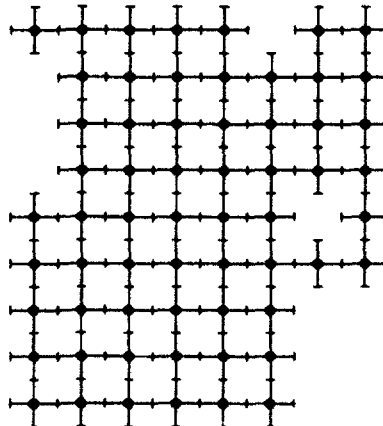


Figure 2. A spatial domain within the TLM mesh



$$\mathbf{P}_B = \mathbf{P}_B \mathbf{P}_D \quad (20)$$

$$\mathbf{P}_B + \mathbf{P}_I = \mathbf{P}_D \quad (21)$$

The inner domain projection operator projects the circuit space  $\mathcal{H}$  on the inner ports of the domain  $D$  (Figure 3). Since the projection operator  $\mathbf{P}_I$  and the connection operator  $\Gamma$  are commuting, i.e.

$$[\mathbf{P}_I, \Gamma] = 0 \quad (22)$$

we obtain

$$|b\rangle_I = \Gamma |a\rangle_I \quad (23)$$

Applying diakoptics to TLM structures requires the computation of the wave pulses scattered at the domain boundaries. The initial conditions or boundary conditions are given by the wave pulses incident on the boundary ports. We apply the projection operators  $\mathbf{P}_I \mathbf{P}_D$  and  $\mathbf{P}_B \mathbf{P}_D$  in order to separate the field states  $|a\rangle$  and  $|b\rangle$  into the inner field states  $|a\rangle_I$  and  $|b\rangle_I$  and the boundary states  $|a\rangle_B$  and  $|b\rangle_B$ . From equation (14) we obtain

$$\begin{aligned} |b\rangle_B &= \mathbf{T} \mathbf{S}_{BB} |a\rangle_B + \mathbf{T} \mathbf{S}_{BI} |a\rangle_I \\ |b\rangle_I &= \mathbf{T} \mathbf{S}_{IB} |a\rangle_B + \mathbf{T} \mathbf{S}_{II} |a\rangle_I \end{aligned} \quad (24)$$

with

$$\begin{aligned} \mathbf{S}_{BB} &= \mathbf{P}_B \mathbf{S} \mathbf{P}_B \\ \mathbf{S}_{BI} &= \mathbf{P}_B \mathbf{S} \mathbf{P}_I \\ \mathbf{S}_{IB} &= \mathbf{P}_I \mathbf{S} \mathbf{P}_B \\ \mathbf{S}_{II} &= \mathbf{P}_I \mathbf{S} \mathbf{P}_I \end{aligned} \quad (25)$$

Using equations (23) and (24), we eliminate the inner domain states  $|a\rangle_I$  and  $|b\rangle_I$  and obtain

$$|b\rangle_B = [\mathbf{T} \mathbf{S}_{BB} + \mathbf{T} \mathbf{S}_{BI} (\mathbf{1} - \Gamma \mathbf{T} \mathbf{S}_{II})^{-1} \Gamma \mathbf{T} \mathbf{S}_{IB}] |a\rangle_B \quad (26)$$

This is the relation between the incident and scattered boundary state. It describes the evolution of the boundary field state without knowledge of the inner-field state. It has to be considered that the operator equation (26) is non-local with respect to both space and time. We expand the operator  $(\mathbf{1} - \Gamma \mathbf{T} \mathbf{S}_{II})^{-1}$  into a Neumann series<sup>10,11</sup> and obtain

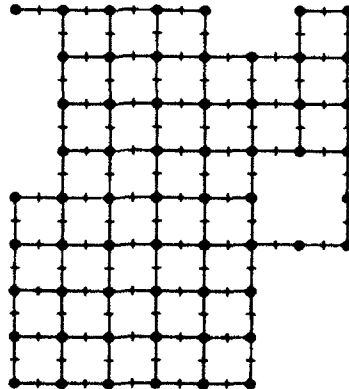


Figure 3. The inner ports of a TLM domain

$$(1 - \Gamma T S_{II})^{-1} = \sum_{l=0}^{\infty} T^l (\Gamma S_{II})^l \quad (27)$$

Inserting this into equation (26) yields the *boundary state evolution equation*

$$|b\rangle_B = G|a\rangle_B \quad (28)$$

with the boundary field evolution operator  $G$  given by

$$G = \left[ T S_{BB} + S_{BI} \left( \sum_{l=0}^{\infty} T^{l+2} (\Gamma S_{II})^l \right) \Gamma S_{IB} \right] \quad (29)$$

The boundary field operator  $G$  gives the relation between the boundary state vector  $|a\rangle_B$  representing the wave pulses incident on the boundary and the boundary state vector  $|b\rangle_B$  representing the wave pulses reflected through the boundary. Equation (28) is the general formulation of the boundary element problem in the Hilbert space. Since the Neumann series is an infinite geometrical series in space- and time-shift operators, the boundary field operator is non-local with respect to space and time.

#### 4. THE DISCRETE TWO-DIMENSIONAL GREEN'S FUNCTION

As an example, we derive the discrete Green's function for the half-plane. The discrete Green's function for the half-plane is given by the projection of the boundary state evolution operator equation (28) onto configuration space for a point-like initial state  $|a\rangle_B$ . The half-plane (Figure 4) is defined by the domain projection operator  $P_D$  given by

$$P_D = \sum_{k,n} \sum_{m=0}^{\infty} |k;m,n\rangle \langle k;m,n| \quad (30)$$

As in the shunt TLM-model, voltage wave amplitudes instead of total voltages are used, a new Green's function for wave amplitudes has to be defined. For a boundary problem, the discrete Green's function is defined by the convolution

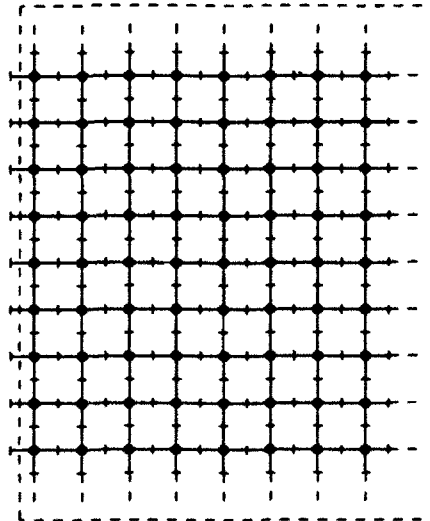


Figure 4. The homogeneous two-dimensional half-space

$$\begin{aligned} {}_k b_n &= \sum_{k', n'} {}_k k' G_{n-n'} {}_k a_{n'} \\ &= {}_k G_n * {}_k a_n \end{aligned} \quad (31)$$

with

$$n \in B \quad (32)$$

where

$$B = \{n_1, n_2, \dots, n_N\} \quad (33)$$

denotes the set of  $N$  boundary nodes.

${}_k a_n$  is the column vector of the incident impulse functions at the time  $k\Delta t$ .  ${}_k b_n$  is the column vector of the scattered output wave pulses at the time  $k\Delta t$ .  ${}_k G_n$  is the discrete Green's function for an arbitrary boundary with  $N$  boundary nodes. It describes the relation between the incident and the scattered wave amplitudes in the boundary ports.

For the half-plane, the boundary is given by  $m=0$  and  $n=-\infty, \dots, -1, 0, 1, \dots, \infty$ . Therefore equation (31) yields

$${}_k b_n = \sum_{n'=-\infty}^{\infty} \sum_{k'=-\infty}^{\infty} {}_k k' G_{n-n'} {}_k a_{n'} \quad (34)$$

The boundary state evolution equation (28) may be expressed by the discrete Green's function, equation (34), via

$$|b\rangle_B = G |a\rangle_B \quad (35)$$

where the boundary field evolution operator is given by

$$G = \begin{bmatrix} 1 & 0 & 0 & 0 \\ 0 & 0 & 0 & 0 \\ 0 & 0 & 0 & 0 \\ 0 & 0 & 0 & 0 \end{bmatrix} \sum_{n=-\infty}^{\infty} \sum_{k=-\infty}^{\infty} {}_k k' G_{n-n'} |k; 0, n\rangle \langle k'; 0, n'| \quad (36)$$

In order to calculate the Green's function for the boundary of the half-plane, we start from an impulsive excitation at  $n'=0$ ,  $k'=0$  given by

$$|a\rangle_{B, k_0=0} = \begin{bmatrix} 1 \\ 0 \\ 0 \\ 0 \end{bmatrix} |0; 0, 0\rangle \quad (37)$$

and obtain

$$|b\rangle_B = \sum_{n=-\infty}^{\infty} \sum_{k=-\infty}^{\infty} \begin{bmatrix} 1 \\ 0 \\ 0 \\ 0 \end{bmatrix} {}_k G_n |k; 0, n\rangle \quad (38)$$

Our result will be the Green's function  ${}_k G_n$ .

Mapping equations (28) with (29) and (37), (35) with (36) and (37) to configuration space by multiplying both equations from the left side with  $\langle k; 0, n|$ , we obtain

$$\langle k; 0, n | b \rangle_B = \langle 0, n | S_{BI} (\Gamma S_{II})^{k-2} \Gamma S_{IB} \begin{bmatrix} 1 \\ 0 \\ 0 \\ 0 \end{bmatrix} | 0, 0 \rangle \quad (39)$$

$$\langle k; 0, n | b \rangle_B = \begin{bmatrix} 1 \\ 0 \\ 0 \\ 0 \end{bmatrix} {}_k G_n \quad (40)$$

where we have used

$$\langle k | T^j | 0 \rangle = \delta_{k,j} \quad (41)$$

so that only one term of the Neumann series in equation (29) contributes to  ${}_k G_n$ , if we restrict ourselves to  $k \geq 2$ .

With this result, we consider equation (29) and formulate the main part of the problem that means the operator  $(T \Gamma S_{II})^j$  recursively

$$|a\rangle_{k+1} = T \Gamma S_{II} |a\rangle_k \quad (42)$$

where

$$|a\rangle_k = \sum_{m,n} \begin{bmatrix} a_1 \\ a_2 \\ a_3 \\ a_4 \end{bmatrix} |k; m, n\rangle \quad (43)$$

With the projection operators  $P_I$  and  $P_B$  given by

$$\begin{aligned} P_I &= \begin{bmatrix} 0 & 0 & 0 & 0 \\ 0 & 1 & 0 & 0 \\ 0 & 0 & 1 & 0 \\ 0 & 0 & 0 & 1 \end{bmatrix} \sum_{k,n} |k; 0, n\rangle \langle k; 0, n| \\ &+ \begin{bmatrix} 1 & 0 & 0 & 0 \\ 0 & 1 & 0 & 0 \\ 0 & 0 & 1 & 0 \\ 0 & 0 & 0 & 1 \end{bmatrix} \sum_{k,n} \sum_{m=1}^{\infty} |k; m, n\rangle \langle k; m, n| \end{aligned} \quad (44)$$

and

$$P_B = \begin{bmatrix} 1 & 0 & 0 & 0 \\ 0 & 0 & 0 & 0 \\ 0 & 0 & 0 & 0 \\ 0 & 0 & 0 & 0 \end{bmatrix} \sum_{k,n} |k; 0, n\rangle \langle k; 0, n| \quad (45)$$

it yields for the operators  $S_{BB}$ ,  $S_{BI}$ ,  $S_{IB}$  and  $S_{II}$ :

$$S_{BB} = \begin{bmatrix} -1 & 0 & 0 & 0 \\ 0 & 0 & 0 & 0 \\ 0 & 0 & 0 & 0 \\ 0 & 0 & 0 & 0 \end{bmatrix} \sum_{k,n} |k; 0, n\rangle \langle k; 0, n| \quad (46)$$

$$S_{BI} = \begin{bmatrix} 0 & \frac{1}{2} & \frac{1}{2} & \frac{1}{2} \\ 0 & 0 & 0 & 0 \\ 0 & 0 & 0 & 0 \\ 0 & 0 & 0 & 0 \end{bmatrix} \sum_{k,n} |k;0,n\rangle \langle k;0,n| \quad (47)$$

$$S_{IB} = \begin{bmatrix} 0 & 0 & 0 & 0 \\ \frac{1}{2} & 0 & 0 & 0 \\ \frac{1}{2} & 0 & 0 & 0 \\ \frac{1}{2} & 0 & 0 & 0 \end{bmatrix} \sum_{k,n} |k;0,n\rangle \langle k;0,n| \quad (48)$$

$$S_{II} = \begin{bmatrix} -\frac{1}{2} & \frac{1}{2} & \frac{1}{2} & \frac{1}{2} \\ \frac{1}{2} & -\frac{1}{2} & \frac{1}{2} & \frac{1}{2} \\ \frac{1}{2} & \frac{1}{2} & -\frac{1}{2} & \frac{1}{2} \\ \frac{1}{2} & \frac{1}{2} & \frac{1}{2} & -\frac{1}{2} \end{bmatrix} \sum_{k,n} \sum_{m=1}^{\infty} |k;m,n\rangle \langle k;m,n|$$

$$+ \begin{bmatrix} 0 & 0 & 0 & 0 \\ 0 & -\frac{1}{2} & \frac{1}{2} & \frac{1}{2} \\ 0 & \frac{1}{2} & -\frac{1}{2} & \frac{1}{2} \\ 0 & \frac{1}{2} & \frac{1}{2} & -\frac{1}{2} \end{bmatrix} \sum_{k,n} |k;0,n\rangle \langle k;0,n| \quad (49)$$

We obtain

$$|a\rangle_{k-1} = T \Gamma S_{IB} \begin{bmatrix} 1 \\ 0 \\ 0 \\ 0 \end{bmatrix} |0;0,0\rangle = \frac{1}{2} \begin{bmatrix} |1;1,0\rangle \\ 0 \\ |1;0,1\rangle \\ |1;0,-1\rangle \end{bmatrix} \quad (50)$$

and

$${}_k G_n \begin{bmatrix} 1 \\ 0 \\ 0 \\ 0 \end{bmatrix} = \langle k;0,n| T S_{BI} |a\rangle_{k-1} = \begin{bmatrix} 0 & \frac{1}{2} & \frac{1}{2} & \frac{1}{2} \\ 0 & 0 & 0 & 0 \\ 0 & 0 & 0 & 0 \\ 0 & 0 & 0 & 0 \end{bmatrix} \langle k-1;0,n|a\rangle_{k-1} \quad (51)$$

Defining

$$\langle k;m,n|a\rangle_k = \begin{bmatrix} a_1 \\ a_2 \\ a_3 \\ a_4 \end{bmatrix}_{m,n}$$

$$= \begin{bmatrix} 1 \\ 0 \\ 0 \\ 0 \end{bmatrix} {}_k [a_1]_{m,n} + \begin{bmatrix} 0 \\ 1 \\ 0 \\ 0 \end{bmatrix} {}_k [a_2]_{m,n}$$

$$+ \begin{bmatrix} 0 \\ 0 \\ 1 \\ 0 \end{bmatrix} {}_k [a_3]_{m,n} + \begin{bmatrix} 0 \\ 0 \\ 0 \\ 1 \end{bmatrix} {}_k [a_4]_{m,n} \quad (52)$$

and assigning  $k=k'-1$ , we obtain the following system of partial difference equations by mapping equation (42) to configuration space

$${}_{k+1}[a_1]_{m+1,n} = \frac{1}{2} ({}_k[a_1]_{m,n} - {}_k[a_2]_{m,n} + {}_k[a_3]_{m,n} + {}_k[a_4]_{m,n}) \quad (53)$$

$${}_{k+1}[a_1]_{m,n} = \frac{1}{2} (-{}_k[a_1]_{m+1,n} + {}_k[a_2]_{m+1,n} + {}_k[a_3]_{m+1,n} + {}_k[a_4]_{m+1,n}) \quad (54)$$

$${}_{k+1}[a_1]_{m,n+1} = \frac{1}{2} ({}_k[a_1]_{m,n} + {}_k[a_2]_{m,n} + {}_k[a_3]_{m,n} - {}_k[a_4]_{m,n}) \quad (55)$$

$${}_{k+1}[a_1]_{m,n-1} = \frac{1}{2} ({}_k[a_1]_{m,n} + {}_k[a_2]_{m,n} - {}_k[a_3]_{m,n} + {}_k[a_4]_{m,n}) \quad (56)$$

for

$$k = 0, 1, 2, \dots, \infty$$

$$n = -\infty, \dots, -1, 0, 1, \dots, \infty$$

$$m = 0, 1, 2, \dots, \infty$$

The initial conditions are given by

$${}_0[a_1]_{1,0} = \frac{1}{2} \quad {}_0[a_3]_{0,1} = \frac{1}{2} \quad (57)$$

$${}_0[a_4]_{0,-1} = \frac{1}{2} \quad \text{all other } m, n: {}_0[a_i]_{m,n} = 0 \quad (58)$$

As the space is not bounded with respect to  $n$ , we only need boundary conditions concerning  $m$ . One boundary value is

$${}_k[a_1]_{0,n} = 0 \quad (59)$$

As we have a system of second order concerning  $m$ , we need another boundary condition. Therefore we apply the Sommerfeld radiation condition.<sup>12</sup>

From equation (51), we obtain for the Green's function for  $k \geq 0$

$${}_{k+2}G_n \equiv {}_k[a_0]_{0,n} = \frac{1}{2} ({}_k[a_2]_{0,n} + {}_k[a_3]_{0,n} + {}_k[a_4]_{0,n}) \quad (60)$$

This system of partial difference equations can be solved by transforming it to frequency- and momentum-space. Concerning  $n$ , we consider  ${}_k[a_i]_{m,n}$  as the Fourier coefficients of the function  ${}_k[A_i(\xi)]_m$ :

$$\xi \{ {}_k[a_i]_{m,n} \} = {}_k[A_i(\xi)]_m = \sum_{n=-\infty}^{\infty} {}_k[a_i]_{m,n} \xi^{-n} \quad (61)$$

with

$$\xi = \exp 2\pi j N \quad (62)$$

Concerning  $m$  and  $k$ , we apply the  $Z$ -transformation<sup>13</sup>

$$Z \{ {}_k[A_i(\xi)]_m \} = [B_i(\xi, \nu)]_m = \sum_{k=0}^{\infty} {}_k[A_i(\xi)]_m \nu^{-k} \quad (63)$$

with

$$\nu = \exp 2\pi j f \quad (64)$$

and in analogy to equation (63) the  $Z$ -transformation with respect to  $m$

$$Y\{[B_i(\xi, \nu)]_m\} = [C_i(\xi, \eta, \nu)] = \sum_{m=0}^{\infty} [B_i(\xi, \nu)]_m \eta^{-m} \quad (65)$$

with

$$\eta = \exp jk \quad (66)$$

As we have

$$\xi\{ {}_k[a_i]_{m,n \pm 1} \} = {}_k[A_i(\xi)]_m \xi^{\pm 1} \quad (67)$$

for a shift in the positive/negative direction of  $n$  and

$$Z\{ {}_{k+1}[A_i(\xi)]_m \} = \nu[B_i(\xi, \nu)]_m - \nu_0[A_i(\xi)]_m \quad (68)$$

$$Y\{[B_i(\xi, \nu)]_{m+1}\} = \eta[C_i(\xi, \eta, \nu)] - \eta[B_i(\xi, \nu)]_0 \quad (69)$$

for a left-shift of  $k$  and  $m$ , we obtain

$$2\nu\eta C_1 - \nu = C_1 - C_2 + C_3 + C_4 \quad (70)$$

$$2\eta C_2 + [B_0]_0 = -C_1 + C_2 + C_3 + C_4 \quad (71)$$

$$2\nu\xi C_3 - \nu = C_1 + C_2 + C_3 - C_4 \quad (72)$$

$$2\xi C_4 - \nu = C_1 + C_2 - C_3 + C_4 \quad (73)$$

where we have used the abbreviation

$$[B_0]_0 = [B_2]_0 + [B_3]_0 + [B_4]_0 \quad (74)$$

This system of algebraic equations has the solution

$$C_1 = \frac{1}{N} (2\xi\nu^4 - \xi\eta\nu^3 - \eta\nu^2 - 2\xi\nu^2 - \eta\xi^2\nu^2 + 3\xi\eta\nu) + \frac{[B_0]_0}{N} (\xi\eta\nu^2 - \eta\nu - \eta\xi^2\nu + \xi\eta) \quad (75)$$

$$C_2 = \frac{1}{N} (\eta^2\nu^3 + \eta^2\xi^2\nu^3 - \xi\eta\nu^3 - 2\xi\eta^2\nu^2 + \xi\eta\nu) - \frac{[B_0]_0}{N} (2\xi\eta^2\nu^3 - \xi\eta\nu^2 - \eta^2\nu^2 - \eta^2\xi^2\nu^2 + \xi\eta) \quad (76)$$

$$C_3 = \frac{1}{N} (2\eta\nu^4 - 2\xi\eta\nu^3 - \eta^2\nu^3 - \xi\eta^2\nu^2 - \eta\nu^2 + \xi\eta\nu) - \frac{[B_0]_0}{N} (\eta^2\nu^2 - \xi\eta^2\nu - \eta\nu + \xi\eta) \quad (77)$$

$$C_4 = \frac{1}{N} (2\xi^2\eta\nu^4 - \xi^2\eta^2\nu^3 - 2\xi\eta\nu^3 + \xi\eta^2\nu^2 - \xi^2\eta\nu^2 + \xi\eta\nu) - \frac{[B_0]_0}{N} (\xi^2\eta^2\nu^2 - \eta\xi^2\nu - \xi\eta^2\nu + \xi\eta) \quad (78)$$

with the nominator  $N$  given by

$$N = 2\eta^2 (\xi\nu - \xi\nu^3) + 2\eta(2\xi\nu^4 - \nu^3 - \xi^2\nu^3 + \nu + \xi^2\nu - 2\xi) + 2\xi\nu - 2\xi\nu^3 \quad (79)$$

For the inverse transformation with respect to  $m$ , we consider the function  $C_4$  and rewrite equation (78):

$$C_4 = \frac{\eta^2 \frac{(\nu + [B_0]_0)(1 - \xi\nu)}{2(1 - \nu^2)}}{\eta^2 - 2\eta \left( \nu + \frac{1}{\nu} - \frac{\xi}{2} - \frac{1}{2\xi} \right) + 1} + \frac{\eta \frac{[B_0]_0 \left( \xi - \frac{1}{\nu} \right) 2\xi\nu^3 - 2\nu^2 - \xi\nu + 1}{2(1 - \nu^2)}}{\eta^2 - 2\eta \left( \nu + \frac{1}{\nu} - \frac{\xi}{2} - \frac{1}{2\xi} \right) + 1} \quad (80)$$

We assign

$$\cosh \alpha = \nu + \frac{1}{\nu} - \frac{\xi}{2} - \frac{1}{2\xi} \quad (81)$$

and

$$\sinh \alpha = \epsilon \sqrt{\cosh^2 \alpha - 1} = \epsilon \sqrt{\left( \nu + \frac{1}{\nu} - \frac{\xi}{2} - \frac{1}{2\xi} \right)^2 - 1} \quad (82)$$

with

$$\epsilon = \begin{cases} 1 & \text{for } \mathcal{R}\{\alpha\} \geq 0 \\ -1 & \text{for } \mathcal{R}\{\alpha\} < 0 \end{cases} \quad (83)$$

It yields

$$C_4 = \frac{\eta^2 - \eta \cosh \alpha}{\eta^2 - 2\eta \cosh \alpha + 1} \frac{(\nu + [B_0]_0)(1 - \xi\nu)}{2(1 - \nu^2)} + \epsilon \frac{\eta \sinh \alpha}{\eta^2 - 2\eta \cosh \alpha + 1} T(\xi, \nu) \quad (84)$$

with the function  $T(\xi, \nu)$  given by

$$T(\xi, \nu) = \frac{\xi\nu^3 - \frac{1}{2}\nu^2 + \frac{1}{2}\xi^2\nu^2 - \frac{\xi}{2}\xi\nu - \frac{\nu}{2\xi} + 2}{2(1 - \nu^2) \sqrt{\left( \nu + \frac{1}{\nu} - \frac{\xi}{2} - \frac{1}{2\xi} \right)^2 - 1}} + [B_0]_0 \frac{-\xi\nu^2 + \frac{3}{2}\nu + \frac{1}{2}\xi^2\nu - \frac{\xi}{2} - \frac{1}{2\xi}}{2(1 - \nu^2) \sqrt{\left( \nu + \frac{1}{\nu} - \frac{\xi}{2} - \frac{1}{2\xi} \right)^2 - 1}} \quad (85)$$

The following correspondences are valid:<sup>13</sup>

$$Y\{\cosh \alpha m\} = \frac{\eta^2 - \eta \cosh \alpha}{\eta^2 - 2\eta \cosh \alpha + 1} \quad (86)$$



$$Y(\sinh \alpha m) = \frac{\eta \sinh \alpha}{\eta^2 - 2\eta \cosh \alpha + 1} \quad (87)$$

with  $m=0,1,2,\dots,\infty$ .

Writing out the  $\sinh(\alpha m)$ - and  $\cosh(\alpha m)$ -function in exponential terms, we obtain for  $[B_4]_m$

$$\begin{aligned} [B_4]_m = & 1/2 \exp(+\alpha m) \left( \frac{(\nu + [B_0]_0)(1 - \xi\nu)}{2(1 - \nu^2)} + \varepsilon T(\xi, \nu) \right) \\ & + 1/2 \exp(-\alpha m) \left( \frac{(\nu + [B_0]_0)(1 - \xi\nu)}{2(1 - \nu^2)} - \varepsilon T(\xi, \nu) \right) \end{aligned} \quad (88)$$

The Sommerfeld radiation condition means that for  $\Re\{\alpha\} \geq 0$ , the terms with  $\exp(-\alpha m)$  and for  $\Re\{\alpha\} \leq 0$ , the terms with  $\exp(+\alpha m)$  must vanish because in passive media, exponentially growing solutions do not correspond to physical solutions. In both cases we obtain

$$\frac{(\nu + [B_0]_0)(1 - \xi\nu)}{2(1 - \nu^2)} = T(\xi, \nu) \quad (89)$$

and for  $[B_0]_0$

$$\begin{aligned} [B_0(\theta, \nu)]_0 = & \frac{2\nu^2(\nu^2 - 1) \sqrt{\left(\nu + \frac{1}{\nu} - \cos \theta\right)^2 - 1}}{\nu^2 - 2\nu \cos \theta + 1} \\ & - \frac{2\nu^3 - 2\nu^4 \cos \theta - \nu^3 + \nu}{\nu^2 - 2\nu \cos \theta + 1} \end{aligned} \quad (90)$$

for  $m=0,1,2,\dots,\infty$  with

$$\cos \theta = \cos 2\pi N = \frac{1}{2} \left( \xi + \frac{1}{\xi} \right) \quad (91)$$

We only need the boundary value  $[B_0(\theta, \nu)]_0$  to calculate  ${}_k G_n$ , because with equation (60) it yields

$${}_k {}_{+2} G_n = {}_k [a_0]_{0,n} = \frac{1}{2} \mathbf{X}^{-1} \{ \mathbf{Z}^{-1} \{ [B_0(\xi, \nu)]_0 \} \} \quad (92)$$

for  $k \geq 0$ . Of course, the result for  $[B_0]_m$  is the same, if we consider the functions  $C_1$ ,  $C_2$  or  $C_3$ .

The transformation back to time-space<sup>1,2</sup> can be achieved by

$${}_k [A_i(\theta)]_m = \frac{1}{2\pi} \oint_C [B_i(\theta, \nu)]_m \nu^{k-1} d\nu \quad (93)$$

where  $C$  is a closed curve in the complex  $\nu$ -plane which surrounds the unity-circle. Integration must be taken in anticlockwise sense.

Owing to the orthogonality relation

$$\int_0^1 [\xi(N)]^{n'-n} dN = \delta_{n',n} \quad (94)$$

the inverse transformation from momentum space to configuration space concerning  $n$  is given by

$$\mathbf{X}^{-1} \{ {}_k [A_i(\theta)]_m \} = {}_k [a_i]_{m,n} = \frac{1}{2\pi} \int_0^{2\pi} {}_k [A_i(\theta)]_m \exp(j\theta n) d\theta \quad (95)$$

As  $B_0(\xi, \nu)$  is an even function of  $\theta$ , it yields with equations (93) and (95) for  ${}_k [a_0]_{0,n}$

$$\begin{aligned}
{}_k[a_0]_{0,n} &= \frac{1}{2\pi j} \oint_C \frac{1}{\pi} \int_0^\pi [B_0(\theta, \nu)]_0 \cos n\theta \nu^{k-1} d\theta d\nu \\
&= \frac{1}{2\pi j} \oint_C \frac{1}{\pi} \int_0^\pi \frac{2\nu^2(\nu^2-1) \sqrt{\left(\nu + \frac{1}{\nu} - \cos \theta\right)^2 - 1}}{\nu^2 - 2\nu \cos \theta + 1} \cos n\theta \nu^{k-1} d\theta d\nu \\
&\quad - \frac{1}{2\pi j} \oint_C \frac{1}{\pi} \int_0^\pi \frac{(\nu^2-1)^2}{\nu^2 - 2\nu \cos \theta + 1} \cos n\theta \nu^{k-1} d\theta d\nu \\
&\equiv I_1 - I_2
\end{aligned} \tag{96}$$

where we have used

$$\oint_C (\text{analytical function}) d\nu = 0$$

For the evaluation of the two integrals  $I_1$  and  $I_2$ , we can restrict ourselves to the case  $n \geq 0$  because

$${}_k[a_0]_{0,n} = {}_k[a_0]_{0,-n} \tag{97}$$

With<sup>14</sup>

$$\int_0^\pi \frac{\cos n\theta d\theta}{\nu^2 - 2\nu \cos \theta + 1} = \frac{\pi \nu^{-n}}{\nu^2 - 1} \tag{98}$$

for  $\nu^2 > 1$ ,  $n \geq 0$  and

$$\frac{1}{2\pi j} \oint_C \nu^{-n} d\nu = \delta_{1,n} \tag{99}$$

we calculate

$$I_2 = \delta_{k,n-3} - \delta_{k,n-1} \tag{100}$$

For the integral  $I_1$ , we apply<sup>15</sup>

$$\frac{1}{\sqrt{1+2\rho x+\rho^2}} = \sum_{l=0}^{\infty} \rho^l P_l(x) \tag{101}$$

for  $|\rho| < 1$  and  $|\xi| \leq 1$  and<sup>16</sup>

$$\frac{1-p^2}{1-2p \cos x + p^2} = 1 + 2 \sum_{k=1}^{\infty} \cos kx \tag{102}$$

for  $|p| < 1$ .

With the integral representation of the Legendre polynomials<sup>17</sup>

$$\frac{1}{2\pi j} \oint_{C'} \frac{t^n dt}{\sqrt{t^2 - 2xt + 1}} = \begin{cases} P_n(x) & \text{for } n \geq 0 \\ 0 & \text{for } n < 0 \end{cases} \tag{103}$$

where  $C'$  is a closed curve in the complex  $\nu$ -plane which encircles the unity-circle in anticlockwise sense, we obtain

$$\begin{aligned}
I_1 &= {}_{k+3}I_n - {}_{k-1}I_n \\
&+ \sum_{j=0}^{k+1} \frac{1}{2} {}_{k+1-j}I_{n+2+j} - \frac{1}{2} {}_{k+1-j}I_{n+j} + \frac{1}{2} {}_{k+1-j}I_{n-2+j} \\
&+ \sum_{j=0}^k \frac{1}{2} {}_{k-j}I_{n+1-j} - \frac{1}{2} {}_{k-j}I_{n-1-j} + \frac{1}{2} {}_{k-j}I_{n-3-j}
\end{aligned} \quad (104)$$

where the function  ${}_kI_n$  is defined by

$${}_kI_n = \sum_{l=0}^k \frac{2}{\pi} \int_0^\pi P_l(\cos^2 \theta/2) P_{k-l}(-\sin^2 \theta/2) \cos n\theta d\theta \quad (105)$$

To calculate  ${}_kI_n$ , we expand  $P_l(\cos^2 \theta/2)$  and  $P_{k-l}(-\sin^2 \theta/2)$  in terms of  $\cos^2 \theta/2$  with the help of References 18 and 19:

$$P_{k-l}(-\sin^2 \theta/2) = (-1)^{k-l} \sum_{r=0}^{k-l} \binom{k-l}{r} \binom{k-l+r}{r} \left(-\frac{1}{2}\right)^r (\cos^2 \theta/2)^{2r} \quad (106)$$

$$P_l(\cos^2 \theta/2) = \frac{1}{2^l} \sum_{s=0}^{[l/2]} (-1)^s \binom{l}{s} \binom{2l-2s}{l} (\cos^2 \theta/2)^{2l-4s} \quad (107)$$

We substitute  $\theta = 2y$ , apply the integral<sup>20</sup>

$$\int_0^{\pi/2} \cos^{2n} t \cos 2mt dt = \begin{cases} \frac{\pi}{2^{2n+1}} \binom{2n}{n-m} & \text{for } n \geq m \\ 0 & \text{for } n < m \end{cases} \quad (108)$$

and obtain for the function  ${}_kI_n$ :

$$\begin{aligned}
{}_kI_n &= 2 \sum_{l=0}^k \sum_{s=0}^{[l/2]} \sum_{r=0}^{k-l} (-1)^{k-l+r-s} \left(\frac{1}{2}\right)^{3l+3r-4s} \binom{l}{s} \binom{2l-2s}{l} \\
&\times \binom{2r}{r} \binom{k-l+r}{2r} \binom{2l-4s+2r}{l-2s+r-n}
\end{aligned} \quad (109)$$

Combining the two integrals yields an algebraic expression for the discrete Green's function

$$\begin{aligned}
{}_kG_n &= \frac{1}{2} \delta_{k,n+1} - \frac{1}{2} \delta_{k,n-1} + \frac{1}{2} {}_{k+1}I_n - \frac{1}{2} {}_{k-3}I_n \\
&+ \sum_{j=0}^{k-1} \frac{1}{2} {}_{k-1-j}I_{n+2+j} - \frac{1}{2} {}_{k-1-j}I_{n+j} + \frac{1}{2} {}_{k-1-j}I_{n-2+j} \\
&+ \sum_{j=0}^{k-2} \frac{1}{2} {}_{k-2-j}I_{n+1-j} - \frac{1}{2} {}_{k-2-j}I_{n-1-j} + \frac{1}{2} {}_{k-2-j}I_{n-3-j}
\end{aligned} \quad (110)$$

for  $n=0,1,2,\dots,\infty$  and  $k=2,3,4,\dots,\infty$ . Because of equation (97) we have for  $n \leq 0$ :

$${}_kG_{-n} = {}_kG_n \quad (111)$$

As already remarked, the general Green's function for an excitation at the time  $k'$  in the boundary node  $n'$  is obtained by the transition

$${}_kG_n \rightarrow {}_{k-k'}G_{n-n'} \quad (112)$$

In Figure 5,  ${}_kG_n$  is depicted for  $n=-9, \dots, -1, 0, 1, \dots, 9$ ;  $k=1, 2, \dots, 10$ .

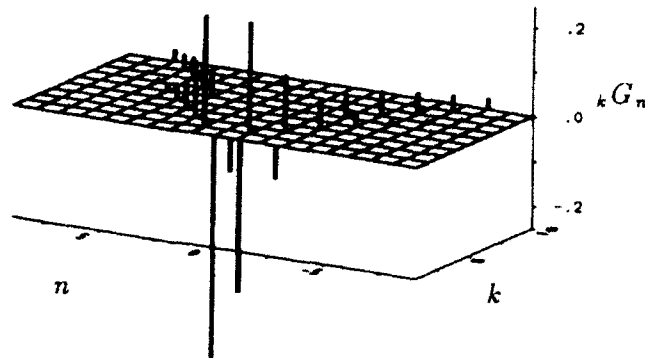


Figure 5. Values of the Green's function

### 5. CONCLUSIONS

In this paper, the TLM-method has been represented in the Hilbert space. The Hilbert space formulation allows the derivation of general algebraic expressions for the field evolution without having regard to the individual geometric conditions. Geometrical structures may be described in a general way by projection operators. A further advantage of the Hilbert space formulation is that the powerful methods of functional analysis<sup>21</sup> can be applied. General investigations of operator equations concerning the existence and the convergence of the solutions are simplified.

The Hilbert space formulation was used for deriving general algebraic expressions for the space and time discrete field evolution. From the local operator equations governing the time evolution of the field state vector, the non-local operator equation describing the time evolution of the boundary state vector was derived.

First applications of this method were demonstrated in calculating the discrete Green's function for the half-plane.

### REFERENCES

1. P. B. Johns and R. L. Beurle, 'Numerical solution of 2-dimensional scattering problems using a transmission-line matrix', *Proc. IEE*, **118**, 1203-1208 (1971).
2. W. J. R. Hofer, 'The transmission line matrix method—theory and applications', *IEEE Trans. Microwave Theory Tech.*, **MTT-33**, 882-893 (1985).
3. W. J. R. Hofer, 'The transmission line matrix (TLM) method', Chapter 8 in *Numerical Techniques for Microwave and Millimeter Wave Passive Structures*, T. Itoh (Ed.), John Wiley, New York, 1989, pp. 496-591.
4. K. E. Gustafson, *Partial Differential Equations and Hilbert Space Methods*, John Wiley, New York, 1987.
5. R. F. Harrington, *Field Computation by Moment Methods*, Krieger, Malabar, FL, 1982.
6. P. A. M. Dirac, *Quantum Mechanics*, 4th edn, Oxford University Press, Oxford.
7. J. von Neumann, *Mathematische Grundlagen der Quantenmechanik*, Springer, Berlin, 1932.
8. R. E. Collin, *Field Theory of Guided Waves*, 2nd edn, IEEE Press, New York, 1991, pp. 55-172.
9. W. J. R. Hofer, 'The discrete time domain Green's function or John's matrix—a new powerful concept in transmission line modelling', *International Journal of Numerical Modelling: Electronic Networks, Devices and Fields*, **2**, 215-225 (1989).
10. J. Weidmann, *Lineare Operatoren in Hilberträumen*, B. G. Teubner, Stuttgart, 1976, pp. 96-105.
11. H. Heuser, *Funktionalanalysis*, B. G. Teubner, Stuttgart, 1986, pp. 106-113.
12. J. A. Kong, *Electromagnetic Wave Theory*, John Wiley, New York, 1986, p. 383.
13. I. N. Bronstein and K. A. Semendjajew, *Taschenbuch der Mathematik*, Verlag Harri Deutsch, Thun, 1985, pp. 649-654.
14. I. S. Gradshteyn and I. M. Ryzhik, *Tables of Integrals, Series and Product*, Academic Press, New York, 1980, 4th edn, p. 366, No. 3.613.
15. J. Lense, *Kugelfunktionen*, Akademische Verlagsgesellschaft Geest & Portig K.-G., Leipzig, 1950, p. 14.
16. I. S. Gradshteyn and I. M. Ryzhik, *Tables of Integrals, Series and Product*, Academic Press, New York, 1980, 4th edn, p. 40.
17. M. Abramowitz and I. Stegun, *Handbook of Mathematic Functions*, Dover Publications, New York, 1970, 9th edn, p. 784.
18. A. P. Prudnikov, Y. A. Brychkow and O. I. Mariakev, *Integrals and Series*, Gordon & Breach, London, 1986, p. 625.
19. M. Abramowitz and I. Stegun, *Handbook of Mathematic Functions*, Dover Publications, New York, 1970, 9th edn, p. 775.
20. I. S. Gradshteyn and I. M. Ryzhik, *Tables of Integrals, Series and Products*, Academic Press, New York, 1980, 4th edn, p. 374, no. 17.
21. S. Grossmann, *Funktionalanalysis: im Hinblick auf ihre Anwendungen in der Physik*, Akad. Verlags-Gesellschaft, 1972, Vols 1 and 2.

**Authors' biographies:**

**Peter Russer** was born in Vienna, Austria, in 1943. He received the Dipl.-Ing. degree in 1967 and the Dr. techn. degree in 1971, both from the Technische Universität in Vienna. From 1968 to 1971 he was an Assistant Professor at the Technische Universität in Vienna. In 1971 he joined the Research Institute of AEG-Telefunken in Ulm, where he worked on fibre-optic communication, high-speed solid-state electronic circuits, laser modulation and fibre-optic gyroscopes. Since 1981 he has held the chair of Hochfrequenztechnik at the Technische Universität München. His current research interests are methods for computer-aided design of microwave circuits, integrated microwave and millimetre-wave circuits, microwave oscillators, microwave applications of superconductors and optical communications. Peter Russer is the author of more than 90 scientific papers in these fields. He is an IEEE Senior Member, and member of the German Informationstechnische Gesellschaft and the Austrian and German Physical Societies. In 1979 he received the NTG award and in 1990 the Peter Johns Prize. From 1987 to 1989 he was the chairman of the German MTT/AP Joint Chapter. In 1990 he was Visiting Professor at the University of Ottawa.



**Michael Krumpholz** was born in Bonn in 1966. He received the Dipl.-Ing. degree in electrical engineering at the Technische Universität München in 1991. Since then, he has been working as a Research Assistant at the Technische Universität München in the field of numerical techniques for microwave circuits.

## SPATIALLY WEIGHTED NUMERICAL MODELS FOR THE TWO-DIMENSIONAL WAVE EQUATION: FD ALGORITHM AND SYNTHESIS OF THE EQUIVALENT TLM MODEL

N. R. S. SIMONS AND A. A. SEBAK

*University of Manitoba, Winnipeg, Manitoba, Canada, R3T 2N2*

### SUMMARY

In this paper a new TLM model for the two-dimensional wave equation is introduced. It is synthesized directly from a FD algorithm. The FD algorithm is second-order-accurate in both space and time, and is explicitly time-stepped. The spatial derivatives in the FD algorithm are approximated by the weighted combination of two standard central difference stencils, one oriented as usual, the other rotated by  $45^\circ$  with its arms extended by a factor of  $(2)^{1/2}$ . The TLM model is realized as the weighted connection of two original models (with the same geometrical configuration as the FD algorithm). The weighting in the TLM model is accomplished by using a variable intrinsic impedance for specific elemental transmission lines. The FD and TLM methods possess identical dispersion relations if the former is operated at its upper limit of stability. Therefore, under these conditions both represent identical models for the simulation of wave propagation. The propagation characteristics of the new model are investigated and the conditions for approximate numerical isotropy are provided. The numerical implementation (scattering matrix and transfer event) is described. To validate the new model, the calculation of cutoff frequencies of various modes in rectangular waveguide is performed. Comparison with analytical results (for an unfilled waveguide) and other numerical results (for a waveguide partially filled with a dielectric) validate the implementation of the model.

### 1. INTRODUCTION

The numerical techniques discussed in this paper are capable of solving arbitrary two-dimensional electromagnetic field problems. If problems independent of the  $z$ -direction are considered, Maxwell's equations are reduced to two independent sets, one of which is given by,

$$\frac{\partial E_z}{\partial x} = \mu \frac{\partial H_y}{\partial t} \quad (1a)$$

$$\frac{\partial E_z}{\partial y} = -\mu \frac{\partial H_x}{\partial t} \quad (1b)$$

$$\frac{\partial H_y}{\partial x} - \frac{\partial H_x}{\partial y} = \sigma E_z + \epsilon \frac{\partial E_z}{\partial t} \quad (1c)$$

where  $E_p$  and  $H_p$  are the electric and magnetic fields, respectively (with  $p = x, y, \text{ or } z$ ) and  $\epsilon$ ,  $\mu$ , and  $\sigma$  are the permittivity, permeability and conductivity of the medium of interest, respectively. Equations 1 can be combined to yield the two-dimensional wave equation in  $E_z$ ,

$$\frac{\partial^2 E_z}{\partial x^2} + \frac{\partial^2 E_z}{\partial y^2} = \sigma \mu \frac{\partial E_z}{\partial t} + \epsilon \mu \frac{\partial^2 E_z}{\partial t^2} \quad (2)$$

The numerical techniques presented in this paper are developed from discrete approximations to (2) rather than (1).

Johns and Beurle introduced the transmission-line matrix (TLM) method in 1971 as a technique which utilizes the equivalence of voltages and currents on transmission lines to electric and magnetic fields in space.<sup>1</sup> An orthogonal grid of transmission lines represents a physical model

which approximates (1) or (2). Hoeter<sup>2,3</sup> presented recent applications and extensions of the method. Another numerical technique used extensively in the computational electromagnetics community is the finite-difference time-domain (FD-TD) method introduced by Yee<sup>4</sup> and extended by others.<sup>5</sup> Both the TLM and FD-TD methods are capable of providing approximate solutions to the time-dependent form of Maxwell's equations. In their most basic forms, both utilize regular rectangular grid structures and explicit time-stepping. Under certain circumstances both methods represent identical models for wave propagation. For all cases in which an equivalence between a TLM model and FD algorithm has been established, the TLM model corresponds to the FD algorithm when the latter is operated at a specific location in its stability range.<sup>6-8</sup>

Recently,<sup>6</sup> the equivalence of the original TLM model<sup>1</sup> and the two-dimensional Yee algorithm<sup>4</sup> is established. In Reference 7 the equivalence of the three-dimensional expanded node<sup>9</sup> and the three-dimensional Yee algorithm<sup>4</sup> is established. In Reference 8, models of (2) based on hexagonal (rather than rectangular) computational grids are investigated, a TLM model is presented and its equivalent FD algorithm derived.

In general, the finite difference (FD) method can be applied in various ways to approximate (2). Grid structures and the accuracy of the difference formulas can be varied, and different time-stepping schemes can be used. The purpose of this paper is to synthesize an equivalent TLM model directly from a FD approximation of (2). The general approach can be extended to the synthesis of other TLM models from FD algorithms.

In the following section, the FD algorithm is presented as a weighted connection of two Yee algorithms,<sup>4</sup> one oriented as usual (arms of the spatial stencil oriented along the  $x$ - $y$  axis), the other rotated by  $45^\circ$  with its arms extended by a factor of  $(2)^{1/2}$ . The dispersive characteristics and stability criterion of the algorithm are derived. In section 3, the equivalent TLM model is presented. Based on the relationship established in Reference 6, the equivalent TLM model is constructed from an interconnection of two original models. One oriented as usual (elemental transmission lines oriented along the  $x$ - $y$  axis), the other rotated by  $45^\circ$  with its arms extended by a factor of  $(2)^{1/2}$ . The weighting is accomplished through the use of a variable intrinsic impedance for specific elemental transmission lines, and synchronism is maintained by increasing the phase velocity along the diagonal elemental transmission lines. The relationship between the FD algorithm and TLM model is established through the equivalence of propagation characteristics, the most fundamental method for establishing the relationship between a TLM model and another numerical method. The TLM model and FD algorithms represent identical methods for the numerical simulation of wave propagation if the latter is operated at the upper limit of its stability range. In section 4, the propagation characteristics of the models are investigated. For the appropriate selection of the weighting factor, the propagation characteristics become approximately isotropic (i.e., the directional dependence of the numerical propagation velocity is removed). This allows the model to be used in conjunction with the velocity error correction technique described in Reference 8. In section 5, the numerical implementation of the new model is described. The scattering and transfer events are presented. The traditional application of calculating cutoff frequencies in rectangular waveguide is used to validate the model. Conclusions and a discussion of the new TLM model are contained in section 6.

## 2. FINITE DIFFERENCE ALGORITHM

Consider the following semi-discretization of (2),

$$\begin{aligned} \frac{E_z(x+\Delta l, y) - 2E_z(x, y) + E_z(x-\Delta l, y))}{\Delta l^2} + \\ \frac{E_z(x, y+\Delta l) - 2E_z(x, y) + E_z(x, y-\Delta l))}{\Delta l^2} = \epsilon\mu \frac{\partial^2 E_z}{\partial t^2} \end{aligned} \quad (3)$$

where the spatial derivatives are replaced with second-order-accurate central difference approximations, we assume  $\sigma = 0$ , and the right-hand side of the expression is evaluated at the spatial location  $(x, y)$ . The stencil for this spatial discretization is shown in Figure 1. We assume a uniform grid spacing of  $\Delta l$  in the  $x$ - and  $y$ -directions.

FD approximations to the wave equation introduce numerical anisotropy and dispersion (i.e.,

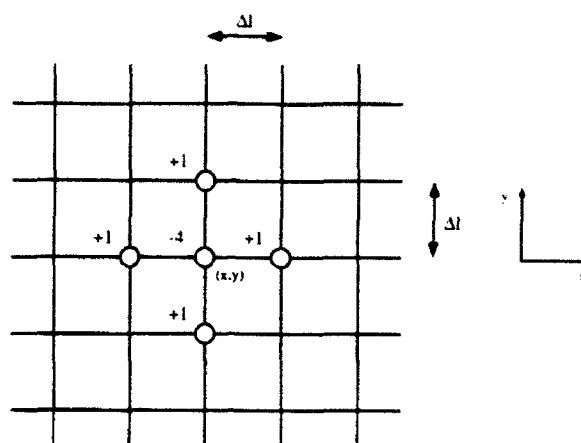


Figure 1. Second-order-accurate, central difference stencil used to approximate the spatial derivatives in the two-dimensional wave equation

the dependence of the numerical propagation velocity on the direction of propagation and frequency content of the signal). To reduce the numerical anisotropy present in the semi-discretization (3), Vichnevetsky and Bowles<sup>10</sup> proposed the weighted combination of two finite difference approximations to the spatial derivatives in (2), as illustrated in Figure 2. This semi-discretization can be expressed mathematically as,

$$\begin{aligned}
 & (1-k) \left\{ \frac{E_z(x+\Delta l, y) - 2E_z(x, y) + E_z(x-\Delta l, y)}{\Delta l^2} \right. \\
 & \quad \left. + \frac{E_z(x, y+\Delta l) - 2E_z(x, y) + E_z(x, y-\Delta l)}{\Delta l^2} \right\} \\
 & + k \left\{ \frac{E_z(x+\Delta l, y+\Delta l) - 2E_z(x, y) + E_z(x-\Delta l, y-\Delta l)}{(\sqrt{2}\Delta l)^2} \right. \\
 & \quad \left. + \frac{E_z(x+\Delta l, y-\Delta l) - 2E_z(x, y) + E_z(x-\Delta l, y+\Delta l)}{(\sqrt{2}\Delta l)^2} \right\} \\
 & = \epsilon \mu \frac{\partial^2 E_z}{\partial t^2}
 \end{aligned} \tag{4}$$

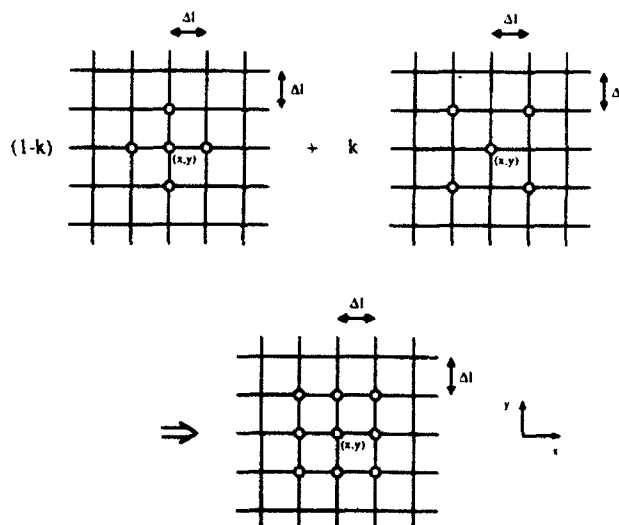


Figure 2. Weighted combination of two 5-point stencils



where  $k$  is a weighting factor restricted between zero and one (and again the right-hand side of (4) is evaluated at the spatial location  $(x, y)$ ). This scheme uses the same grid as the semi-discretization (3) and has the same memory storage requirements.

With the appropriate selection of  $k$ , the propagation characteristics of (4) become isotropic i.e., the propagation velocity becomes independent of the direction of propagation. In this paper we investigate time-dependent rather than time-harmonic solutions of (2). Therefore approximation of the temporal derivative in (4) is required. Using a second-order-accurate central difference approximation, (4) becomes,

$$\begin{aligned}
 (1-k) & \left\{ \frac{E_z(x+\Delta l, y) - 2E_z(x, y) + E_z(x-\Delta l, y)}{\Delta l^2} \right. \\
 & \left. + \frac{E_z(x, y+\Delta l) - 2E_z(x, y) + E_z(x, y-\Delta l)}{\Delta l^2} \right\} \\
 & + k \left\{ \frac{E_z(x+\Delta l, y+\Delta l) - 2E_z(x, y) + E_z(x-\Delta l, y-\Delta l)}{(\sqrt{2}\Delta l)^2} \right. \\
 & \left. + \frac{E_z(x+\Delta l, y-\Delta l) - 2E_z(x, y) + E_z(x-\Delta l, y+\Delta l)}{(\sqrt{2}\Delta l)^2} \right\} \\
 & = \epsilon \mu \frac{E_z^{t+\Delta t}(x, y) - 2E_z^t(x, y) + E_z^{t-\Delta t}(x, y)}{\Delta t^2} \quad (5)
 \end{aligned}$$

where  $\Delta t$  denotes the time step, and the left-hand side of (5) is evaluated at time  $t$ . (5) represents an explicitly time-stepped finite difference algorithm for the solution of (2). We classify this algorithm as an explicitly-time-stepped, second-order-accurate in time, and geometrically weighted second-order-accurate in space, FD algorithm. Trefethen<sup>11</sup> has investigated this algorithm and determined the conditions for approximate numerical isotropy.

The dispersion relation for a numerical method yields the relationship between the dispersed (or numerical) and mathematically exact quantities. We use the notation of Vichnevetsky and Bowles,<sup>10</sup> where dispersed quantities are denoted by  $a^*$  superscript and physical (exact) quantities are otherwise unscripted. In the following section, the dispersive analysis of the equivalent TLM model is outlined. It is necessary to distinguish the quantities associated with the elemental transmission lines of the model from both the numerical and physical quantities. We use an  $(l)$  subscript to denote elemental transmission line quantities. A monochromatic numerical plane wave propagating through the numerical mesh at an angle  $\phi$  to the  $x$  axis can be expressed as,

$$E_z = E_0 e^{j\omega t + j\beta^* (x \cos \phi + y \sin \phi)} \quad (6)$$

where  $\beta^*$  represents the numerical phase constant. Frequency is regarded as an absolute quantity defined in terms of numerical or exact quantities,

$$f = \frac{c^*}{\lambda^*} = \frac{c^* \beta^*}{2\pi} = \frac{c}{\lambda} = \frac{c \beta}{2\pi} \quad (7)$$

where  $c^*$  and  $\lambda^*$  are the numerical propagation velocity and wavelength, respectively;  $c$ ,  $\lambda$ , and  $\beta$  are the exact propagation velocity, wavelength and phase constant, respectively ( $c = (\epsilon \mu)^{-1/2}$ ). Substitution of (6) into (5) yields the dispersion relation for the finite difference algorithm,

$$\begin{aligned}
 & \frac{k}{2} \left\{ \sin^2 \frac{\beta^* \Delta l (\cos \phi + \sin \phi)}{2} + \sin^2 \frac{\beta^* \Delta l (\cos \phi - \sin \phi)}{2} \right\} \\
 & + (1-k) \left\{ \sin^2 \frac{\beta^* \Delta l \cos \phi}{2} + \sin^2 \frac{\beta^* \Delta l \sin \phi}{2} \right\} = \frac{\Delta l^2}{c^2 \Delta t^2} \sin^2 \frac{\omega \Delta t}{2} \quad (8)
 \end{aligned}$$

Expression (8) describes the fundamental manner in which plane waves propagate through an

infinite FD grid. Given a spatial and temporal discretization ( $\Delta l$  and  $\Delta t$  respectively), frequency of excitation ( $\omega$ ), direction of propagation ( $\phi$ ), and the weighting factor ( $k$ ), the numerical phase constant ( $\beta^*$ ) can be obtained from (8). This value can be compared to the exact physical phase constant to determine the amount of dispersion introduced by the algorithm. Therefore, (8) is a fundamental representation of the fidelity of the algorithm as a method for the simulation of wave propagation.

The stability criterion for this algorithm (obtained using the Von Neumann method, discussed in Reference 12) is given by,

$$\Delta t \leq \frac{1}{\sqrt{2-k}} \frac{\Delta l}{c} \quad (9)$$

### 3. TRANSMISSION-LINE MATRIX MODEL

#### 3.1. Synthesis

We now synthesize a TLM model equivalent to the FD algorithm presented in the previous section. The FD algorithm is constructed from the weighted combination of two second-order-accurate central difference stencils, one oriented as usual (arms of the stencil located along the  $x$  and  $y$  axis), the other rotated by  $45^\circ$  with its arms extended by a factor of  $(2)^{1/2}$ . It has been demonstrated that the original TLM model<sup>1</sup> and the FD algorithm (3) (with temporal derivatives approximated by a second-order-accurate central difference approximation) are equivalent.<sup>6</sup> Therefore, the new TLM model should consist of the weighted combination of two original models. One oriented as usual (with elemental transmission lines oriented along the  $x$  and  $y$  axis), the other rotated by  $45^\circ$  with its arms extended by a factor of  $(2)^{1/2}$ . The basic geometry of the model is shown in Figure 3. The new model is realized as a shunt connection of transmission lines (as in Reference 1). A mesh of nodes is provided in Figure 4. Note that a direct electrical connection between diagonal and axial transmission lines exists only at the centres of nodes, located at even multiples of  $\Delta l$  in both the  $x$ - and  $y$ -directions (denoted by the black dots in the figure). To

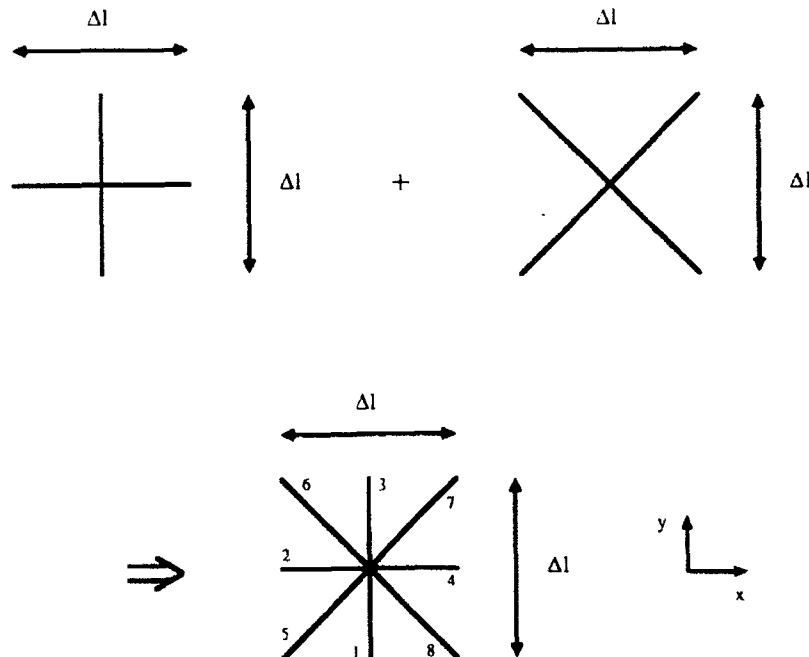


Figure 3. Basic geometry of the new TLM model, created from the combination of two original models

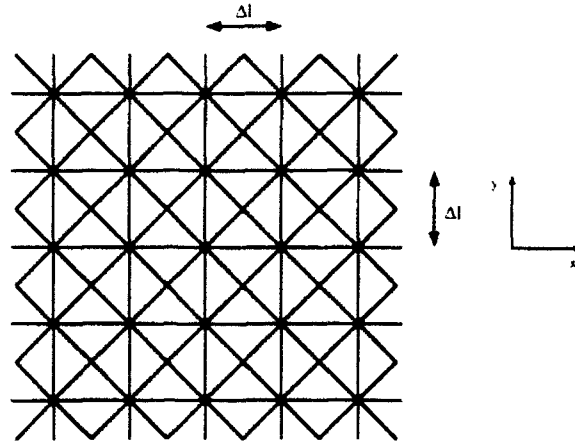


Figure 4. Mesh of new nodes. Electrical connections in the mesh are denoted by black dots. These spatial locations are the centres of nodes

complete the model, the electrical characteristics of the elemental transmission lines must be determined.

The electrical circuit analogue of a weighting factor is a variable impedance. To implement the ability to weight the two interconnected original models, the diagonal and axial elemental transmission lines are permitted to have different characteristic impedances. The intrinsic impedance of the axial elemental transmission lines (i.e., associated with the original model with elemental transmission lines along the  $x$  and  $y$  axis) is  $Z_l$ , and the intrinsic impedance of the diagonal transmission lines (i.e., associated with the original model rotated by  $45^\circ$ ) is  $mZ_l$ , where  $m$  is the impedance weighting factor ( $0 \leq m < \infty$ ).

In the evaluation of the FD algorithm (5), communication of information between spatial locations in the axial direction takes place at the same speed as communication of information between spatial locations in the diagonal direction. Therefore, propagation along diagonal elemental transmission lines should be  $(2)^{1/2}$  times faster than propagation along the axial elemental transmission lines, or

$$v_i' = \sqrt{2} v_j' \quad (10)$$

where  $v_i'$  refers to the propagation velocity along the  $n$ th elemental transmission-line,  $j = 5-8$ , and  $i = 1-4$ . A beneficial consequence of (10) is that the synchronism of voltage pulses is preserved in the new model. The electrical and geometrical description of the new model is complete.

### 3.2. Propagation analysis

The topology of the model is provided in Figure 5. To model a medium of arbitrary permittivity, an open circuit stub is added to the centre of a TLM node.<sup>9</sup> The new model is the weighted combination of two original shunt nodes. Therefore, to maintain consistency, two open circuit stubs are added. One of length  $\Delta l/2$  and admittance  $Y_0/Z_l$  (associated with the shunt node with elemental transmission lines along the  $x$  and  $y$  axis), the other length  $\Delta l/(2^{1/2})$  and admittance  $Y_0/mZ_l$  (associated with the rotated shunt node).

The propagation analysis of the model proceeds in the same manner as performed in References 6, 8 and 13. Superposition and transmission-line theory yield the characteristic equation which describes the behaviour of voltages on the model,

$$2(m+1) \left( 2 \cos \beta_l \Delta l - Y_0 \sin^2 \frac{\beta_l \Delta l}{2} \right) = m \sum_{i=1}^4 v_i + \sum_{j=5}^8 v_j \quad (11)$$

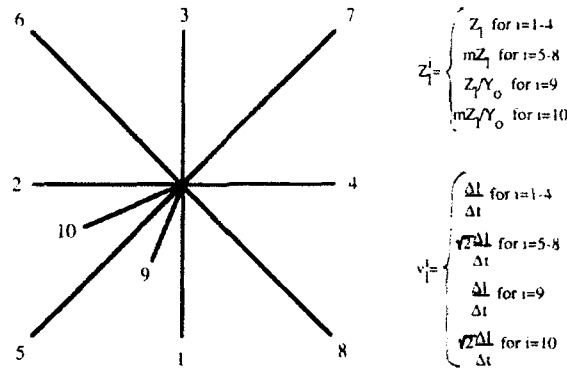


Figure 5. Complete electrical and geometric description of the new model with permittivity stubs

A monochromatic numerical plane voltage wave propagating through the numerical mesh at an angle  $\phi$  to the  $x$  axis can be expressed as,

$$V_z = V_0 e^{j\omega t + j\beta^* (x \cos \phi + y \sin \phi)} \quad (12)$$

where the parameters in the exponential term of (12) are as defined in section 2. Substitution of (12) into (11) yields the dispersion relation for the TLM model,

$$\sin^2 \frac{\beta^* \Delta l (\cos \phi + \sin \phi)}{2} + \sin^2 \frac{\beta^* \Delta l (\cos \phi - \sin \phi)}{2} + m \left\{ \sin^2 \frac{\beta^* \Delta l \cos \phi}{2} + \sin^2 \frac{\beta^* \Delta l \sin \phi}{2} \right\} = \frac{m+1}{2} (4 + Y_0) \sin^2 \frac{\beta_l \Delta l}{2} \quad (13)$$

Expression (13) describes the fundamental manner in which plane waves propagate through an infinite TLM mesh. Given a spatial discretization ( $\Delta l$ ), frequency of excitation (described through  $\beta_l$ ), direction of propagation ( $\phi$ ), and the electrical properties of the model ( $m$  and  $Y_0$ ), the numerical phase constant ( $\beta^*$ ) can be obtained from (13). This value can be compared to the exact physical phase constant to determine the amount of dispersion introduced by the model. Therefore, (13) is a fundamental representation of the fidelity of the model as a method for the simulation of wave propagation.

### 3.3. Equivalence of the TLM model and FD algorithm

We now establish the equivalence of the TLM and FD methods and demonstrate that both can represent identical models for wave propagation. This is accomplished by determining the conditions for which (8) and (13) are equivalent.

The term  $\beta_l \Delta l$  in the right-hand side of (13) can be re-expressed as  $\omega \Delta t$  by noting the following relationships,

$$\beta_l = \frac{2\pi}{\lambda_l} \quad (14a)$$

$$\lambda_l = \frac{2\pi v_l}{\omega} \quad (14b)$$

$$v_l = \frac{\Delta l}{\Delta t} \quad (14c)$$

(14b) is a direct extension of (7), (i.e., frequency is considered as an absolute quantity and can be defined in terms of exact, numerical, or elemental transmission-line quantities). If we divide the FD dispersion relation (8) by  $k/2$  we obtain,

$$\sin^2 \frac{\beta^* \Delta l (\cos \phi + \sin \phi)}{2} + \sin^2 \frac{\beta^* \Delta l (\cos \phi - \sin \phi)}{2} + \frac{2(1-k)}{k} \left\{ \sin^2 \frac{\beta^* \Delta l \cos \phi}{2} + \sin^2 \frac{\beta^* \Delta l \sin \phi}{2} \right\} = \frac{2\Delta l^2}{kc^2 \Delta t^2} \sin^2 \frac{\omega \Delta t}{2} \quad (15)$$

(15) and (13) have fundamentally the same form. Equating coefficients of the left-hand side of (8) and (13) yields the relationship between the TLM and FD weighting factors,

$$m = \frac{2(1-k)}{k} \quad (16a)$$

or

$$k = \frac{2}{m+2} \quad (16b)$$

Equating the coefficients on the right-hand side of (15) and (13) yields,

$$c = \frac{2}{\sqrt{k(m+1)(4+Y_0)}} \frac{\Delta l}{\Delta t} \quad (17a)$$

substitution of (16a) into (17a) yields,

$$c = \frac{2}{\sqrt{(2-k)(4+Y_0)}} \frac{\Delta l}{\Delta t} \quad (17b)$$

or if we desire  $c$  in terms of TLM model parameters alone, substitution of (16a) and (14c) into (17b) yields,

$$c = \sqrt{\frac{2(m+2)}{(m+1)(4+Y_0)}} v_l \quad (17c)$$

If the FD algorithm is operated such that (17b) is satisfied, the dispersion relations for both are identical, and therefore the two methods fundamentally represent identical methods for the simulation of wave propagation.

It is interesting to note that for the condition  $Y_0 = 0$  (a 'free space' TLM model), the condition (17b) corresponds to the upper limit of the FD stability range. As was found for the original node and the Yee algorithm,<sup>6</sup> the TLM model and FD algorithm are identical when the latter is operated at the upper limit of its stability range. This was not the case for the hexagonal TLM and FD methods.<sup>8</sup>

If we return to the context of modelling electromagnetic phenomena, we can establish the relationship between the admittance of the open circuit stub and the material properties of the medium modelled by the entire model. The physical propagation velocity is defined as,

$$c = \frac{1}{\sqrt{\epsilon_r \epsilon_0 \mu_r \mu_0}} \quad (18)$$

where  $\epsilon_r$  and  $\mu_r$  are the relative permittivity permeability, respectively and  $\epsilon_0$  and  $\mu_0$  are the free space permittivity and permeability, respectively. Relating this to the propagation velocity in the TLM model (given by (17c)), we obtain,

$$\frac{1}{\sqrt{\epsilon_r \epsilon_0 \mu_r \mu_0}} = \sqrt{\frac{2(m+2)}{(m+1)(4+Y_0)}} \frac{\Delta l}{\Delta t} \quad (19)$$

If we consider the case  $Y_0 = 0$  to represent free space, i.e.,  $\epsilon_r = \mu_r = 1$ , (19) becomes,

$$\frac{1}{\epsilon_0 \mu_0} = \frac{(m+2) \Delta l^2}{2(m+1) \Delta r^2} \quad (20)$$

The relative permittivity and relative permeability are related to the stub admittance  $Y_0$  by,

$$\epsilon_r \mu_r = \left(1 + \frac{Y_0}{4}\right) \quad (21)$$

#### 4. PROPAGATION CHARACTERISTICS

Numerical models for wave propagation represent a discretized medium that is both dispersive and anisotropic, i.e., the propagation velocity of waves in the numerical mesh depends on both the frequency content of a signal and the direction of propagation. This undesired effect is referred to as velocity error and is determined from the dispersion relation for the particular model. The ratio  $c^*/c$  (the ratio of the numerical propagation velocity to the physical propagation velocity), can be used as a quantitative measure of velocity error. The TLM dispersion relation (13) can be rewritten as,

$$\begin{aligned} & \sin^2 \pi (\cos \phi + \sin \phi) \frac{\Delta l}{\lambda^*} + \sin^2 \pi (\cos \phi - \sin \phi) \frac{\Delta l}{\lambda^*} \\ & + m \left\{ \sin^2 \pi \cos \phi \frac{\Delta l}{\lambda^*} + \sin^2 \pi \cos \phi \frac{\Delta l}{\lambda^*} \right\} \\ & = \frac{m+1}{2} (4 + Y_0) \sin^2 \pi \sqrt{\frac{2(m+2)}{(m+1)(Y_0+4)}} \frac{\Delta l}{\lambda} \end{aligned} \quad (22)$$

Given the free space discretization ratio ( $\Delta l/\lambda$ ), direction of propagation ( $\phi$ ), and the electrical properties of the model ( $m$  and  $Y_0$ ), (22) can be searched to determine the dispersed discretization ratio ( $\Delta l/\lambda^*$ ). Given  $\Delta l/\lambda$  and  $\Delta l/\lambda^*$ , the ratio  $c^*/c$  can be determined from,

$$\frac{c^*}{c} = \frac{\Delta l/\lambda}{\Delta l/\lambda^*} \quad (23)$$

In Figure 6(a), (b), (c), (d), (e), and (f),  $c^*/c$  is provided as a function of  $\phi$  for  $m = 900, 6, 4, 3, 2$  and  $0.01$ , respectively. For each case, contours for  $\Delta l/\lambda = 0.10, 0.20, 0.30$ , and  $0.35$  are provided ( $Y_0 = 0$  for all cases). Note that in light of the equivalence established in section 3.3, Figure 6(a), (b), (c), (d), (e) and (f) are applicable to the FD algorithm provided the FD algorithm is operated at its upper limit of stability,  $\epsilon_r = \mu_r = 1$  and  $k = 0.002217, 0.25, 0.333, 0.4, 0.5$ , and  $0.995$ , respectively.

In the limit as  $m$  approaches infinity, the new model is equivalent to a mesh of original nodes<sup>1</sup> with elemental transmission lines oriented along the  $x$  and  $y$  axis. In Figure 7,  $c^*/c$  is provided as a function of  $\phi$  for the original model<sup>1</sup> (for  $Y_0 = 0$ ). As expected the contours of Figure 7 and Figure 6(a) are indistinguishable. In the limit as  $m$  approaches zero, the new model is equivalent to the original model rotated by  $45^\circ$  and mesh spacing extended by a factor of  $(2)^{1/2}$ . In Figure 8,  $c^*/c$  is provided as a function of  $\phi$  for the original model rotated by  $45^\circ$  and mesh spacing extended by a factor of  $(2)^{1/2}$  (for  $Y_0 = 0$ ). As expected the contours of Figure 8 and Figure 6(f) are indistinguishable.

For moderate values of  $m$ , directions for propagation with no dispersion do not exist with the new model. From the results of Figure 7, we note that no numerical dispersion exists for waves which propagate diagonally through the mesh ( $\phi = 45^\circ + n90^\circ, n = 0, 1, 2, 3$ ). Numerical dispersion is maximum for axial propagation ( $\phi = n90^\circ, n=0, 1, 2, 3$ ). For the rotated original model, the complementary situation is present. No numerical dispersion exists for ( $\phi = n90^\circ, n = 0, 1, 2, 3$ ), and numerical dispersion is maximum for ( $\phi = 45^\circ + n90^\circ, n = 0, 1, 2, 3$ ). From Figure 6(b)–(e) we note that the new model blends the propagation characteristics of the original and rotated original models. Therefore, propagation along the directions for maximum numerical

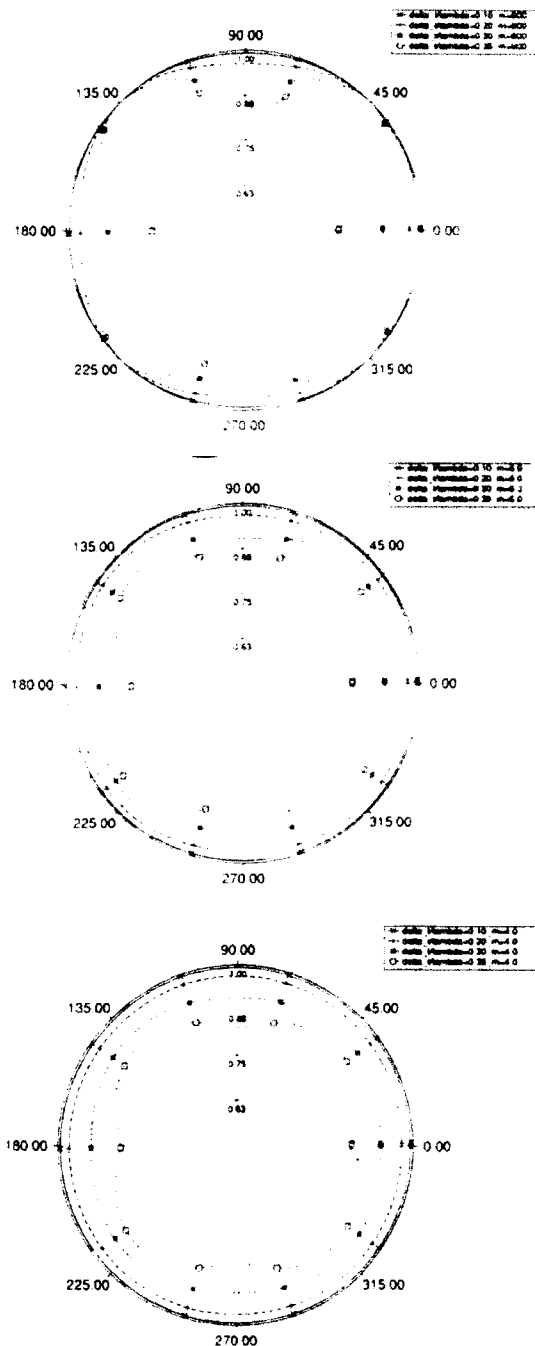


Figure 6. Contours of  $c^*/c$  for the new TLM model ( $Y_0 = 0$ ) for (a)  $m = 900$ , (b)  $m = 6$ , (c)  $m = 4$ , (d)  $m = 3$ , (e)  $m = 2$  and (f)  $m = 0.01$

dispersion is improved, but directions for perfect propagation are eliminated. Therefore, in this context the propagation characteristics of the original model are superior to those of the new model.

However, from Figure 6 it can be noted that for the appropriate selection of the weighting factor, the new model can possess propagation characteristics with approximate isotropy. The appropriate conditions have been investigated in the context of the equivalent FD algorithm.<sup>10,11</sup> The appropriate weighting factor for the semi-discretization (4) is  $k = 0.5$  (see Reference 10).

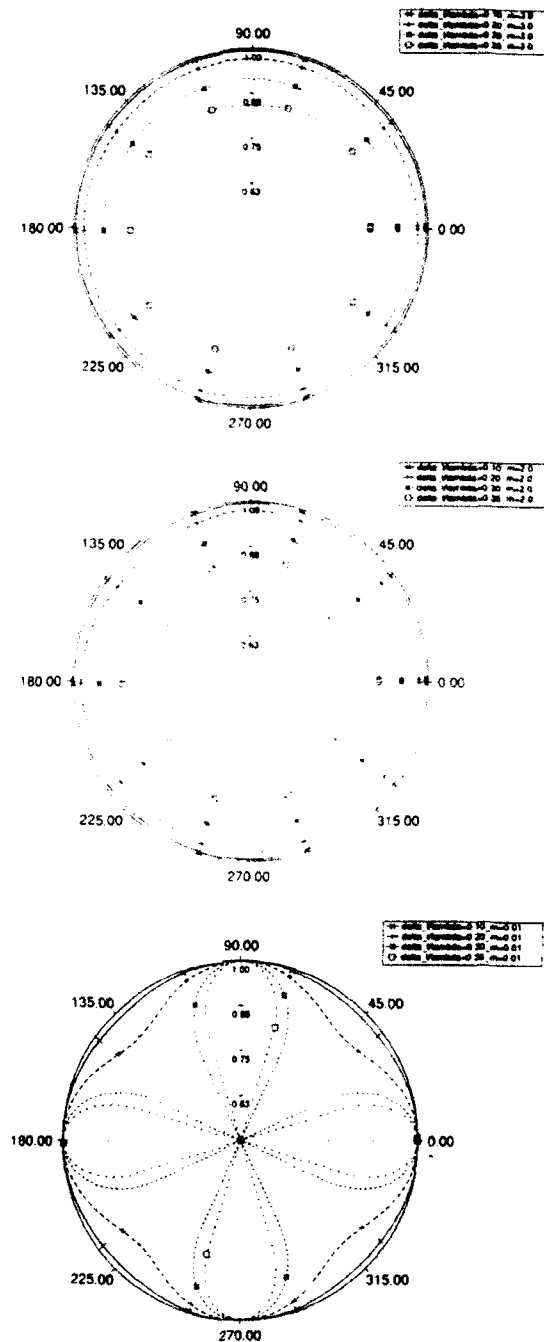


Figure 6. Continued

For the full discretization (5), Trefethen<sup>11</sup> has determined a weighting factor of  $k = 1/3$  provides isotropy to order  $(\Delta t)^4$  (note that the difference in  $k$  for the semi-discretization and full discretization is a result of effect of temporal discretization in the later). Therefore, isotropy to order  $(\Delta t)^4$  should be obtained from the new TLM model for  $m = 4.0$  (using (16a) to convert  $k$  to  $m$ ), as shown in Figure 6(c).

Obtaining approximate numerical isotropy is equivalent to reducing the dependence of the propagation velocity on the direction of propagation. Consider the simulation of a homogeneous problem that employs a regular mesh. If the numerical propagation velocity is independent of the



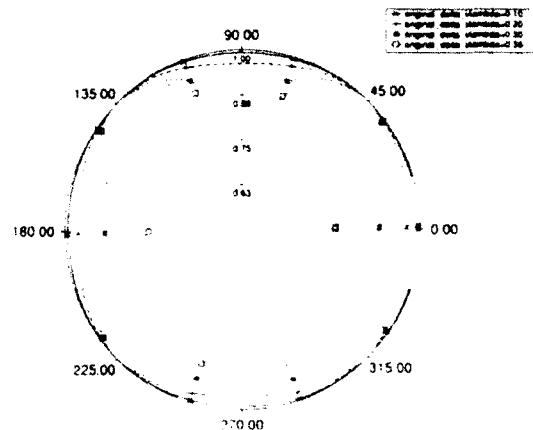


Figure 7. Contours of  $c^*/c$  for the original TLM model.<sup>1</sup> Contours are indistinguishable from those of Figure 6(a)

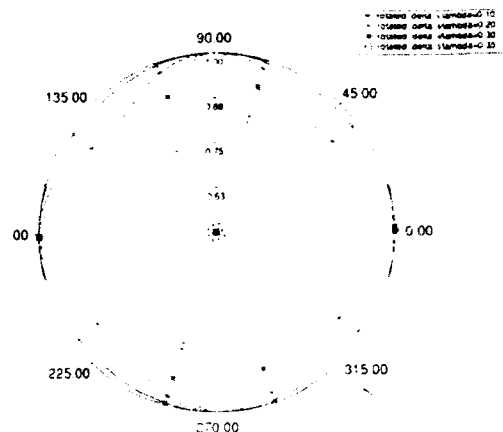


Figure 8. Contours of  $c^*/c$  for the original TLM model rotated by  $45^\circ$  and mesh spacing extended by a factor  $(2)^{1/2}$ . Contours are indistinguishable from those of Figure 6(f)

direction of propagation, the amount of velocity error at a given frequency can be accurately estimated from the dispersion relation. Therefore, after the simulation is complete, the velocity error can be corrected at each output frequency. This method was used in Reference 8 (with the hexagonal two-dimensional TLM model) to correct for the cutoff frequencies in a rectangular waveguide with no *a priori* assumption regarding the directional dependence of a particular mode. In this context the propagation characteristics of the new model can be considered as superior to those of the original model.<sup>1</sup>

In Figure 9, the propagation characteristics of the new model and the hexagonal TLM model<sup>8</sup> are compared. The ratio  $c^*/c$  is provided as a function of the physical discretization ratio ( $\Delta l/\lambda$ ) for propagation directions  $\phi = 0^\circ, 22.5^\circ, 39^\circ$ , and  $45^\circ$  for (a) the new model with  $m = 3.0$ , (b) the new model with  $m = 4.0$  and (c) the hexagonal TLM model. The results contained in the figure indicate that the hexagonal model is superior to the new model in terms of both the cutoff frequency of the model, and the degree of approximate isotropy. Therefore, in the context of isotropic models for the simulation of wave propagation, the hexagonal model is preferred.

An advantage of the new node is that it is realized on a regular grid with equal spacing in the  $x$ - and  $y$ -directions ( $\Delta l$ ). The hexagonal model is also realized using a mesh with equal inter-nodal spacing. However, owing to the nature of the hexagonal grid, the spacing in the  $x$ - and  $y$ -directions is unequal,  $\Delta l$  and  $(3)^{1/2}\Delta l/2$ , respectively. This creates a disadvantage for the hexagonal model in the modelling of structures with regular geometric features.

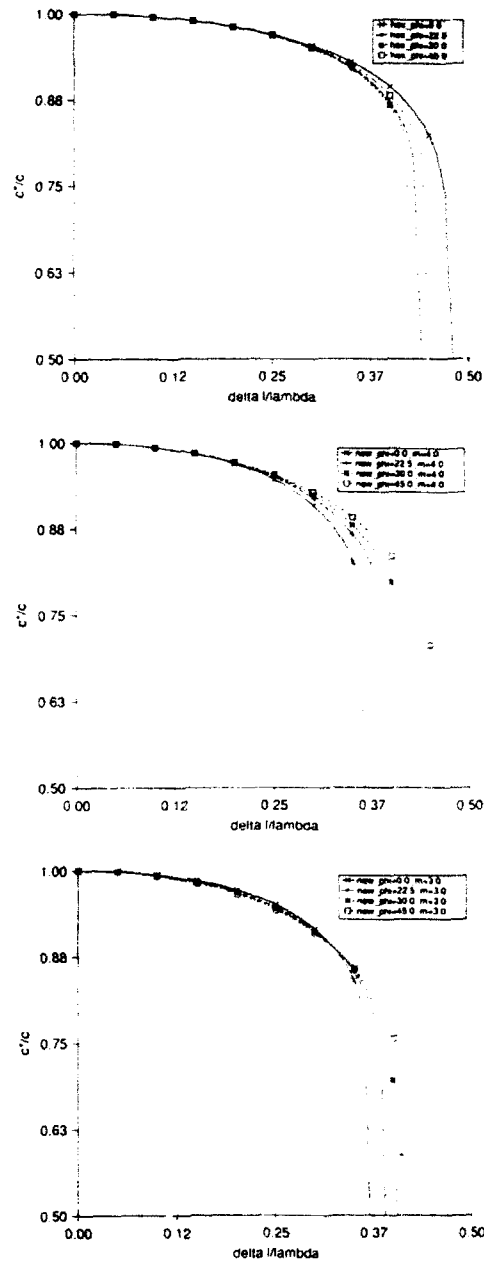


Figure 9.  $c^*/c$  versus  $\Delta/\lambda$  (the exact (physical) discretization ratio) for various of  $\phi$  for (a) the new model with  $m = 3$ , (b) the new model with  $m = 4$  and (c) the hexagonal TLM model

## 5. NUMERICAL IMPLEMENTATION AND RESULTS

### 5.1. Scattering matrix

In the previous sections we have examined some of the theoretical aspects of the new TLM model. We now describe the numerical implementation of the model in terms of the traditional scattering and transfer events.<sup>2,3</sup> TLM algorithms operate by simulating the progression of voltage pulses as they are scattered throughout the mesh of transmission lines. Applying the appropriate initial conditions and reflection coefficients (to model boundary conditions) the transmission-line

simulation becomes analogous to an electromagnetic field problem. The implementation of the new model follows the same procedure as all other models, i.e., scattering of incident impulses at the junction of nodes and transfer of the reflected pulses to adjacent nodes. The algorithm can be expressed formally as,

$${}_k V^r = S {}_k V^i \quad (24)$$

and

$${}_{k+1} V^i = C {}_k V^r \quad (25)$$

where  ${}_k V^i$  and  ${}_k V^r$  are the vectors of the incident and reflected voltage pulses at all nodes at time-step  $k$ ,  $S$  is the global scattering matrix describing the interaction of pulses at all nodes in the mesh, and  $C$  is the connection matrix describing how nodes are connected (and includes the boundary conditions for the particular problem). These two equations include all information required to perform the simulation.

The nodal scattering matrix can be assembled by examining the reflection and transmission coefficients of a voltage pulse on each of the ten elemental transmission lines of the model. A voltage pulse on the  $i$ th elemental transmission line 'sees' a reflection coefficient of,

$$\Gamma = \frac{Z_L - Z_i}{Z_L + Z_i} \quad (26)$$

where  $Z_L$  is the parallel combination of all but the  $i$ th elemental transmission line and  $Z_i$  is the intrinsic impedance of the  $i$ th elemental transmission line. The intrinsic impedance of the elemental transmission lines (from section 3.1 and shown in Figure 5), is,

$$Z_i = \begin{cases} Z_l & \text{for } i = 1-4 \\ mZ_l & \text{for } i = 5-8 \\ Z_l/Y_0 & \text{for } i = 9 \\ mZ_l/Y_0 & \text{for } i = 10 \end{cases} \quad (27)$$

The associated transmission coefficient is,

$$T = 1 + \Gamma \quad (28)$$

From (26)–(28), the nodal scattering matrix can be assembled as,

$$\begin{bmatrix} v_1 \\ v_2 \\ v_3 \\ v_4 \\ v_5 \\ v_6 \\ v_7 \\ v_8 \\ v_9 \\ v_{10} \end{bmatrix} = \begin{bmatrix} a & b & b & b & d & d & d & d & f & h \\ b & a & b & b & d & d & d & d & f & h \\ b & b & a & b & d & d & d & d & f & h \\ b & b & b & a & d & d & d & d & f & h \\ b & b & b & b & c & d & d & d & f & h \\ b & b & b & b & d & c & d & d & f & h \\ b & b & b & b & d & d & c & d & f & h \\ b & b & b & b & d & d & d & c & f & h \\ b & b & b & b & d & d & d & d & e & h \\ b & b & b & b & d & d & d & d & f & g \end{bmatrix} \begin{bmatrix} v_1 \\ v_2 \\ v_3 \\ v_4 \\ v_5 \\ v_6 \\ v_7 \\ v_8 \\ v_9 \\ v_{10} \end{bmatrix} \quad (29)$$

where

$$a = \frac{-2m - 4 - Y_0(m+1)}{4 + 4m + Y_0(m+1)}$$

$$\begin{aligned}
b &= \frac{2m}{4 + 4m + Y_0(m+1)} \\
c &= \frac{-2 - 4m - Y_0(m+1)}{4 + 4m + Y_0(m+1)} \\
d &= \frac{2}{4 + 4m + Y_0(m+1)} \\
e &= \frac{-4 - 4m - Y_0(1-m)}{4 + 4m + Y_0(m+1)} \\
f &= \frac{2mY_0}{4 + 4m + Y_0(m+1)} \\
g &= \frac{-4 - 4m - Y_0(m-1)}{4 + 4m + Y_0(m+1)} \\
h &= \frac{2Y_0}{4 + 4m + Y_0(m+1)}
\end{aligned}$$

The nodal transfer event is described by,

$$\begin{aligned}
v_1^i(i,j) &= v_3^i(i,j-1) \\
v_2^i(i,j) &= v_4^i(i-1,j) \\
v_3^i(i,j) &= v_1^i(i,j+1) \\
v_4^i(i,j) &= v_2^i(i+1,j) \\
v_5^i(i,j) &= v_7^i(i-1,j-1) \\
v_6^i(i,j) &= v_8^i(i-1,j+1) \\
v_7^i(i,j) &= v_5^i(i+1,j+1) \\
v_8^i(i,j) &= v_6^i(i+1,j-1) \\
v_9^i(i,j) &= v_9^i(i,j) \\
v_{10}^i(i,j) &= v_{10}^i(i,j)
\end{aligned} \tag{30}$$

where  $(i,j)$  denotes the discrete  $(x,y)$  location of a node in the mesh.

If the TLM method is considered as a differential-equation-based numerical method for solving (2), (29) and (30) represent the approximate model for wave propagation (in the same way the FD method is considered as a differential-equation-based numerical method for solving (2) and (5) represents the approximate model for wave propagation). The solution of a specific problem requires the application of initial and boundary conditions. The treatment of boundary conditions is an important subject for the practical application of the method. In this paper we are primarily concerned with the development of the new TLM model as an approximate model for wave propagation and establishing the equivalence with the FD algorithm. Therefore we do not treat the subject of boundary conditions in detail. The traditional methods of specifying reflection coefficients at locations half-way between the centres of nodes (in both the axial and diagonal direction) should be applicable.<sup>2,3</sup> Potential users should be cautioned that the intrinsic impedance of the elemental transmission lines is not always the same for this model and care should be taken in the evaluation of the appropriate reflection coefficients for a specific boundary condition. The method described by Chen *et al.*<sup>14</sup> of enforcing boundary conditions at the centre of nodes should also be applicable to the new model.

## 5.2. Calculation of cutoff frequencies

To validate the new TLM model, we investigate the traditional TLM application of the calculation of cutoff frequencies of various modes in a waveguide.<sup>2,3</sup> The cross-section of the partially

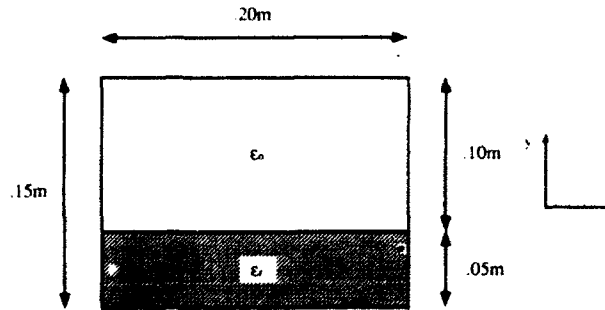


Figure 10. The geometry of the waveguide cross-section analysed using the new TLM model

Table I. Cutoff frequencies (in GHz) for rectangular waveguide

Mode	New TLM model	Analytical <sup>15</sup>	% difference
(1,1)	1.244	1.2490	0.4
(1,2)	1.784	1.8015	0.9
(2,1)	2.126	2.1345	0.4
(1,3)	2.429	2.4605	1.3
(2,2)	2.481	2.4983	0.7

Table II. Cutoff frequency (in GHz) of the dominant mode in partially filled waveguide

$\epsilon_r$	New TLM model	Finite element <sup>16</sup>	% difference
2.5	1.054	1.063	0.8
5.0	0.846	0.852	0.7
10.0	0.614	0.623	1.4

filled rectangular waveguide and the physical dimensions are provided in Figure 10. The walls of the guide are considered to be perfectly conducting. To realize this boundary condition, reflection coefficients of magnitude  $-1.0$  are placed at locations half-way between nodes. A mesh spacing of  $\Delta l = 0.01$  metres is selected, resulting in a total TLM mesh with 20 nodes in the  $x$ -direction and 15 nodes in the  $y$ -direction. Calculations were performed such that the true physical cutoff frequencies are obtained directly from the simulation. Normalization for a non-free space medium is not required.

The TLM simulation yields the cutoff frequencies of TM modes. Table I contains the cutoff frequencies for the first five modes for  $\epsilon_r = 1.0$  ( $Y_0 = 0$ ). A total of 1000 iterations (i.e.,  $1000\Delta t$ , where  $\Delta t$  can be obtained from (17c)) and a weighting factor of  $m = 6$  was used. The TLM results are compared to analytical results.<sup>15</sup> The percentage difference is provided in the table. Reasonable accuracy is obtained. In Table II, the cutoff frequency of the dominant mode is provided for  $\epsilon_r = 2.5$ , 5 and 10. As a comparison results generated by a finite element code are provided.<sup>16</sup> Again, reasonable agreement is obtained.

## 6. CONCLUSIONS

In this paper we have presented a new TLM model for the simulation of the two-dimensional wave equation. The TLM model was synthesized directly from an FD algorithm<sup>10,11</sup> as a shunt connection of two-wire transmission lines. The new model is a spatially weighted connection of two original models.<sup>1</sup> One oriented as usual, the other rotated by  $45^\circ$ . The weighting is accomplished through the use of a variable intrinsic impedance for specific elemental transmission lines. Synchronism is maintained by increasing the propagation velocity along diagonal elemental

transmission lines. In general, the synthesis of other TLM models from FD algorithms is possible using the same basic steps.

The relationship between the FD algorithm and TLM model is established through the equivalence of propagation characteristics. We feel this is the most fundamental method for establishing the relationship between a TLM model and another numerical method. It is possible to demonstrate that the TLM model satisfies the FD algorithm (by examining the scattering and transfer of voltage pulses at a node and its neighbours). In Reference 17, the original TLM model was shown to satisfy the two-dimensional Yee algorithm. To demonstrate the equivalence, the definitions for magnetic field quantities in terms of voltage pulses were altered. Rather than define the magnetic field components at the centres of nodes at each iteration, the magnetic fields were defined at the intersection of nodes at half iterations. Chen *et al.*<sup>18</sup> have recently reported a complete algorithmic equivalence of two- and three-dimensional TLM models and FD algorithms. We regard the calculation of field values from voltage pulses to be a post-processing task associated with the TLM method. The basic algorithm (scattering and transfer of voltage pulses) operates independently of these definitions. One of the often-quoted advantages of the TLM approach is the ability to define field components at various spatial and temporal locations (as long as a certain consistency is maintained). Therefore, we feel that establishing an equivalence between a TLM model and another numerical method without specific definitions for field quantities in the TLM model, is the most fundamental and rigorous. We accomplish this by demonstrating the propagation characteristics of the TLM model and FD algorithm are identical if the latter is operated at the upper limit of its stability range.

The propagation characteristics of the new model have been examined. For moderate values of  $m$ , directions for propagation with no dispersion do not exist for the new model. Therefore, in this context the propagation characteristics of the original model are superior to those of the new model. However, an advantage of the new model is that for appropriate values of  $m$ , approximate numerical isotropy is obtained. This allows the model to be combined with an error-correction method to remove the contribution of velocity error from the results.<sup>8</sup> Comparison of the characteristics of the new model to those of the hexagonal TLM model<sup>18</sup> indicate the hexagonal model is preferred (in terms of both the amount of approximate numerical isotropy and cutoff frequency). This conclusion is supported by analogous finite element (FE) studies. Consider the relationship of the various FD algorithms and TLM models (References 6 and 8, and section 3 of this paper), and the relationship of the FD and FE methods.<sup>19,20</sup> Based on these relationships, the original TLM model<sup>1</sup> is analogous to using square quadrilateral finite elements of sides  $\Delta l$ ; the hexagonal TLM model<sup>18</sup> is analogous to using equilateral triangular finite elements, each triangle having sides of  $\Delta l$  and angles of  $60^\circ$ ; and the new TLM model is in some way analogous to using right triangular finite elements, each triangle having sides of  $\Delta l$ ,  $\Delta l$ ,  $(2)^{1/2}\Delta l$  and angles  $90^\circ$ ,  $45^\circ$ ,  $45^\circ$ . Mullen and Belytschko have determined that modelling with equilateral triangles (analogous to the hexagonal TLM model) is the optimum triangular discretization if isotropy is desired.<sup>21</sup> This supports the analysis performed in this paper.

Finally, the scattering and transfer events for the new model were presented and were applied to the analysis of a rectangular waveguide partially filled with a dielectric. The cutoff frequencies calculated using the new TLM model agreed well with both analytic and numerical finite element results.

In 1976, Johns presented an interesting paper in which the original TLM model is described as a discrete form of Huygens' Principle.<sup>22</sup> Hofer has continued this view and has provided a brief historical review and description of the discretization process.<sup>3</sup> The hexagonal model can be considered as a logical extension of the original model. The improvement in numerical isotropy over the original model is intuitively obvious. The model presented in this paper could also be described as a discrete form of Huygens' Principle. However, the model would have been developed with a specific value for the weighting factor (presumably such that energy would be scattered isotropically). While selecting a variable weighting factor may be of more theoretical interest than practical value, the motivation for allowing this flexibility may not be obvious from the perspective of a discrete form of Huygens' Principle.

The original model,<sup>1</sup> the hexagonal model<sup>18</sup> and the new model presented in this paper are equivalent to FD algorithms that approximate spatial derivatives with second-order-accurate central difference formulas. The difference between the various models is the geometric configuration and weighting of the difference approximations. Future work will investigate the synthesis of a

TLM model equivalent to an FD algorithm that approximates the spatial derivatives in the wave equation with fourth-order-accurate central difference formulas.

#### ACKNOWLEDGEMENT

The authors wish to thank Mr Yves Cassivi (École Polytechnique, Montréal, Canada) for providing the finite element results contained in Table II, and the Communications Research Centre (Ottawa, Canada) for providing computational facilities.

#### REFERENCES

1. P. B. Johns and R. L. Beurle, 'Numerical solution of two-dimensional scattering problems using a transmission line matrix', *Proceedings of the IEE*, **118**, 1203-1208 (1971).
2. W. J. R. Hoefer, 'The transmission-line matrix method — theory and applications', *IEEE Trans MTT*, **33**, 882-893 (1985).
3. W. J. R. Hoefer, 'The transmission line matrix (TLM) method', in *Numerical Techniques for Microwave and Millimeter Wave Passive Structures*, T. Itoh (Ed.), John Wiley, New York, 1989.
4. K. S. Yee, 'Numerical solution of initial boundary value problems involving Maxwell's equations in isotropic media', *IEEE Trans. Ant. Propagat.*, **14**, 302-307 (1966).
5. A. Taflov and K. R. Umashankar, 'The finite-difference time-domain (FD-TD) method for electromagnetic scattering and interaction problems', *Journal of Electromagnetic Waves and Applications*, **1**, 243-267 (1987).
6. N. R. S. Simons and E. Bridges, 'Equivalence of propagation characteristics for the transmission-line matrix and finite-difference time-domain methods in two dimensions', *IEEE Trans. Microwave Theory Techniques*, **39**, 354-357 (1991).
7. D. H. Choi, 'A comparison of the dispersion characteristics associated with the TLM and FD-TD methods', *Int. J. Num. Modelling*, **2**, 203-214 (1989).
8. N. R. S. Simons and A. A. Sebak, 'New transmission-line matrix node for two-dimensional electromagnetic field problems', *Canadian J. Physics*, **69**, 1388-1398 (1991).
9. S. Akhtarzad and P. B. Johns, 'Solution of Maxwell's equations in three space dimensions and time by the TLM method of numerical analysis', *Proceedings of the IEE*, **122**, 1344-1348 (1975).
10. R. Vichnevetsky and J. B. Bowles, *Fourier Analysis of Numerical Approximations of Hyperbolic Equations*, SIAM, Philadelphia, PA, 1982.
11. L. N. Trefethen, 'Group velocity in finite difference schemes', *SIAM Review*, **24**, 113-136 (1982).
12. G. G. O'Brien, M. A. Hyman and S. Kaplan, 'A study of the numerical solution of partial differential equations', *J. Math. and Phys.*, **29**, 223-251 (1950).
13. C. R. Brewitt-Taylor and P. J. Johns, 'On the construction and numerical solution of transmission-line and lumped network models of Maxwell's equations', *Int. J. Num. Meth. Eng.*, **15**, 13-30 (1980).
14. Z. Chen, M. M. Ney and W. J. R. Hoefer, 'A new boundary description in two-dimensional TLM models of microwave circuits', *IEEE Trans. Microwave Theory Techniques*, **39**, 377-382 (1991).
15. R. F. Harrington, *Time-Harmonic Fields*, McGraw-Hill, New York, 1961.
16. Y. Cassivi, 'Conception de coupleurs directionnels micro-ondes à l'aide de la méthode des éléments finis', Mémoire de maîtrise ès sciences appliquées, Département de génie électrique, École Polytechnique de Montréal, 1991.
17. N. R. S. Simons, 'Application of the TLM method to open region field problems', M.Sc. Thesis, University of Manitoba, 1989.
18. Z. Chen, M. M. Ney and W. J. R. Hoefer, 'A new finite-difference time-domain formulation and its equivalence with the TLM symmetrical condensed node', *IEEE Trans. Microwave Theory Techniques*, **39**, 2160-2169 (1991).
19. W. G. Gray and G. F. Pinder, 'On the relationship between the finite element and finite difference methods', *Int. J. Num. Meth. Eng.*, **10**, 893-923 (1976).
20. D. R. Lynch and K. D. Paulsen, 'Origin of vector parasites in numerical Maxwell solutions', *IEEE Trans. Microwave Theory Techniques*, **30**, 383-394 (1991).
21. R. Mullen and T. Belytschko, 'Dispersion analysis of finite element semidiscretizations of the two-dimensional wave equation', *Int. J. Num. Meth. Eng.*, **18**, 11-29 (1982).
22. P. B. Johns, 'A new mathematical model to describe the physics of propagation', *The Radio and Electronic Engineer*, **44**, 657-666 (1974).

#### Authors' biographies:



Neil R. S. Simons was born in Winnipeg, Canada, in 1965. He received the B.Sc. degree with distinction in Electrical Engineering in 1987 and the M.Sc. degree in 1990, both from the University of Manitoba. From 1987 to 1989 he was employed with Quantic Laboratories, Winnipeg, Canada. He is currently a Ph.D. student at the University of Manitoba. His research interests include the numerical solution of electromagnetic field problems and applications of artificial neural networks.

Abdel Razik Sebak received the B.Sc. degree (with honours) in Electrical Engineering from Cairo University, Egypt, in 1976 and the B.Sc. degree in Applied Mathematics from Ein Shams University, Egypt, in 1978. He received the M.Eng. and Ph.D. degrees from the University of Manitoba, Winnipeg, Canada, in 1982 and 1984, respectively, both in electrical engineering.

From 1984 to 1986, he was with the Canadian Marconi Company, Kanata, Ontario, working on the design

of microstrip phased array antennas. He is currently an Associate Professor of Electrical and Computer Engineering, at the University of Manitoba. His current research interests include electromagnetic theory, computational electromagnetics, detection of subsurface conducting objects, electromagnetic interference, and integrated antennas.

Dr Sebak has served as Vice-Chairman/Treasurer (1990-91) and Chairman (1991-92) of the joint IEEE AP/MTT/VT Winnipeg Chapter. He is a Senior Member of the IEEE, and a member of the International Union of Radio Science Commission B. He was the Publicity Chairman of ANTEM'90 Symposium. Currently, he is the Finance Chairman of ANTEM'92 Symposium.



## MULTIPORT APPROACH FOR THE ANALYSIS OF MICROWAVE NON-LINEAR NETWORKS

M. I. SOBHY AND E. A. HOSNY

*Electronic Engineering Laboratories, University of Kent, Canterbury, CT2 7NT, U.K.*

AND

M. A. NASSEF

*Electrical Engineering Department, Military Technical College, Cairo, Egypt*

### SUMMARY

The state and output equations of the overall networks are derived from the state and output equations of individual multiports and knowledge of the interconnections between them. A generalized lumped-distributed L/D multiport is described by its associated state, output and non-linear equations in the time domain. Any network can be considered as composed of a set of multiports and independent sources. These equations have been incorporated into a computer-aided procedure for the analysis of L/D networks. The procedure can be used for the simulation of any non-linear microwave circuit and offers the facility of developing a multiport equivalent circuit for any linear or non-linear device or subcircuit. Several examples are successfully analysed using the developed general program.

### 1. INTRODUCTION

The analysis of non-linear dynamic networks by using state-space approach has been established since the 1960s and well documented in many reference books.<sup>5,6</sup> Computer-aided state-space analysis of lumped and lumped/distributed networks has been developed.<sup>1,3,4,7,8</sup> The capacitor voltages (or charges) and the inductor currents (or fluxes) are usually chosen as the lumped state variables. The reflected voltages at the transmission lines can be chosen as the distributed state variables. In all these cases the state and output equations are established from the circuit element values and the topology of the whole network.

It is highly desirable and convenient for circuit designers to consider the non-linear network composed of subcircuits. These subcircuits are represented by functional blocks described by a set of equations. In this case the formulation of the whole network equations starts from the top level of the subcircuits (multiports). The graph of the network is only describing the interconnection of all network multiports.

Multiport representation is common for linear networks in the frequency domain where any of the usual multiport parameters ( $x$ ,  $y$ ,  $h$ ,  $g$ ) or the scattering parameters can be used. When any of these parameters are known, the topology and element values of the multiport are no longer required. No such treatment has so far been available for non-linear networks. Non-linear networks are usually solved in the time domain either by direct integration of the network equations,<sup>1</sup> by using associated discrete circuit modelling (Spice) or by the harmonic balance technique.<sup>2</sup> In the harmonic balance method the non-linear subnetwork is still solved in the time domain. It is then a great advantage to develop a method of characterizing non-linear networks from their terminal behaviour and treat them as multiports.

In this work multiports can represent networks with lumped, distributed and non-linear elements. Each multiport is represented by non-linear state and output equations and the overall network is composed of a number of individual multiports connected in an arbitrary fashion. The state and output equations of the overall network are derived and solved in the time domain. Thus the method enables the hierarchical development of non-linear networks. At the lowest level of hierarchy the multiport equivalent is developed from individual circuit elements (linear and/or

non-linear) using a tabular approach. At the higher levels only the multiport equivalent is required. Any number of hierarchical levels can be developed.

The present formulation gives separate differential, difference and non-linear equations for the overall network and for each of the individual multiports. This leads to an efficient and numerically stable algorithm. No difficulties have been encountered in analysing networks with very unequal time constants such as microwave mixers.

The advantages of this approach are summarized below:

- (1) A large network can be divided into smaller subnetworks and the equations for each subnetwork are derived separately.
- (2) A library of subnetworks can be developed and stored for future use without the need of an equivalent circuit. This includes transistors, FETs, diodes, matching sections, filters and couplers.
- (3) The equations characterizing a non-linear device can be derived to match experimental data without the need to develop a physically realizable equivalent circuit. This gives a greater flexibility in modelling active devices.
- (4) The subnetworks developed can be used in either a direct integration subroutine or a harmonic balance subroutine.

## 2. THE GENERALIZED L/D MULTIPORT

A general multiport composed of individual multiports is shown in Figure 1. The individual multiports are composed of lumped, distributed elements and dependent sources. The lumped elements are linear and non-linear resistors, capacitors and inductors. The distributed elements are transmission lines coupled or uncoupled embedded in homogeneous or inhomogeneous media. The overall network is composed of all individual multiports and independent sources. Each multiport has current-driven and voltage-driven ports. These are ports for which either the current or the voltage is considered as the input. The  $j$ th multiport is described by

$$\bar{x}^j = A^j x^j + B^j u^j + B_n^j u_n^j \quad (1a)$$

$$y^j = C^j x^j + D^j u^j + D_n^j u_n^j \quad (1b)$$

$$F_n^j = C_n^j x^j + D_n^j u^j + D_{nn}^j u_n^j \quad (1c)$$

where

$x^j = [x_1^j(t) \ x_2^j(t)]^T$ ,  $x_1^j(t)$  and  $x_2^j(t)$  are the lumped and distributed state vectors of the  $j$ th multiport, respectively,

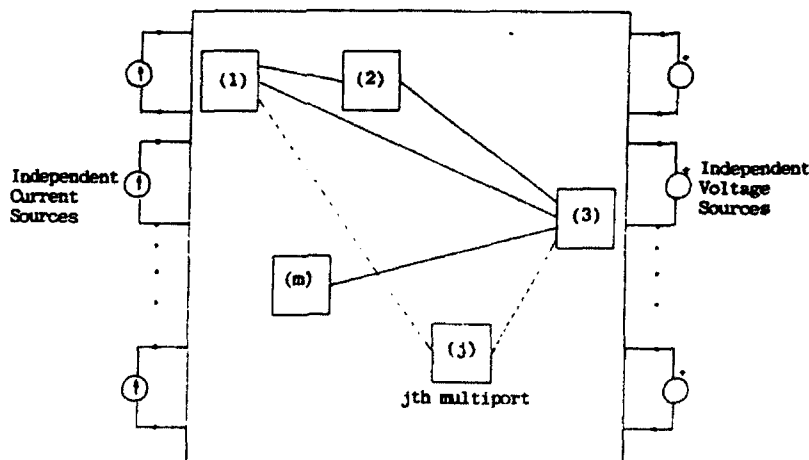


Figure 1. General lumped-distributed non-linear multiport

$$\begin{aligned}
\bar{x}^j &= \left[ \frac{dx_1^j(t)}{dt} x_2^j(t + T_k) \right]^T, \quad T_k \text{ is the delay of the } k\text{th transmission line,} \\
u^j &= [i_{cp}^j v_{cp}^j]^T \text{ is the input vector,} \\
y^j &= [v_{cp}^j i_{vp}^j]^T \text{ is the output vector,} \\
u_n^j &\text{ is the vector of the controlling voltages and currents of the non-linear elements,} \\
F_n^j &= [f_n(x^j, u^j, u_n^j, t)]^T \text{ is the vector of the non-linear functions,} \\
A^j, B^j, \dots &\text{ are real matrices of the state and output equations of the } j\text{th multiport,} \\
&\text{and the subscripts cp and vp refer to the current-driven or voltage-driven ports.}
\end{aligned}$$

With each non-linear lumped distributed multiport being represented by equation (1) we now proceeded to derive the state equations of the overall network which consists of any number of individual multiports.

### 3. THE NETWORK TOPOLOGY

The whole network is obtained by interconnecting all multiports and independent sources. The topology of these interconnections is represented by unconnected graphs. The edges of each graph have to satisfy Kirchhoff's laws. A forest is defined and Kirchhoff's laws can be expressed in the hybrid form.

$$\begin{bmatrix} i_f \\ v_c \end{bmatrix} = \begin{bmatrix} 0 & D \\ -D^T & 0 \end{bmatrix} \begin{bmatrix} v_f \\ i_c \end{bmatrix} \quad (2)$$

where  $D$  is the dynamical transformation matrix.<sup>3,4</sup>

$$D = \begin{bmatrix} D_{vs, cp} & D_{vs, vp} & D_{vs, cs} \\ \hline D_{cp, cp} & D_{cp, vp} & D_{cp, cs} \\ \hline D_{vp, cp} & D_{vp, vp} & D_{vp, cs} \end{bmatrix} \quad (3)$$

$$i_f = [i_{vs, cp, f} \ i_{vp, f}]^T \quad v_f = [v_{vs, cp, f} \ v_{vp, f}]^T$$

$$v_c = [v_{cp, c} \ v_{vp, c} \ v_{cs}]^T \quad i_c = [i_{cp, c} \ i_{vp, c} \ i_{cs}]^T$$

and the subscripts f, c, vs, cs refer to the forest, coforest, independent voltage source and independent current source respectively.

Let us define the following vectors

$$u_1 = [i_{cp, f} v_{vp, c}]^T, \quad u_2 = [v_{vp, f} i_{cp, c}]^T, \quad u_3 = [v_{vs} i_{cs}]^T$$

$$y_1 = [v_{cp, f} i_{vp, c}]^T, \quad \text{and } y_2 = [i_{vp, f} v_{cp, c}]^T$$

where  $u_3$  is the source vector containing all the independent voltage and current sources of the whole network.

It should be noted that the independent voltage and current source edges must be always in the forest and coforest, respectively. Without loss of generality, the maximum number of current-driven ports of all multiports are assigned to the forest ( $D_{vp, cp} = 0$ ).

The following equations can be obtained from (2) and (3).

$$u_1 = F_1 y_1 + F_2 u_2 + F_3 u_3 \quad (4a)$$

$$y_2 = -F_2 y_1 + F_4 u_3 \quad (4b)$$

where

$$F_1 = \begin{bmatrix} 0 & D_{cp.vp} \\ -D_{cp.vp}^T & 0 \end{bmatrix}, F_2 = \begin{bmatrix} 0 & D_{cp.cp} \\ -D_{vp.vp}^T & 0 \end{bmatrix}$$

$$F_3 = \begin{bmatrix} 0 & D_{cp.cs} \\ -D_{vs.vp}^T & 0 \end{bmatrix} \text{ and } F_4 = \begin{bmatrix} 0 & D_{vp.cs} \\ -D_{vs.cp}^T & 0 \end{bmatrix}$$

Equations (4) are auxiliary equations which will be used in the derivation of the network equations in the next section.

#### 4. FORMULATION OF THE NETWORK EQUATIONS

The state, output and non-linear equations of the whole network consisting of a number of multiports is written in the form.

$$\dot{\bar{x}}_p = \hat{A}_p \bar{x}_p + \hat{B}_p u_p + \hat{B}_{np} u_n \quad (5a)$$

$$y_p = \hat{C}_p \bar{x}_p + \hat{D}_p u_p + \hat{D}_{np} u_n \quad (5b)$$

$$F_{np} = \hat{C}_{1p} \bar{x}_p + \hat{D}_{1p} u_p + \hat{D}_{1np} u_n \quad (5c)$$

where  $\bar{x}_p$ ,  $x_p$ ,  $u_p$ ,  $u_n$  and  $F_{np}$  are real vectors, each vector contains the elements of the corresponding vectors of all multiports (e.g.  $x_p = [x^1 x^2 \dots x^m]^T$ ,  $m$  is the number of all multiports).  $\hat{A}_p$ ,  $\hat{B}_p$ ,  $\hat{B}_{np}$ ,  $\hat{C}_p$ ,  $\hat{D}_p$ ,  $\hat{D}_{np}$ ,  $\hat{C}_{1p}$ ,  $\hat{D}_{1p}$ , and  $\hat{D}_{1np}$  are real quasidiagonal matrices, each matrix contains the elements of the corresponding matrices of all multiports.

The state vector is rearranged to contain all the lumped state variables followed by the distributed ones of the whole network. The vectors  $u_p$  and  $y_p$  are also rearranged according to the forest and coforest edges of the defined vectors  $u_1$ ,  $u_2$ ,  $y_1$  and  $y_2$ . Hence the following relations are obtained:

$$x = P_1 x_p \quad (6a)$$

$$u = P_2 u_p \quad (6b)$$

and

$$y = P_2 y_p \quad (6c)$$

where  $P_1$  and  $P_2$  are elementary transformation matrices, with element values of zero or one,

$$u = [u_1 u_2]^T, \quad y = [y_1 y_2]^T$$

From (5) and (6) the overall network of multiports is described by

$$\dot{\bar{x}} = A_p \bar{x} + B_p u + B_{np} u_n \quad (7a)$$

$$y = C_p \bar{x} + D_p u + D_{np} u_n \quad (7b)$$

and

$$F_n = C_{1p} \bar{x} + D_{1p} u + D_{1np} u_n \quad (7c)$$

where

$$A_p = P_1 \hat{A}_p P_1^T, \quad B_p = P_1 \hat{B}_p P_2^T, \quad B_{np} = P_1 \hat{B}_{np}$$

$$C_p = P_2 \hat{C}_p P_1^T, \quad D_p = P_2 \hat{D}_p P_2^T, \quad D_{np} = P_2 \hat{D}_{np}$$

$$C_{1p} = C_{1p} P_1^T, \quad D_{1p} = \hat{D}_{1p} P_2^T \quad \text{and} \quad D_{1np} = \hat{D}_{1np}$$

Equation (7b) is partitioned as follows,

$$\begin{bmatrix} y_1 \\ y_2 \end{bmatrix} = \begin{bmatrix} C_{p1} \\ C_{p2} \end{bmatrix} x + \begin{bmatrix} D_{p1} & D_{p2} \\ D_{p3} & D_{p4} \end{bmatrix} u + \begin{bmatrix} D_{np1} \\ D_{np2} \end{bmatrix} u_n \quad (8)$$

From (4) and (8), we get

$$w_0 u = w_1 x + w_2 u_s + w_3 u_n \quad (9)$$

Table I. State-space representation of basic lumped elements

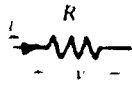
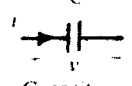
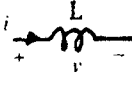
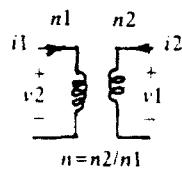
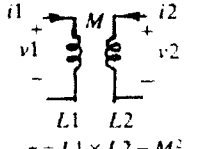
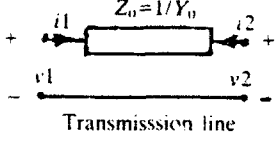
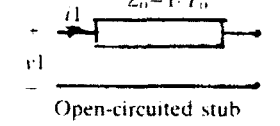
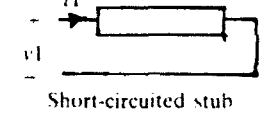
Element	Inputs	Matrices of state and output equations			
		$A$	$B$	$C$	$D$
 Resistor	$u = v$	—	—	—	$1/R$
	$u = i$	—	—	—	$R$
 Capacitor	$u = i$	0	$1/C$	1	0
 Inductor	$u = v$	0	$1/L$	1	0
 $n = n_2/n_1$	$u = \begin{bmatrix} v_1 \\ i_2 \end{bmatrix}$	—	—	—	$\begin{bmatrix} 0 & n \\ -n & 0 \end{bmatrix}$
	$u = \begin{bmatrix} i_1 \\ v_2 \end{bmatrix}$	—	—	—	$\begin{bmatrix} 0 & 1/n \\ -1/n & 0 \end{bmatrix}$
 $\tau = L_1 \times L_2 - M^2$ Non-ideal transformer	$u = \begin{bmatrix} v_1 \\ v_2 \end{bmatrix}$	—	$\begin{bmatrix} L_2/\tau & M/\tau \\ M/\tau & L_1/\tau \end{bmatrix}$	$\begin{bmatrix} 1 & 0 \\ 1 & 0 \end{bmatrix}$	—

Table II. State-space representation of transmission lines

Element	Inputs	Matrices of state and output equations			
		$A$	$B$	$C$	$D$
	$u = \begin{bmatrix} v1 \\ v2 \end{bmatrix}$	$\begin{bmatrix} 0 & -1 \\ -1 & 0 \end{bmatrix}$	$\begin{bmatrix} 0 & 1 \\ 1 & 0 \end{bmatrix}$	$\begin{bmatrix} -2Y_0 & 0 \\ 0 & -2Y_0 \end{bmatrix}$	$\begin{bmatrix} Y_0 & 0 \\ 0 & Y_0 \end{bmatrix}$
	$u = \begin{bmatrix} i1 \\ i2 \end{bmatrix}$	$\begin{bmatrix} 0 & 1 \\ 1 & 0 \end{bmatrix}$	$\begin{bmatrix} 0 & Z_0 \\ Z_0 & 0 \end{bmatrix}$	$\begin{bmatrix} 2 & 0 \\ 0 & 2 \end{bmatrix}$	$\begin{bmatrix} Z_0 & 0 \\ 0 & Z_0 \end{bmatrix}$
	$u = \begin{bmatrix} i1 \\ v2 \end{bmatrix}$	$\begin{bmatrix} 0 & -1 \\ 1 & 0 \end{bmatrix}$	$\begin{bmatrix} 0 & 1 \\ Z_0 & 0 \end{bmatrix}$	$\begin{bmatrix} 2 & 0 \\ 0 & -2Y_0 \end{bmatrix}$	$\begin{bmatrix} Z_0 & 0 \\ 0 & Y_0 \end{bmatrix}$
	$u = \begin{bmatrix} v1 \\ i2 \end{bmatrix}$	$\begin{bmatrix} 0 & 1 \\ -1 & 0 \end{bmatrix}$	$\begin{bmatrix} 0 & Z_0 \\ 1 & 0 \end{bmatrix}$	$\begin{bmatrix} -2Y_0 & 0 \\ 0 & 2 \end{bmatrix}$	$\begin{bmatrix} Y_0 & 0 \\ 0 & Z_0 \end{bmatrix}$
	$u = v1$	$\begin{bmatrix} 0 & 1 \\ -1 & 0 \end{bmatrix}$	$\begin{bmatrix} 0 \\ 1 \end{bmatrix}$	$\begin{bmatrix} -2Y_0 & 0 \end{bmatrix}$	$\begin{bmatrix} Y_0 \end{bmatrix}$
	$u = i1$	$\begin{bmatrix} 0 & 1 \\ 1 & 0 \end{bmatrix}$	$\begin{bmatrix} 0 \\ Z_0 \end{bmatrix}$	$\begin{bmatrix} 2 & 0 \end{bmatrix}$	$\begin{bmatrix} Z_0 \end{bmatrix}$
	$u = v1$	$\begin{bmatrix} 0 & -1 \\ -1 & 0 \end{bmatrix}$	$\begin{bmatrix} 0 \\ 1 \end{bmatrix}$	$\begin{bmatrix} -2Y_0 & 0 \end{bmatrix}$	$\begin{bmatrix} Y_0 \end{bmatrix}$
	$u = i1$	$\begin{bmatrix} 0 & -1 \\ 1 & 0 \end{bmatrix}$	$\begin{bmatrix} 0 \\ Z_0 \end{bmatrix}$	$\begin{bmatrix} 2 & 0 \end{bmatrix}$	$\begin{bmatrix} Z_0 \end{bmatrix}$

where

$$w_0 = \begin{bmatrix} I_0 - F_1 D_{p1} & -F_1 D_{p2} - F_2 \\ D_{p3} + F_2^T D_{p1} & F_2^T D_{p2} + D_{p4} \end{bmatrix}$$

$$w_1 = \begin{bmatrix} F_1 C_{p1} \\ -F_2^T C_{p1} - C_{p2} \end{bmatrix}$$

$$w_2 = \begin{bmatrix} F_3 \\ F_4 \end{bmatrix}$$

$$w_3 = \begin{bmatrix} F_1 D_{np} \\ -F_2^T D_{np1} - D_{np2} \end{bmatrix}$$

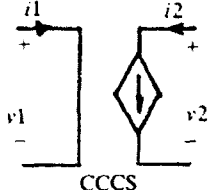
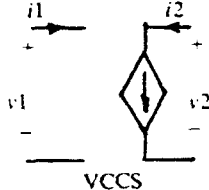
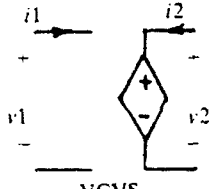
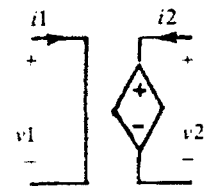
and  $I_0$  is a unit matrix.

Finally, the network equations are obtained from (7) and (9).

$$\dot{x} = Ax + Bu_i + B_n u_n \quad (10a)$$

$$y = Cx + Du_i + D_n u_n \quad (10b)$$

Table III. State-space representation of linear controlled sources

Element	Linear relations	Excitation inputs	Matrices of state and output equations			
			A	B	C	D
 CCCS	$i2 = \alpha i1$ $v1 = 0$	$u = \begin{bmatrix} i1 \\ v2 \end{bmatrix}$	—	—	—	$\begin{bmatrix} 0 & 0 \\ \alpha & 0 \end{bmatrix}$
 VCCS	$i2 = g v1$ $i1 = 0$	$u = \begin{bmatrix} v1 \\ v2 \end{bmatrix}$	—	—	—	$\begin{bmatrix} 0 & 0 \\ g & 0 \end{bmatrix}$
 VCVS	$v2 = \beta v1$ $i2 = 0$	$u = \begin{bmatrix} i2 \\ v1 \end{bmatrix}$	—	—	—	$\begin{bmatrix} 0 & \beta \\ 0 & 0 \end{bmatrix}$
 CCVS	$v2 = r i1$ $v1 = 0$	$u = \begin{bmatrix} i1 \\ i2 \end{bmatrix}$	—	—	—	$\begin{bmatrix} 0 & 0 \\ r & 0 \end{bmatrix}$

$$F_n = C_1 x + D_1 u_s + D_{1n} u_n \quad (10c)$$

where

$$A = B_p w_0^{-1} w_1 + A_p$$

$$B = B_p w_0^{-1} w_2$$

$$B_n = B_p w_0^{-1} w_3 + B_{np}$$

$$C = D_p w_0^{-1} w_1 + C_p$$

$$D = D_p w_0^{-1} w_2$$


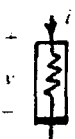
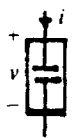



$$D_n = D_p w_0^{-1} w_3 + D_{np}$$

$$C_1 = D_{1p} w_0^{-1} w_1 + C_{1p}$$

$$D_1 = D_{1p} w_0^{-1} w_2$$

$$D_{1n} = D_{1p} w_0^{-1} w_3 + D_{1np}$$

Table IV. State-space representation of basic non-linear elements

Element	Non-linear relations	Inputs	Matrices of state and output equations									
			A	B	B <sub>n</sub>	C	D	D <sub>n</sub>	C <sub>1</sub>	D <sub>1</sub>	D <sub>1n</sub>	
<div></div> <div>Voltage-controlled resistor</div>	$i = f(v)$	$u = v$ $u_n = i$	—	—	—	0	0	1	0	0	1	
		$u = i$ $u_n = v$	—	—	—	0	0	1	0	1	0	
<div></div> <div>Current-controlled resistor</div>	$v = f(i)$	$u = v$ $u_n = i$	—	—	—	0	0	1	0	1	0	
		$u = i$ $u_n = v$	—	—	—	0	0	1	0	0	1	
<div></div> <div>Non-linear capacitor</div>	$v = g(q)$ $E = g(v_0, C_0) - v_0$	$u = i$ $u_n = E$	0	$\frac{1}{C_0}$	0	1	0	1	0	0	1	
<div></div> <div>Non-linear inductor</div>	$i = f(\psi)$ $J = f(i_0, L_0) - i_0$	$u = v$ $u_n = J$	0	$\frac{1}{L_0}$	0	1	0	1	0	0	1	
<div></div> <div>Non-linear voltage source</div>	$E = f(x, u, u_n, t)$	$u = i$ $u_n = E$	—	—	—	0	0	1	0	0	1	
<div></div> <div>Non-linear current source</div>	$J = f(x, u, u_n, t)$	$u = v$ $u_n = J$	—	—	—	0	0	1	0	0	1	



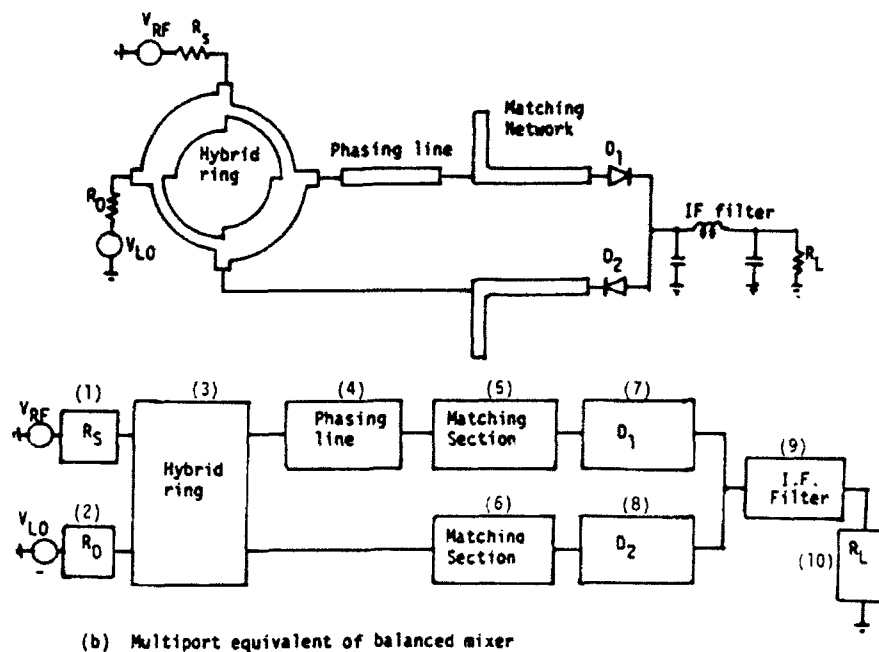


Figure 2. Circuit diagram and multiport equivalent of balanced mixer. (a) Schematic diagram of balanced mixer. (b) Multiport equivalent of balanced mixer

The matrix  $w_0$  may be singular due to the dependence between some of the lumped state variables. Such dependence which is due to the interconnection of all multiports can only arise under the following conditions:

- (1) The network has some cutsets consisting of only inductors and current sources.
- (2) The network has some loops consisting of only capacitors and voltage sources.
- (3) The presence of dependent sources in some special cases. This condition does not occur in practical networks.

The dependent state variables can be eliminated by elementary row and column operations on the coefficient matrices in (9).

## 5. SIMULATION

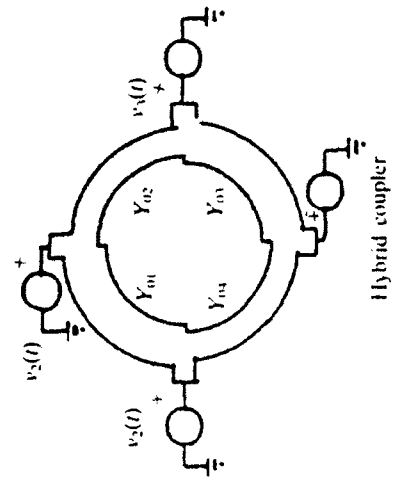
A general computer program has been developed for the analysis of non-linear L/D networks. The formulation of the network equations has been established by using sparse matrix techniques. The solution of (10) can be obtained as explained in Reference 1.

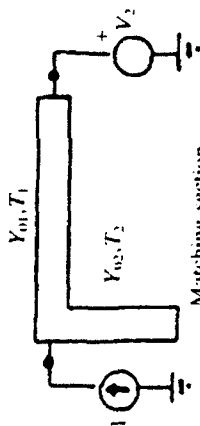
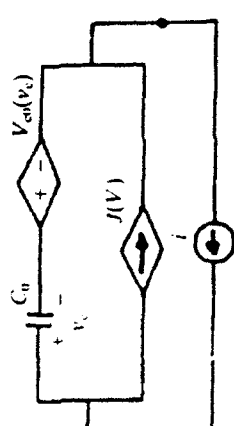
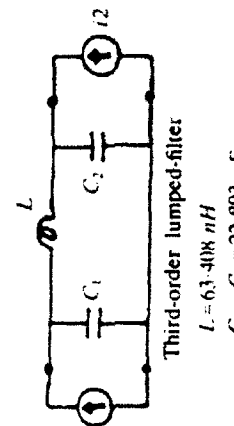
The explicit forms of the matrices of network equations, describing the devices and subcircuits commonly used are implemented in the program. The advantage of the proposed method is that the developed program deals with these circuits as multiports, describing their terminal behaviour instead of dealing with their basic circuit elements. Basic linear and non-linear circuit elements (such as resistors, inductors, capacitors, controlled sources and transmission lines) can also be represented as multiports. The state space representation of these elements is given in Tables I, II, III and IV.

## 6. EXAMPLES

The developed program has been applied to several examples. In the following examples, the circuit is partitioned into multiports using some of the implemented subcircuits in the program such as diodes, MESFET's and matching sections.

Table V. Multiport circuits of diode balanced mixer

Multiport number	Number of multiports	Non-zero elements of the state and output matrices	Multiport circuit
1 2 10	1	See Table I	$R_s = R_o = R_l = 50 \Omega$
3	4	<p><b>A matrix:</b>  <math>a_{15} = a_{26} = a_{37} = a_{48} = -1</math>  <math>a_{51} = a_{62} = a_{73} = a_{84} = 1</math></p> <p><b>B matrix:</b>  <math>b_{12} = b_{23} = b_{34} = a_{41} = 1</math>  <math>b_{41} = b_{63} = b_{73} = b_{84} = 1</math></p> <p><b>D matrix:</b>  <math>d_{11} = Y_{01} + Y_{03}</math>  <math>d_{22} = Y_{01} + Y_{02}</math>  <math>d_{33} = Y_{02} + Y_{03}</math>  <math>d_{44} = Y_{03} + Y_{04}</math></p> <p><b>C matrix:</b>  <math>c_{11} = c_{25} = -2Y_{01}</math>  <math>c_{22} = c_{36} = -2Y_{02}</math>  <math>c_{33} = c_{47} = -2Y_{03}</math>  <math>c_{44} = c_{58} = -2Y_{04}</math></p>	 <p>Hybrid coupler</p> <p> <math>Y_{01} = Y_{03} = 0.02 \text{ S}</math>  <math>Y_{02} = Y_{04} = 0.02828 \text{ S}</math>  <math>T_1 = T_2 = T_3 = T_4 = 35.714 \text{ ps}</math> </p>
4	2	See Table II	<p>Phasing line</p> <p><math>Y_0 = 0.02 \text{ S}</math>, <math>T = 35.714 \text{ ps}</math></p>

5 6	2	<p><b>A matrix:</b>  <math>a_{13} = -a_{24} = -1</math>  <math>a_{31} = -a_{42} = (Y_{01} - Y_{02})/(Y_{01} + Y_{02})</math>  <math>a_{32} = a_{41} = 2Y_{01}/(Y_{01} + Y_{02})</math></p> <p><b>B matrix:</b>  <math>b_{12} = 1</math>  <math>b_{31} = b_{41} = 1/(Y_{01} + Y_{02})</math></p> <p><b>C matrix:</b>  <math>c_{11} = 2Y_{01}/(Y_{01} + Y_{02})</math>  <math>c_{12} = 2Y_{02}/(Y_{01} + Y_{02})</math>  <math>c_{23} = -2Y_{01}</math></p> <p><b>D matrix:</b>  <math>d_{11} = 1/(Y_{01} + Y_{02})</math></p>	 <p>Matching section  <math>Y_{01} = Y_{02} = 0.02 \text{ S}</math>  <math>T_1 = 11.429 \text{ ps}</math>  <math>T_2 = 45.818 \text{ ps}</math></p>
7 8	2	<p><b>B<sub>n</sub> matrix:</b>  <math>b_{n11} = -1/c_0</math></p> <p><b>D<sub>n</sub> matrix:</b>  <math>d_{n21} = 1</math></p> <p><b>F<sub>n</sub> vector:</b>  <math>F_n = [JV_{co}]^T, V_{co} = -v^2/4V_u</math>  <math>J = J_d \exp(-v/v_T) - 1</math></p>	 <p>Schottky diode  <math>J_0 = 10^{-6} \text{ A}, V_T = 0.68 \text{ V}</math>  <math>V_{co} = 0.8 \text{ V}, C_0 = 0.15 \text{ pF}</math></p>
9	2	<p><b>A matrix:</b>  <math>a_{11} = -1/C_1, a_{21} = -1/C_2</math>  <math>a_{12} = -a_{21} = 1/L</math></p> <p><b>C matrix:</b>  <math>c_{11} = c_{22} = 1</math></p>	 <p>Third-order lumped-filter  <math>L = 63.408 \text{ nH}</math>  <math>C_1 = C_2 = 22.803 \text{ pF}</math></p>

### 6.1. Schottky diode balanced mixer

A balanced microwave mixer circuit using two silicon Schottky diodes DC1533G was analysed. The local oscillator and intermediate frequencies are 7 and 0.144 GHz, respectively. The schematic diagram of the mixer is shown in Figure 2(a). The network is divided into a number of multiports and models of each multiport, including the Schottky diodes, are developed and stored in the program library. The overall network is then analysed as an interconnection of the multiports, as shown in Figure 2(b). The equivalent representations of each multiport are given in Table V. A higher level of hierarchy is also possible and larger multiport representations can be made if required. The output waveforms before and after IF filter are shown in Figure 3. The variation of the conversion loss with RF frequency is shown in Figure 4.

### 6.2. MESFET frequency doubler

A similar procedure has been used to analyse a 2.5 GHz frequency doubler, using a Plessey P35-1105-1 MESFET, shown in Figure 5(a) and the multiport equivalent is shown in Figure 5(b). The output waveform is shown in Figure 6. The output is further analysed and the frequency response is obtained. The circuit has been built and tested and the theoretical frequency response is compared with the practical measurements in Figure 7. Good agreement is shown between measured and predicted results which gives confidence in the developed method.

## 7. CONCLUSION

Non-linear lumped-distributed networks can now be analysed in the time domain as an interconnection of multiports. The overall network is divided into a number of subnetworks and each

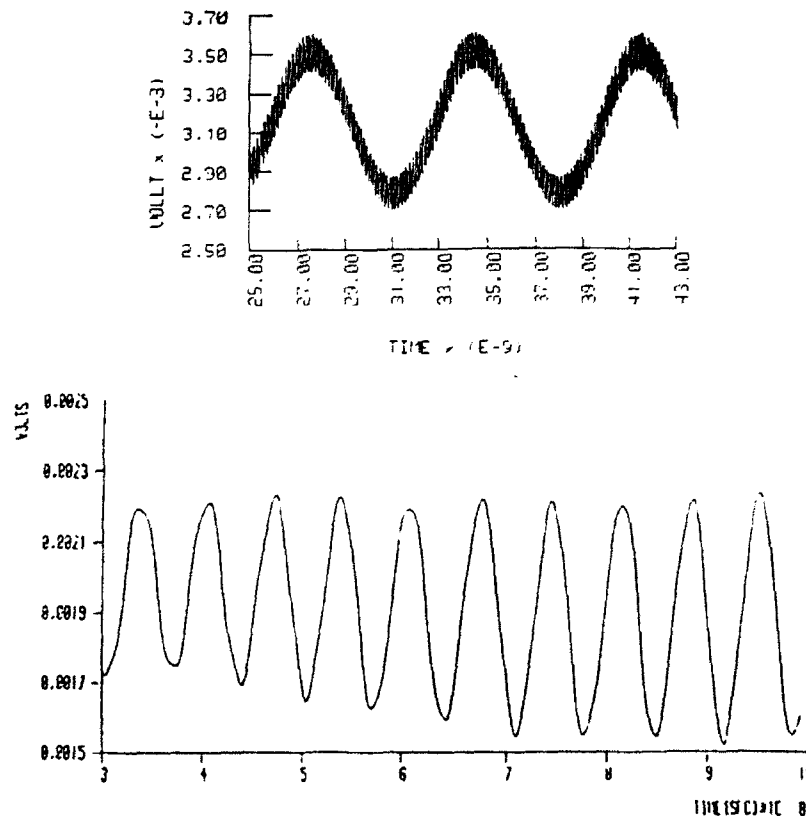


Figure 3. Simulated output of microwave mixer

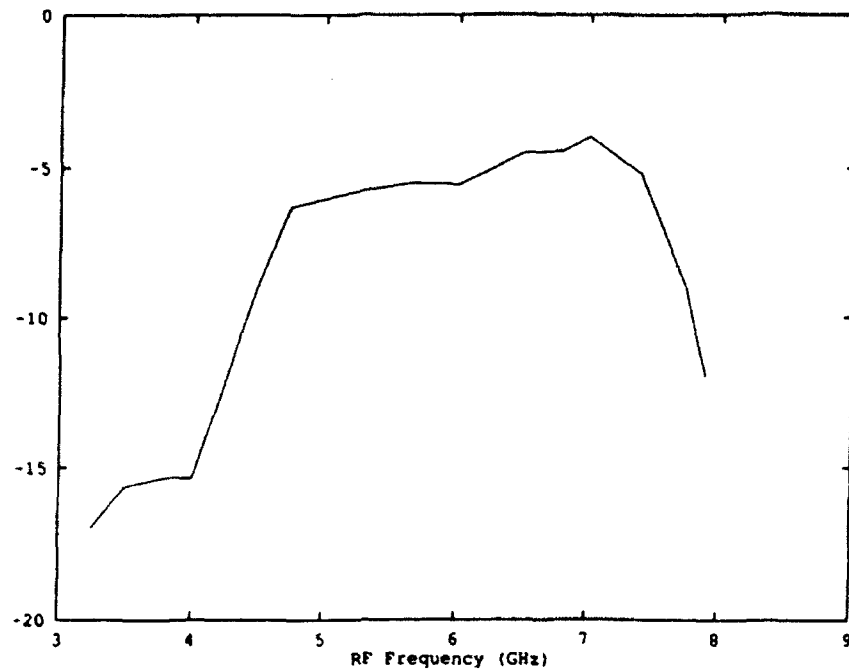
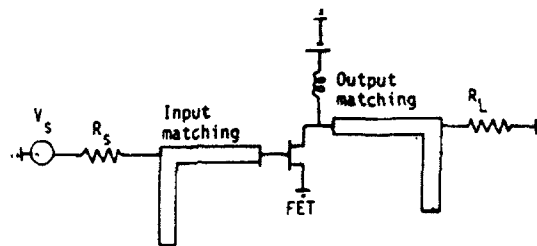
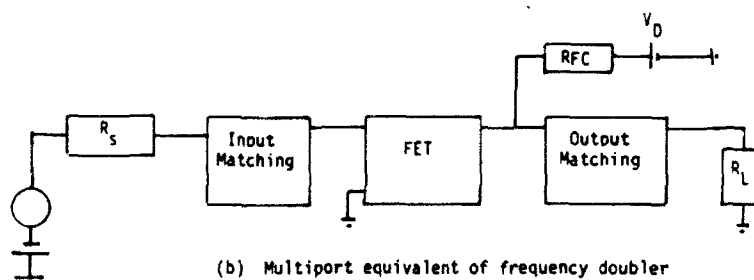


Figure 4. Frequency response of microwave mixer



(a) Schematic diagram of frequency doubler



(b) Multiport equivalent of frequency doubler

Figure 5. Circuit diagram and multiport equivalent of frequency doubler. (a) Schematic diagram of frequency doubler. (b) Circuit diagram and multiport equivalent of frequency doubler

subnetwork is characterized separately. A library of subnetworks can be developed from active elements such as transistors, FETs, diodes, etc. with very little storage required. The non-linear multiports can be used in either a direct integration subroutine or using the harmonic balance method.

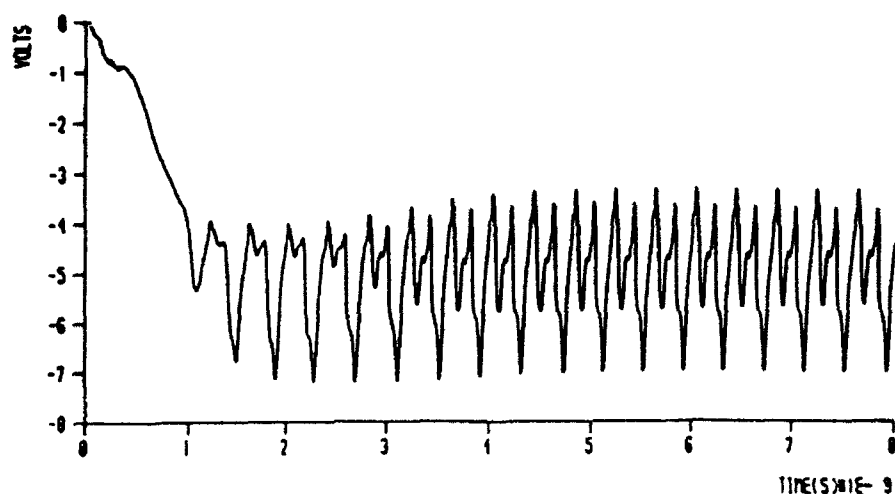


Figure 6. Output waveform of frequency doubler

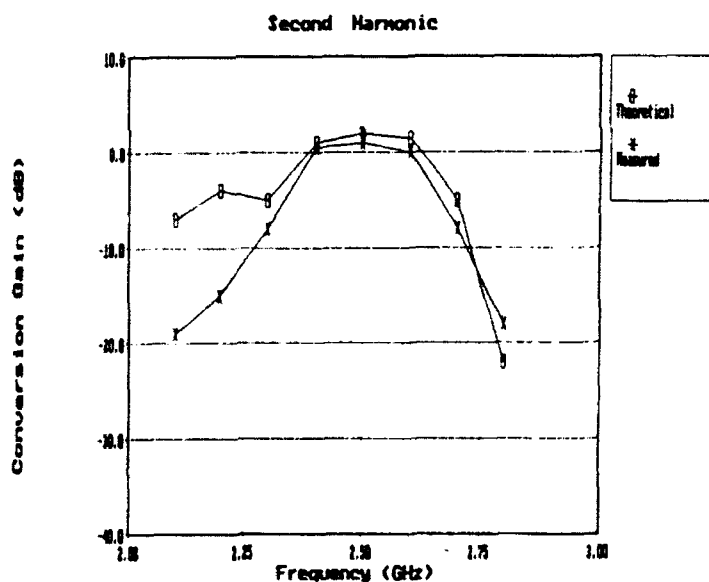


Figure 7. Frequency response of frequency doubler

## REFERENCES

1. M. I. Sobhy and A. K. Jastrzebski, 'Direct integration methods of non-linear microwave circuits', *15th European Microwave Conference*, pp. 1110-1118, Paris, September 1985.
2. V. Rizzoli and C. Cecchetti, 'A user-oriented software package for the analysis of and optimization of non-linear microwave circuits', *IEEE Trans. Microwave Theory and Techniques*, MTT-31, 636-640 (1985).
3. M. I. Sobhy and M. H. Keriakos, 'Computer aided analysis and design of networks containing commensurate and non-commensurate delay lines', *IEEE Trans. Microwave Theory and Techniques*, MTT-28, 348-358 (1980).
4. M. I. Sobhy and E. A. Hosny, 'State-space analysis of lumped-distributed networks in the time and frequency domains', *IEE Proc.*, 128, 293-298 (1981).
5. L. O. Chua and P. Lim, *Computer-aided Analysis of Electronic Circuits*, Prentice Hall, Englewood Cliffs, NJ, 1975.
6. D. A. Calahan, *Computer-aided Network Design*, McGraw-Hill, NY, 1972.
7. S. S. Bedair and M. I. Sobhy, 'Approximate solution for propagation modes on lossy multiconductor transmission lines in inhomogeneous media', *Electr. Letters*, 16, 914-915 (1980).
8. M. I. Sobhy, S. S. Bedair and M. H. Keriakos, 'State-space approach for the analysis of networks containing lossy coupled transmission lines in inhomogeneous media', *IEE Proc.*, 129 (1982).

**Authors' biographies:**

**M. I. Sobhy** received the B.Sc. degree in electrical engineering from the University of Cairo, Egypt, in 1956 and the Ph.D. degree from the University of Leeds, England, in 1966.

He was a teaching assistant at the Department of Electrical Engineering, University of Cairo, until 1962 when he joined the University of Leeds, first as a research student and later as a lecturer working on microwave ferrite devices. In 1966 he joined Microwave Associates Ltd., Luton, England, as a research engineer, where he worked on the development of microwave solid-state devices. He joined the University of Kent at Canterbury in 1967, where he is now leading a research group engaged on projects on solid-state devices and microwave circuits. He is also a consultant to a number of industrial establishments.

Professor Sobhy has published more than 100 papers in the fields of microwave circuits, computer-aided design of non-linear circuits digital filters, switched capacitor filters and microwave solid-state devices.

He is now Director of the Electronic Engineering Laboratories at the University of Kent at Canterbury, U.K.

Professor Sobhy is a Fellow of the Institute of Electrical Engineers.



**Essam A. Hosny** received the B.Sc. (Hons) degree in Electrical Engineering from the University of Cairo, Egypt, in 1965, the M.Sc. degree from the Technical University of Prague (CVUT), Czechoslovakia, in 1976 and the Ph.D. degree from the University of Kent, Canterbury, England, in 1980.

From 1965 to 1985 he was a member of the teaching staff in the Electrical Engineering Department, The Military Technical College, Cairo, Egypt. From 1986 to 1990 he was an associate professor of Electrical Engineering and head of the Circuits and Systems Group, Department of Electrical Engineering, The Military Technical College, Cairo, Egypt. Since 1990 he has been a Senior Research Fellow in the Electronic Engineering Laboratories, University of Kent, Canterbury, England.

His research interest is in the field of computer-aided design of electrical networks.



**Dr. Nassef** was born in Cairo, Egypt. He received his B.Sc. (Hons) in Electrical Engineering from the Military Technical College (MTC), Cairo, Egypt, in 1971, his M.Sc. from the University of Cairo in 1981 and his Ph.D. from the University of Kent at Canterbury, Canterbury, Kent, U.K., in 1987.

Since graduating he became a member of the academic staff at MTC, where he is now an associate professor. His research interests include the computer-aided analysis and design of non-linear microwave circuits, satellite and long-distance communications and radar systems.

Dr. Nassef won a state prize for his work in designing microstrip radar circuits.

Dr. Nassef is a member of the IEEE, a member of the Egyptian Society for Engineers and a member of the Engineering Syndicate.

## New Text Books from Wiley

### Instrumentation for Engineering Measurements, 2nd Edition

*James Dally, University of Maryland and William Riley, Iowa State University (Retired)*

This new text provides detailed coverage of the many aspects of digital instrumentation currently being employed in industry for engineering measurements and process control. Heavy emphasis is placed on electronic measurements and a section on fundamentals of digital processes has been added.

0471 60004 0 approx 704pp due April 1993 (WIE) £18.95 \$33.50

0471 55192 9 approx 704pp due April 1993 (cl) £53.00 \$86.95

### Introduction to Electric Circuits, 2nd Edition

*Richard Dorf, University of California*

Thoroughly updated with additional material, this text continues to succeed in bringing circuits to life through enriching historical vignettes and an informal writing style. Students will appreciate the relevancy of the material due to an abundance of realistic problems actually faced by practicing engineers.

0471 60011 3 approx 976pp due March 1993 (WIE) approx £21.50 \$37.95

0471 57451 1 approx 976pp due March 1993 (cl) approx £55.50 \$92.00

### Modern Control Systems Analysis and Design

*Walter Grantham, Washington State University and*

*Thomas L. Vincent, University of Arizona*

This new text provides an introduction to the analysis techniques used in the design of linear feedback control systems. It introduces general state space systems and input-output systems, and presents design methods in a building block sequence, with an analysis of first-order systems and higher-order systems.

0471 59958 1 approx 512pp due April 1993 (WIE) approx £18.50 \$32.50

0471 81193 9 approx 512pp due April 1993 (cl) approx £48.50 \$79.50

### Analysis and Design of Analog Integrated Circuits, 3rd Edition

*Paul Gray and Robert Meyer, University of California*

This new edition presents a unified treatment of bipolar, CMOS, and BICMOS analog integrated-circuit design. It stresses their commonalities and differences to give students insights into the strengths and weaknesses of each technology. The text features extensive use of the SPICE program.

0471 59984 0 approx 816pp due March 1993 (WIE) approx £18.95 \$33.50

0471 57495 3 approx 816pp due March 1993 (cl) approx £61.50 \$102.00

### Computer Aided Logical Design with Emphasis on VLSI, 4th Edition

*Frederick Hill, University of Arizona*

This book bridges the gap between logical design and VLSI design. This new edition now covers CAD tools, PLA's and VLSI systems, and NMOS and standard-cell based CMOS methodologies are now stressed.

0471 59987 5 approx 576pp due March 1993 (WIE) approx £19.95 \$34.95

0471 57527 5 approx 576pp due March 1993 (cl) approx £57.50 \$95.95

*Prices may be higher outside the UK/Europe.*

### Inspection Copy Order Form

Inspection copies are available to bona fide lecturers only.

I am a lecturer and wish to consider the title(s)

Name (PLEASE PRINT): \_\_\_\_\_

I have indicated below for course use:

☐ 0471600040 WIE Dally Instrumentation

Dept: \_\_\_\_\_

☐ 0471600113 WIE Dorf Electric Circuits

☐ 0471599581 WIE Grantham Modern Control

Address: \_\_\_\_\_

☐ 0471599840 WIE Gray Integrated Circuits

☐ 0471599875 WIE Hill Computer Aided

Course Title: \_\_\_\_\_

Enrolment: \_\_\_\_\_

Signature: \_\_\_\_\_

☐ Please tick this box if you do not wish to be mailed by other companies

Return to: Textbook Dept, John Wiley & Sons Ltd,  
Baffins Lane, Chichester, West Sussex PO19 1UD, UK  
Tel No: 0243 770372 Fax No: 0243 527944

☐ Please send me the latest catalogue.

JNM





# JOHN WILEY & SONS LIMITED

## WILEY JOURNAL AUTHOR PUBLISHING AGREEMENT

John Wiley & Sons, Ltd requires a grant of copyright from authors of articles contributed to our journals in order to effectively publish and distribute these journals worldwide. Therefore, we ask you to confirm your acceptance of the following terms by signing and returning this agreement to us:

1. The undersigned (individually or collectively the "Author") hereby assigns to John Wiley & Sons, Ltd (the "Publisher") for the full term of copyright, the sole and exclusive rights in the whole copyright in and to the article entitled \_\_\_\_\_

\_\_\_\_\_ (the "Article")  
for initial publication in the journal entitled \_\_\_\_\_

\_\_\_\_\_ (the "Journal"). This grant of rights includes, but is not limited to, the rights to republish and use the Article and the material contained therein, throughout the world, in all languages and in all media of expression now known or later developed, and to license or permit others to do so.

2. The Publisher will not withhold permission for any reasonable request from the Author to use material from the Article in connection with any other work by the Author, except for inclusion of all or a substantial part of the Article in a competing publication, provided the material appears with an appropriate credit to the Publisher and to the Journal and with copyright notice as set forth in the Journal. Such permission must be obtained from the Publisher in writing and in advance.
3. If the Article was written by the Author in the course of employment, the employer shall sign this agreement in the space provided below.
4. Any proprietary rights other than copyright (e.g. patent rights) are retained by the Author or the employer, as applicable.
5. If the Author is a U.S. government employee and this Article was prepared as part of his/her official duties, the Article will constitute a "U.S. Government Work" not protected by copyright in the U.S., but protectable outside the U.S. In such case, this assignment applies only outside the U.S. (If applicable, please mark the appropriate box provided below.) Note: If at least one co-Author is not a government employee, it is not a U.S. Government Work and said co-Author should sign this agreement.
6. In case of work prepared under U.S. Government contract, if the contract so requires the U.S. Government may reproduce, royalty free, all or portions of the Article and may authorise others to do so, for official U.S. Government purposes only. (If applicable, please mark the appropriate box provided below and attach a copy of the relevant contract.)
7. The Author warrants that the Article is the Author's original work and has not been published before. If excerpts from copyrighted works or illustrations provided by others are included, the Author will obtain written permission from the copyright owners and show credit to the sources in the manuscript. The Author also warrants that he or she has the right to enter into this Agreement, the Article contains no libelous or unlawful statements, contains no instructions that may cause harm or injury, and does not violate the copyright or trademark, or infringe on the rights or the privacy of others; and that all statements in the Article asserted as fact are either true or are based upon reasonable research.
8. If the article was prepared jointly by more than one Author, the Author warrants that he or she has been authorised by all co-Authors to sign on their behalf.
9. If the Article is accepted, publication in the Journal is deemed to constitute consideration. In addition, the Publisher will furnish the Author with a number of free copies of the Article, in accordance with its current applicable policies. If the Article is rejected, this assignment is null and void.

AGREED:

\_\_\_\_\_  
(Author) Date \_\_\_\_\_

\_\_\_\_\_  
(Employer (if applicable)) Date \_\_\_\_\_

☐ U.S. Government Employee

☐ U.S. Government Contract attached

## AIMS AND SCOPE

Prediction through modelling forms the basis of engineering design. The computational power at the fingertips of the professional engineer is increasing enormously and techniques for computer simulation are changing rapidly. Engineers need models which relate to their design area and which are adaptable to new design concepts. They also need efficient and friendly ways of presenting, viewing and transmitting the data associated with their models.

The *International Journal of Numerical Modelling: Electronic Networks, Devices and Fields* provides a communication vehicle for numerical modelling methods and data preparation methods associated with electrical and electronic circuits and fields. It concentrates on numerical modelling rather than abstract numerical mathematics.

Contributions on numerical modelling will cover the entire subject of electrical and electronic engineering. They will range from electrical distribution networks to integrated circuits on VLSI design, and from static electric and magnetic fields through microwaves to optical design. They will also include the use of electrical networks as a modelling medium.

## PRINCIPAL TOPICS

- Electromagnetic field modelling from d.c. to optical frequencies
- Modelling of information networks, analogue and digital circuits, power distribution
- Modelling of solid state devices, electronic tubes, electrical components
- Moving boundary problems, coupled problems
- Network modelling, energy and moment methods, element and ray methods, graphs
- Pre- and post-processing of data

## NOTES FOR CONTRIBUTORS

1. Four copies of the manuscript should be submitted either to Dr Wolfgang J. R. Hoefer, NSERC MPR Teltech Research Chair in RF-Engineering, Department of Electrical & Computer Engineering, P.O. Box 3055, University of Victoria, B.C., Canada V8W 3P6 or to Professor Brian Tuck, Department of Electrical and Electronic Engineering, University of Nottingham, University Park, Nottingham NG7 2RD, UK. Papers should not normally exceed 8,000 words.

In order to enable the publisher to do everything to ensure prompt publication, the full postal address should be given for the author who will check proofs, as well as telephone, telex and telefax numbers where possible.

2. Only original papers will be accepted, and copyright in published papers will be vested in the publisher.\*

3. The language of the journal is English.

4. Twenty-five offprints of each paper and one copy of the journal issue in which it appears will be provided free of charge. Additional copies may be purchased using an offprint order form which will accompany the proofs.

5. Manuscripts should be typed double-spaced with wide margins, on one side of the paper only, and submitted in triplicate. Illustrations should be submitted with the manuscript on separate sheets. Authors should write concisely. Contributors are requested to submit a photograph, in black and white, together with brief biographical details (50-100 words), with their manuscripts for publication in the journal.

6. The title should be brief, typed on a separate sheet and the author's name should be typed on the line below the title; the affiliation and address should follow on the next line. In the case of co-authors, respective addresses should be clearly indicated. Correspondence and proofs for correction will be sent to the first-named author, unless otherwise indicated.

7. The body of the manuscript should be preceded by a Summary (maximum length 200 words) which should be a summary of the entire paper, not of the conclusions alone.

8. The papers should be reasonably subdivided into sections and, if necessary, subsections.

9. Mathematical symbols may be either handwritten or type-written. Greek letters and unusual symbols should be identified separately in the margin. Distinction should be made between capital and lower case letters; between the letter *O* and zero; between the letter *I*, the number one and prime; between *k* and *kappa*.

10. Computer programs should be on an original print-out on plain paper and will be reproduced photographically to avoid errors. A distinct black image must always be used.

11. Half-tone illustrations are to be restricted in number to the minimum necessary. Good glossy bromide prints should accompany the manuscripts and should not be attached to manuscript pages. Photographs should be enlarged sufficiently to permit clear reproduction in half-tone after reduction. If words or numbers are to appear on a photograph two prints should be sent, the lettering being clearly indicated on one print only.

12. Original line drawings (not photocopies) should be submitted suitable for immediate reproduction. Drawings should be about twice the final size and the lettering must be clear and 'open' and must also be large enough to be reduced in the same proportion. If this is not possible the lettering should be provided on an overlay.

13. Figure legends should be typed on a separate sheet and placed at the end of the manuscript. The amount of lettering on a drawing should be reduced as far as possible by transferring it to the legend.

14. It is the author's responsibility to obtain written permission to quote material which has appeared in another publication.

15. Tables should be numbered consecutively and titled. All table columns should have an explanatory heading. Tables should not repeat data which are available elsewhere in the paper, e.g. in a line diagram.

16. References to published literature should be quoted in the text by superior numbers and grouped together at the end of the paper in numerical order. Journal references should be arranged thus:

1. M. LeRoy, 'Original improvements of TLM method', *Electron. Lett.*, 17, 684-685 (1981).

Book references should be given as follows:

2. P. Hammond, *Energy Methods in Electromagnetism*, Clarendon Press, Oxford, 1986.

17. The *International Journal of Numerical Modelling* will feature a letters section, allowing accelerated publication of original and significant contributions of high quality in numerical modelling. A small number of pages will be allocated per issue for short letters that do not exceed two printed pages, including illustrations. A submission including the equivalent of more than two and one-half pages will be returned for shortening immediately, and not be given an official received date.

Manuscripts for such letters should be submitted in the same form as regular papers, together with a signed publishing agreement. However, photographs and biographical notes should not be submitted with letters. Using accelerated reviewing procedures which rely heavily on Fax transmission of reviewers' comments, we will attempt to publish manuscripts within three to six months after they have been received by the Editors, provided the authors respond immediately to all communications. Acknowledgement cards will not be sent to the authors. Proofs will be sent, but there may not be time to wait for their return in certain cases, as this may result in a publication delay of three months.

18. No manuscript or figures will be returned following publication unless a request for a return is made when the manuscript is originally submitted.

19. The publisher will do everything possible to ensure prompt publication. It will therefore be appreciated if manuscripts and illustrations conform from the outset to the style of the journal. Corrected proofs must be returned to the publishers within three days to minimize the risk of the author's contribution having to be held over to a later issue.

20. Copies of redrawn or re-lettered diagrams will only be submitted to authors if time permits. Authors should check the illustrations carefully when reading their proofs.

21. The Editors and Publishers cannot accept responsibility for the correctness of published programs. The responsibility is that of the author who will have an opportunity to check the program at proof stage.

\*NOTE: Because of recent changes in copyright laws the transfer of copyright from author to publisher, previously implicit in the submission of a manuscript, must now be explicitly transferred to enable the publisher to ensure maximum dissemination of the author's work. A copy of the Publishing Agreement to be used for *International Journal of Numerical Modelling: Electronic Networks, Devices and Fields* is reproduced in each volume. Additional copies are available from the journal editors or from the publisher; or contributors may photocopy the agreement from this journal. A copy of this agreement, signed by the author, must accompany every article submitted for publication.

## CONTENTS

**Special Issue on the Workshop on Discrete Time Domain Modelling of  
Electromagnetic Fields and Networks**

*Munich, 24-25 October, 1991*

**Part 2**

*Guest Editor: Professor Dr Peter Russer*

**VOLUME 6, ISSUE No 1**

*February 1993*

Editorial.....	1
Efficient Analytical-Numerical Modelling of Ultra-wideband Pulsed Plane Wave Scattering from a Large Strip Grating: L. Carin and L. B. Felsen .....	3
Calculating Frequency-domain Data by Time-domain Methods: M. Dehler, M. Dohlus and T. Weiland .....	19
The Hilbert Space Formulation of the TLM Method: P. Russer and M. Krumpholz ..	29
Spatially Weighted Numerical Models for the Two-dimensional Wave Equation: FD Algorithm and Synthesis of the Equivalent TLM Model: N. R. S. Simons and A. A. Sebak .....	47
Multiport Approach for the Analysis of Microwave Non-linear Networks: M. I. Sobhy, E. A. Hosny and M. A. Nassef .....	67



0894-3370(199302)6:1;1-4

### COPYING OF ARTICLES

The code and the copyright notice appearing at the bottom of the first page of an article in this journal indicates the copyright owner's consent that copies of the articles may be made for personal or internal use, or for the personal or internal use of specific clients, on the condition that the copier pay for copying beyond that permitted by Sections 107 or 108 of the US Copyright Law. The per-copy fee for each article appears after the dollar sign, and is to be paid through the Copyright Clearance Center Inc. This consent does not extend to other kinds of copying, such as copying for general distribution, for advertising or promotional purposes, for creating new collective works, or for resale. Such permission requests, or other inquiries, should be addressed to the publisher.